Mechanism of Membrane Penetration by Nonenveloped Polyomavirus and Papillomavirus

by

Allison Jade Dupzyk

A dissertation submitted in partial fulfillment of the
requirements of the degree of
Doctor of Philosophy
(Microbiology and Immunology)
in the University of Michigan
2019

Doctoral Committee:

Professor Billy Tsai, Chair
Associate Professor Diane Fingar
Professor Michael J. Imperiale
Professor Katherine R. Spindler

Allison J. Dupzyk

adupzyk@umich.edu

ORCID iD: 0000-0003-1474-4489

Dedication

I dedicate this thesis to Michael James Bennett. Thank you for the unconditional love and support.

Acknowledgments

I'd like to acknowledge Bill Tsai for being a wonderful mentor. Bill leads by example, and teaches his trainees what it means to be a responsible scientist, and a mentor. He has always managed to make me feel like a valuable lab member, even when I was just joining the lab. Bill goes out of his way to provide support for his trainees, whether it's writing recommendation letters at midnight, or while on vacation, or sitting down and discussing our future endeavors. His enthusiasm for science is contagious, and despite his productivity, he always makes research enjoyable. I would also like to thank my committee members for their time and valuable insight.

I would like to thank the Tsai lab, both current and past members, for assistance in my training, support and lively discussions. I owe a great deal to the past postdocs who trained me during my first year in the lab- specifically Dr. Madhu Ravindran, Dr. Parikshit Bagchi, and especially Dr. Takamasa Inoue. I would like to thank Corey Cunningham for being an enthusiastic lab sibling, and Dr. Chelsey Spriggs, one of the more recent Tsai lab postdocs, for being a supportive friend and mentor. Lastly, I'd like to thank Mara Harwood, for being a great teammate on the HPV project.

I discovered my love for basic science during my time as an undergraduate at University of California, Santa Cruz. My time spent in lab would not have been possible without the financial and professional support of the IMSD program. I would like to thank my undergraduate mentor, Professor Victoria Auerbach Stone, who taught me that sometimes you have to push back when told "no." I'd also like to thank Dr. Miles Duncan, who was patient while training me in the Auerbach Stone lab- even when I aspirated his cells.

I am grateful to my family who have provided their love and support from the west coast. Both my mother and father have inspired me to give my all in everything I pursue. I would like to give a special thanks to my in-laws, who have treated me like their own daughter, and made my undergraduate degree a possibility. Lastly, I would like to acknowledge my husband and best friend, Michael Bennett, for moving to Michigan with me and partaking on this adventure. I'm excited for our next adventure together.

Chapters 1 (the SV40 introduction), 2, and 3 are all multi-author publications. Figures 2-3c and 2-3d were produced by Jeffrey Williams. Figure 2-6a contains data produced by Dr. Parikshit Bagchi. Figure 4-1a was generated by Dr. Takamasa Inoue. Figures 4-1c, and 4-1d were generated by Mara Harwood. Figure 4-2 was a joint effort with Mara Harwood.

Table of Contents

List of Figures

Abstract

Membrane penetration represents a critical step during virus infection. As nonenveloped viruses lack a surrounding lipid bilayer, they are unable to penetrate host membranes by a membrane fusion mechanism. Consequently, nonenveloped viruses must devise alternative strategies to enter the host cell. In the case of polyomavirus SV40 and human papillomavirus (HPV), these two nonenveloped DNA tumor viruses must hijack selective host factors in order to promote their membrane penetration.

Upon endocytosis, SV40 traffics through the endosomal pathway to reach the endoplasmic reticulum (ER). Here the virion is inserted into the ER membrane and is extracted into the cytosol by the cytosolic extraction machinery composed of the Hsc70, SGTA, and Hsp105 chaperones. From the cytosol, the virus is transported into the nucleus to cause infection. My thesis work unambiguously identified Hsc70 as a critical component of the cytosolic extraction machinery that ejects SV40 from the ER into the cytosol, clarified the structure-function relationship of SGTA during this process, and unveiled SGTA's ability to negatively regulate Hsc70's action during this the ER-to-cytosol membrane transport step. Moreover, my studies revealed that the Bag2 nucleotide exchange factor (NEF) is a new component of the cytosolic extraction machinery. In this context, Bag2 stimulates SV40 release from Hsc70, promoting successful arrival of SV40 to the cytosol, leading to infection. Collectively, my findings identify a novel component of a cytosolic extraction machinery essential during

membrane penetration of a nonenveloped virus, and provide further mechanistic insights into this process.

Similar to SV40, HPV membrane penetration requires host factors that are poorly characterized. After initial entry, HPV reaches the endosome, where the viral L2 minor capsid protein is inserted into the endosomal membrane. Membrane insertion of L2 is a decisive event because this step recruits the cytosolic sorting retromer complex to endosome-localized HPV, which in turn directs the virus to the Golgi apparatus. From this compartment, the virus enters the nucleus during mitosis where viral DNA is replicated. Through classic biochemical analyses, we recently reported that the transmembrane protease γ-secretase acts as a novel chaperone that binds to and inserts L2 into the endosomal membrane, an essential HPV infection step. In this thesis, we now identify the γ-secretase-binding partner δ-catenin/p120 as a new host factor that interacts with L2 and promotes HPV infection. Our analysis further suggests a model in which p120 engages HPV early in infection, delivering the virus to γ–secretase so that HPV can properly insert into the endosome membrane. In sum, my results provide fundamental insights into the infectious entry pathway of the nonenveloped SV40 and HPV by illuminating their membrane penetration mechanism.

Chapter 1: Introduction

Viruses must hijack cellular machineries in order to enter and infect host cells. Because the host's cell surface and internal organelles are surrounded by membranes composed of a lipid bilayer, viral entry requires penetration of at least one of these cellular membrane barriers. In the case of an enveloped virus ensheathed by a lipid bilayer, membrane penetration occurs when the viral membrane fuses with the host membrane. However, because a nonenveloped virus is not surrounded by a lipid bilayer, membrane penetration must occur by a fundamentally different mechanism.

Indeed, nonenveloped viruses have developed unique strategies to penetrate host membranes, enabling them to deliver the viral nucleic acids to appropriate cellular destinations to cause infection. In general, this process requires trafficking along a productive infectious route to a specific sub-cellular location where host factors induce viral conformational changes. For example, endocytosis of the nonenveloped adenovirus targets the virus to the endosome, enabling the low pH in this compartment to trigger release of the viral lytic protein VI from the core viral particle (1). Protein VI in turn binds to and ruptures the endosomal membrane, allowing the virus to reach the cytosol. Similarly, for the nonenveloped poliovirus, after reaching the endosome from the cell surface, structural changes experienced by the viral particle in this organelle induce the viral proteins VP1 and VP4 to insert into the endosomal membrane, promoting release of the viral RNA into the cytosol (2). While these examples reveal a

level of insight into membrane penetration of nonenveloped viruses, a more comprehensive and mechanistic understanding of this process remains largely undefined, especially in comparison to our understanding of enveloped virus membrane fusion.

PyV and disease

A central focus of my thesis project is to clarify membrane penetration of the small nonenveloped DNA tumor polyomavirus (PyV). The first two human PyVs, JC and BK PyV, were discovered in 1971 (3,4). Since then, an additional 11 human PyVs have been identified (5-7), including some more prominent viruses such as the Merkel cell PyV, the causative agent of an aggressive skin cancer called Merkel cell carcinoma (8). PyVs are highly prevalent in the human population, with some such as the BK PyV estimated to infect up to 90% of the human population (5, 9-11). Although PyV infections are generally benign in healthy immunocompetent individuals, they pose a significant threat to immunocompromised patients (11). For instance, BK PyV, the causative agent of PyV-associated nephropathy (10), becomes problematic in transplant patients. Because no therapies currently exist for PyV-associated nephropathy, treatment requires reducing immunosuppressants, which often leads to graft rejection. As another example, JC PyV is a neurotropic virus that causes progressive multifocal leukoencephalopathy (PML), a demyelinating disease of the central nervous system (12). In immunocompromised patients such as those infected by human immunodeficiency virus and suffering acquired immune deficiency syndrome (HIV/AIDS), JC PyV-induced PML is rather common. Despite the fact that PyVs were

discovered 45 years ago, effective treatments are currently lacking. However, recent advances in PyV research have made therapeutic development a realistic possibility.

SV40 structure and entry pathway

SV40 is the archetype PyV, displaying both genetic and structural similarity to human PyVs. Accordingly, elucidating SV40 entry should illuminate the human PyV infection pathway. Structurally, SV40 contains a circular doubled-stranded DNA genome of approximately five kilobase-pairs that encodes seven genes: three structural genes called VP1, VP2, VP3, and four non-structural genes called VP4, large T antigen, small T antigen, and agno protein (5,7,11,13). As a nonenveloped virus, SV40 lacks a surrounding envelope and instead contains a protein capsid composed of 360 VP1 copies arranged as 72 pentamers that are displayed on the viral surface (Figure 1-1A). The pentamers are stabilized by disulfide bonds, as well as by interactions between the VP1 C-terminus, which invades a neighboring pentamer (14,15). VP1 also associates with the underlying internal hydrophobic proteins VP2 and VP3, which along with VP1, bind to the genome (16). When fully assembled, SV40 is approximately 45–50 nm in diameter (7,11,14).

To infect cells, SV40 first binds to the glycolipid receptor ganglioside GM1 on the cell surface (17-19), becomes internalized, and traffics to the early and late endosomes (Figure 1-1B, step 1; (20)). The virus then sorts to the endoplasmic reticulum (ER) using a lipid-directed mechanism (Figure 1-1B, step 2; (17, 21,22)), from where it ejects across the ER membrane to reach the cytosol (Figure 1-1B, step 3). Upon reaching the cytosol, SV40 mobilizes to the nucleus (Figure 1-1B, step 4), where ensuing

transcription and replication of the viral genome cause lytic infection or cellular transformation (23,24). Although SV40 ER-to-cytosol membrane penetration - a decisive infection step - is not entirely understood, key concepts and cellular components involved in this pathway are slowly being unraveled (25). The emerging principle posits that SV40 hijacks elements of a major protein quality control pathway called ER-associated degradation (ERAD) during its ER membrane penetration. In typical ERAD, misfolded ER proteins are ejected to the cytosol by transporting across the ER membrane via the so-called Hrd1-Sel1L membrane complex; upon reaching the cytosol, the misfolded proteins are polyubiquitinated and degraded by the proteasome machinery (26).

ER luminal events

After reaching the ER from the cell surface, SV40 is thought to disguise as a "misfolded" substrate, co-opting components of the ERAD machinery in order to penetrate the ER membrane and reach the cytosol. To do so, SV40 first undergoes conformational changes that partially uncoat the virus. This conformational change generates a hydrophobic viral particle that binds to and inserts into the ER membrane, a step required for successful membrane transport. Multiple PDI family members impart structural alterations to SV40 in the ER, including PDI, ERp57, and ERdj5 (27-29); there is evidence that ERdj5 also executes an important role during BK PyV infection (29). In the case of the murine PyV, another PDI family member called ERp29 was found to locally unfold the VP1 C-terminal arm (30,31), a reaction that in conjunction with PDI and ERp57 (28,32) generates a hydrophobic virus by exposing the internal hydrophobic

proteins VP2 and VP3 (33,34). Of note, the PDI-ERp57-ERp29 triad has also been reported to act on JC PyV during infection (35).

Uncoating of SV40 (and other PyVs) by PDI family members exposes the underlying hydrophobic proteins VP2 and VP3. While the newly-generated hydrophobic viral particle can bind to and integrate into the hydrophobic ER membrane, this virus is also prone to aggregation. To prevent aggregation, the BiP chaperone is recruited to the virus (36,37), similar to its role in preventing aggregation of a misfolded client during ERAD (38). BiP's ability to engage SV40 (and other cellular substrates) is strictly dependent on its nucleotide-bound states (39). In the ADP-bound form, BiP has a high affinity for its substrate, while ATP-BiP displays a low substrate-binding affinity. J-proteins activate BiP's intrinsic ATPase activity, converting ATP-BiP to ADP-BiP. By contrast, nucleotide exchange factors (NEFs) release ADP from ADP-BiP, enabling ATP to re-engage BiP and generate ATP-BiP. In this context, the ER-resident J-protein ERdj3 was found to promote SV40 ER membrane transport by stimulating SV40-BiP interaction (37), presumably after hydrophobic proteins VP2 and VP3 are exposed. When the SV40-BiP complex is proximal to the luminal surface of the ER membrane, the virus must be released from BiP to initiate ER membrane penetration and transport. Of the two established ER luminal NEFs, only glucose-regulated protein 170 kDa (Grp170), but not Sil1, promotes SV40 release from BiP in order to prime the virus for membrane penetration (40). Grp170 was also shown to bind directly to the Hrd1 adapter Sel1L (41). This positions Grp170 next to the ER membrane, suggesting that SV40 release from BiP occurs proximal to the membrane. Such a scenario raises the possibility that release of the virus from BiP is coupled to membrane transport.

Interestingly, only Sel1L (27) but not Hrd1 (36) plays a role in SV40 and JC PyV infection (35). Why this is the case is unclear, but there is the possibility that Sel1L might operate independent of Hrd1 in some instances. For instance, there may exist a pool of Sel1L that does not bind to Hrd1. Instead, this Sel1L pool might recruit previously uncharacterized ER (or possibly cytosolic) proteins that promote PyV infection.

While not identical for all PyV family members, a coherent theme has come into focus for ER luminal events initiating the virus membrane transport process. Specifically, upon reaching the ER from the plasma membrane, the virus initially undergoes conformational changes induced by ERAD factors such as the PDI family members - these reactions expose the inner hydrophobic VP2 and VP3 proteins and generate a hydrophobic viral particle. The hydrophobic virus is prevented from aggregation by the recruitment of ERAD molecular chaperones such as BiP. In the final phase, the hydrophobic virus disengages from the molecular chaperone, binds to and inserts into the ER membrane, and is now primed for penetration across the lipid bilayer.

ER membrane events

When the hydrophobic SV40 particle inserts into the ER membrane, the N-terminal region of the exposed VP2 protein binds to an ER membrane protein called B-cell receptor-associated protein 31 (BAP31) (36), which is thought to stabilize the membrane-embedded virus. Additional ER membrane components such as the Derlins have also been reported to mediate ER-to-cytosol transport of SV40 (27), as well as the

murine PyV (42), and BK PyV (43). However, the precise molecular contribution of Derlins to the membrane penetration event is unclear.

In an unbiased RNA interference (RNAi) screen, three ER transmembrane J proteins (B12, B14, and C18) were found to be essential in promoting SV40 and BK PyV infection (37). Of these J proteins, B12 and B14 have been previously implicated in ERAD (44-46). Not surprisingly, due to their localization to the ER membrane, B12, B14, and C18 regulate the decisive virus ER-to-cytosol membrane transport step (37,47,48). Because these J proteins display their catalytic J-domain towards the cytosol, part of their mechanism of action likely involves the recruitment of cytosolic Hsc70 and associated co-chaperones used to extract the virus into the cytosol. Interestingly, using a knockdown-rescue approach, all three J proteins were shown to exert non-redundant roles during SV40 ER membrane penetration (48). These results suggest that each J protein imparts a unique function within the viral membrane transport pathway. One possibility is that an individual J protein binds to a distinct set of luminal, membrane, or cytosolic partners that are all necessary to support the membrane transport process.

An outstanding question is whether there are specific regions within the vast ER membrane, which is composed of a complicated network of sheets and tubules (49), that serve as selective membrane penetration sites for the virus. To address this question, we and others reported that many of the ER membrane proteins that promote SV40 ER membrane transport, including BAP31, B12, B14, and C18, reorganize into distinct subdomains within the ER membrane called foci during SV40 infection (36, 47,48,50); SV40 itself also accumulates in these virus-induced foci (36,47,48,50). Importantly, the VP2/VP3-exposed, membrane penetration-competent form of SV40 is

found predominantly in these punctate structures (48). These collective findings suggest that virus-triggered foci represent viral cytosol entry sites from the ER. Consistent with this idea, the rate of focus formation was found to temporally parallel SV40 cytosol arrival from the ER (47), SV40 mutants which cannot transfer across the ER membrane to reach the cytosol also fail to trigger focus formation (48), and impairing SV40 release into the cytosol traps SV40 in the foci, leading to expansion of the foci structures (50). While these are compelling data to support the notion that SV40 possesses a unique ability to construct specific penetration sites on the ER membrane, the precise molecular mechanism by which the viral particle stimulates focus formation remains unclear. For instance, assuming that individual components of the foci structures must reorganize laterally within the ER lipid bilayer to generate the focus structure, how does SV40 exploit cellular mechanical forces to accomplish this difficult feat? In this regard, the force generated by the cytosolic kinesin-1 motor was shown to promote SV40-induced focus formation (51). Whether forces derived from additional ER luminal, membrane, or cytosolic factors are harnessed to drive focus formation are unknown. Clearly, clarifying the nature of the virus-induced foci, as well as elucidating their precise physiologic functions, deserve more attention.

Cytosolic events

Although SV40 is partially uncoated when it penetrates the ER membrane, the size of these viral particles remains relatively large, with reports ranging from approximately 35 nm (36) up to 45 nm (29,52) in diameter. Thus it is unlikely that the membrane-inserted SV40 passively slips through the ER lipid bilayer to reach the cytosol. Instead, we postulate that a cytosolic extraction machinery “pulls” the viral particle into the

cytosol. During ERAD, the p97 chaperone normally provides the primary driving force to extract a misfolded client from the ER into the cytosol (53). However, this cytosolic ATPase is not involved in SV40 infection (36). Motivated by this observation, we used a classical biochemical approach to identify the putative cytosolic extraction machinery, guided by the basic premise that the membrane-bound J proteins B12, B14, and C18 would recruit such a machinery. These efforts pinpointed a cytosolic ternary protein complex composed of Hsc70, Hsp105, Bag2, and SGTA that we called the virus "extraction machinery" (47,50,54,55). Within this extraction machinery, Hsc70 is a well-established chaperone that uses its ATPase activity to drive numerous protein folding, degradation, and quality control processes (56). Hsp105 is an atypical Hsc70 family member that also harbors a bonafide chaperone activity which can be used to promote protein disaggregation (56,57). Bag2 is NEF of Hsc70, while SGTA is a Hsc70 co-chaperone that controls the action of Hsc70 (58-61). In addition to its role regulating Hsc70, SGTA also catalyzes an important step in the guided entry of tail-anchored proteins (GET) pathway, which inserts tail-anchored (TA) proteins from the cytosol into the ER membrane (62,63). It is worth noting that individual components of the Hsc70-Hsp105-Bag2-SGTA complex executes a role during ERAD (64,65,66).

At the on-set of my thesis project, Hsp105 and SGTA were shown to play pivotal roles in promoting ER-to-cytosol membrane penetration of SV40 (47,50). Specifically, Hsp105 is thought to disassemble SV40 as the virus is extracted from the ER into the cytosol, while SGTA guides the virus from the ER into the cytosol via a poorly characterized mechanism (47,50). However, the functions of Hsc70 and Bag2, as well as whether any individual components of this extraction machinery mutually regulate

each other's function during the virus membrane penetration process, remained unknown. Chapter 2 and 3 of this thesis will demonstrate the key findings of my thesis work, firmly establishing critical roles of Hsc70 and Bag2 in driving ER-to-cytosol membrane penetration of SV40 (54,55). Additionally, my results reveal that Hsc70's action during SV40 ER membrane transport is negatively impacted by SGTA (54). Finally, I also demonstrate that SGTA – via its N-terminal domain – exerts an unanticipated role post ER membrane penetration (54). By revealing the molecular basis by which SV40 accomplishes its ER-to-cytosol membrane penetration, this thesis thus clarifies a decisive step during infectious entry of a nonenveloped virus. We envision these insights may illuminate membrane penetration of other PyV family members and perhaps other nonenveloped viruses.

HPV and disease

In addition to PyV, the human papillomavirus (HPV) is another nonenveloped DNA tumor virus that causes morbidity and mortality. There are more than 200 types of HPVs, which are divided into 5 genera: alpha, beta, gamma, mu and nu (67). Of these viruses, only viruses belonging to the alpha genera infect cutaneous and mucosal epithelia (67). High risks HPVs, including HPV16 and HPV18, are not only responsible for almost all cases of cervical cancer, but also cause anogenital and oropharyngeal cancer (68). Although a highly effective HPV vaccine exists, vaccination cannot be used to treat pre-existing HPV infections. In addition, many people worldwide do not have access to HPV vaccines, further highlighting the need for insights into HPV entry which might provide new therapeutic strategies (69,70).

HPV structure and receptor-engagement

Structurally, HPV is approximately 55 nm in diameter (71). The icosahedral viral capsid is composed of 72 pentamers of the L1 major capsid protein, which encase up to 72 copies of the L2 minor capsid protein (72). Protected inside the viral capsid is the double-stranded DNA genome of approximately 8 kilobase-pairs (73). While the HPV genome varies between types, four genes are conserved among all HPVs: the viral capsid genes L1 and L2, and the replication genes E1 and E2 (67).

Productive HPV entry begins with damage to the outermost layer of tissue of the stratified epithelium, which provides the virus physical access to the basal tissue layer (74). Infection at this basal layer allows for long-term, persistent infection to occur (75,76). The viral lifecycle is highly dependent on cell differentiation, as receptor binding and viral entry does not occur at the squamous stratified epithelial, but instead occurs only at the basal epithelial cells (75). As cell differentiation occurs, viral genome replication and gene expression becomes detectable (77).

HPV endocytosis is a slow and asynchronous process, with the half-time of uptake varying from 4 to 12 hours (71). Initial binding of the virus to the cell surface occurs quickly, suggesting that the rate-limiting step during entry occurs post-attachment (78). To date, the HPV entry receptor remains unknown. Prior to engaging the unknown entry receptor, HPV L1 binds to the primary attachment receptor heparin sulfate proteoglycans on the cell surface or laminin 332 of the extracellular matrix (79-82). A conformational change ensues that results in cleavage of L1 by kallikrein-8 (KLK8) (83). Presence of extracellular cyclophilins on HSPGs allows for their direct

access to HPV, and induces conformational changes that exposes the N-terminus of L2 (84,85). The L2 N-terminus is then cleaved by the transmembrane protein furin (81, 86, 87). This cleavage promotes release of HPV from the attachment receptor, enabling the virus to be transferred to the postulated entry receptor (88, 89). There is evidence that receptor-dependent internalization mediated by the postulated entry receptor acts as a rate-limiting step during viral endocytosis (90).

Endocytosis and transport to endosome

Although HPV endocytosis is actin-dependent, the role of clathrin remains controversial, possibly due to studies using different pseudoviruses, cell lines, and means of disrupting clathrin function (71, 91). After endocytosis, HPV reaches the endosome. Here, virus disassembly is initiated when the low pH and the action of cyclophilins promote dissociation of the majority of L1 from the L2-DNA complex (92-94). Importantly, L2 remains associated with the viral DNA, guiding transport of the viral DNA to the nucleus (95). In the endosome, HPV encounters the transmembrane protease γ-secretase complex (96-99). Our lab recently revealed that γ-secretase promotes insertion of L2 across the endosomal membrane (99), initiating virus membrane penetration essential during HPV infection (100).

Targeting to the Golgi

Insertion of L2 into the endosomal membrane is critical for HPV infection, because this step exposes the C-terminus of L2 to the cytosol (100). As the L2 C-terminus harbors a retromer-binding motif, L2 membrane insertion can recruit the

cytosolic retromer complex to the membrane-inserted virus (98, 99, 101-103). Because the retromer complex normally targets cargos from the endosome to the trans Golgi network (TGN) and Golgi, its recruitment to the virus sorts endosome-localized HPV to the Golgi (99, 101,102,104).

Nuclear entry

The L2-viral DNA complex remains in the Golgi until the host cell undergoes mitosis. Two critical events occur during mitosis essential for HPV infection: the Golgi membrane fragments and the nuclear envelope disassembles (105). Golgi membrane fragmentation generates Golgi-derived vesicles (GDVs) that harbor HPV, which can gain entry to the nucleus due to disassembly of the nuclear envelope (106). In this manner, HPV is deposited into the nucleus upon re-assembly of the nuclear envelope at the end of mitosis. Within the nucleus, HPV (harbored in the GDV) is physically tethered to mitotic chromosomes as a result of the exposed L2 C-terminus, which contains a DNA binding-site (107-109). Topologically, the L2-viral DNA complex can only be exposed to the nucleoplasm when it penetrates the limiting membrane of the GDV; how this is accomplished is not known. Regardless, transcription and replication of the viral genome is postulated to occur in or surrounding the promyelocytic leukemia protein (PML) nuclear bodies within the nucleus (95).

p120 catenin in HPV infection

In addition to elucidating ER membrane penetration of SV40, this thesis will also clarify the molecular basis by which HPV penetrates the endosomal membrane, a

critical step that properly directs the virus to the Golgi *en route* for successful infection. Although penetration of HPV into the endosomal membrane depends on γ-secretase, how HPV is targeted to γ-secretase in the endosome is unknown. My thesis work will clarify this targeting step.

Using an unbiased immunoprecipitation (IP)-mass spectrometry approach, p120 catenin (ctn) was implicated as a host factor that binds to HPV L2 during infection. p120 is a member of the p120ctn family (110). Members of this family belong to the larger catenins family including alpha and beta catenin, as well as plakoglobin (111). Catenins are well-known for their role in cell-cell adhesion junctions, specifically through their interactions with cadherins (112,113), which are transmembrane receptors that form cell-cell adhesions via their extracellular domains (111). Importantly, p120 is known to interact with γ-secretase (114). In fact, one critical function of p120 is to deliver a transmembrane protein to γ-secretase, enabling γ-secretase to proteolytically cleave the transmembrane protein in order to generate a cleaved product that elicits a defined cellular response (115). This thesis will assess the role of p120 during HPV infection, with the central objective of understanding how p120 might target HPV to γ-secretase so that the virus can initiate membrane penetration – a critical infection step.

In sum, the overarching theme of my thesis is to elucidate the mechanism of membrane penetration by the nonenveloped PyV and HPV. Chapters 2 and 3 will focus on the role of a specific host cytosolic extraction complex that completes the last phase of ER-to-cytosol membrane penetration of SV40, while chapter 4 will examine the action of p120 in targeting HPV to the γ-secretase complex, which in turn promotes endosomal membrane penetration of the virus. I will then conclude this thesis with chapter 5,

bringing into perspective the contributions that I have made, as well as important questions that should be addressed in the future.

Introduction Figures

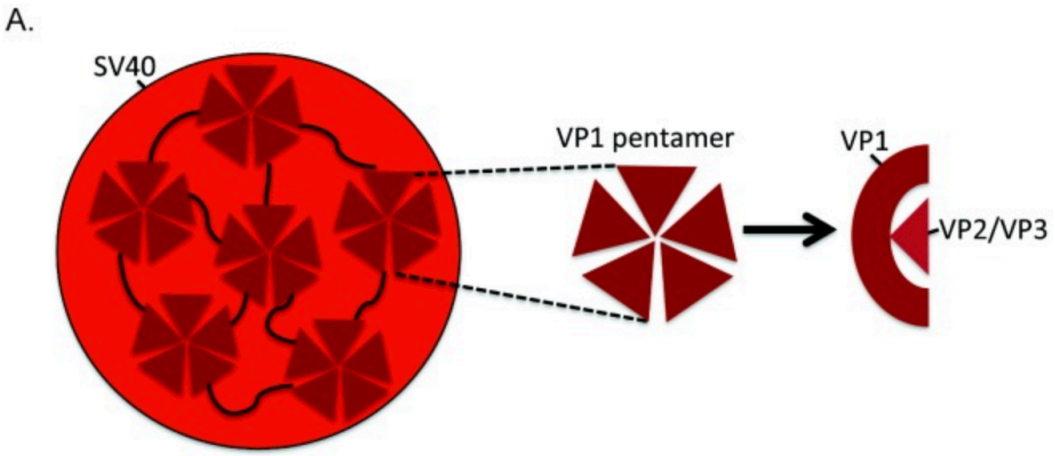

B.

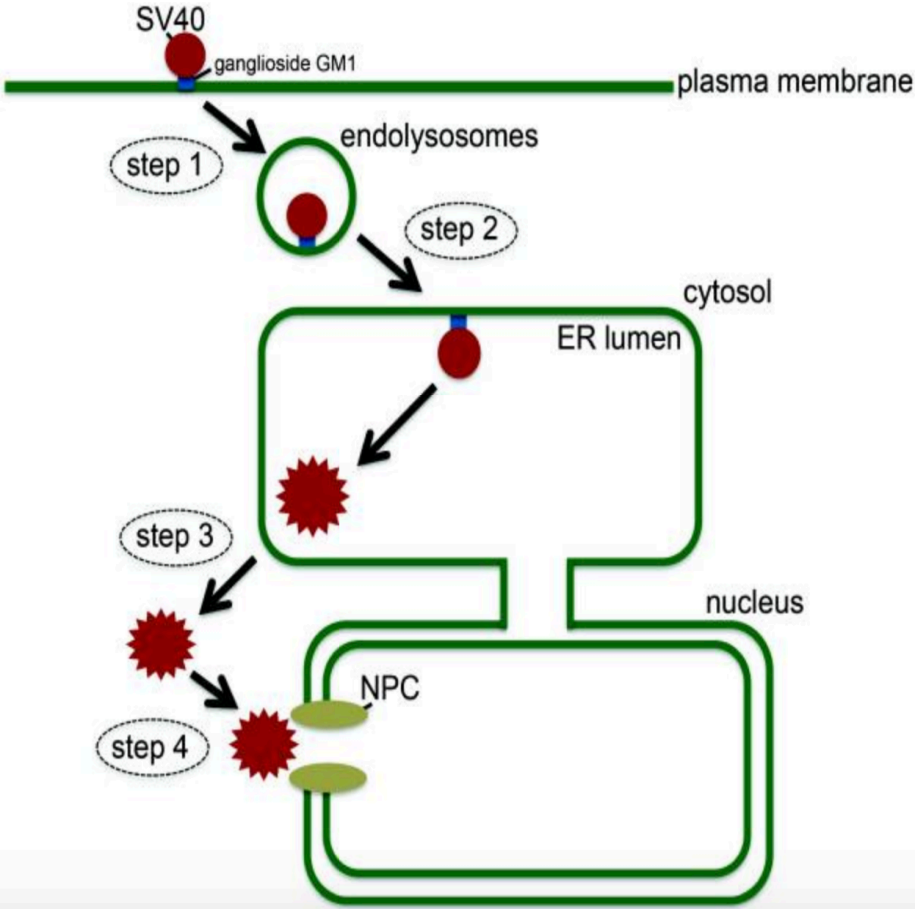
SV40
ganglioside GM1
plasma membrane
endolysosomes
step 1
step 2
cytosol
ER lumen
step 3
nucleus
NPC
step 4

Figure 1-1. Simian virus 40 (SV40) structure and entry pathway.

(A) SV40 consists of 360 VP1 copies arranged as 72 pentamers, which are localized on the viral surface. The pentamers are stabilized by disulfide bonds, as well as by interactions between the VP1 carboxy-terminus, which invades a neighboring pentamer (black curved lines). VP1 also binds to the underlying internal hydrophobic proteins VP2 and VP3.
(B) To infect cells, SV40 interacts with the glycolipid receptor ganglioside GM1 on the plasma membrane, internalizes, and traffics to the endolysosomes (step 1). The virus then targets to the endoplasmic reticulum (ER) using a lipid-sorting mechanism (step 2), from where it crosses the ER membrane to access the cytosol (step 3). Upon entering the cytosol, SV40 mobilizes into the nucleus (step 4), where ensuing transcription and replication of the viral genome causes lytic infection or cellular transformation. NPC: nuclear pore complex.

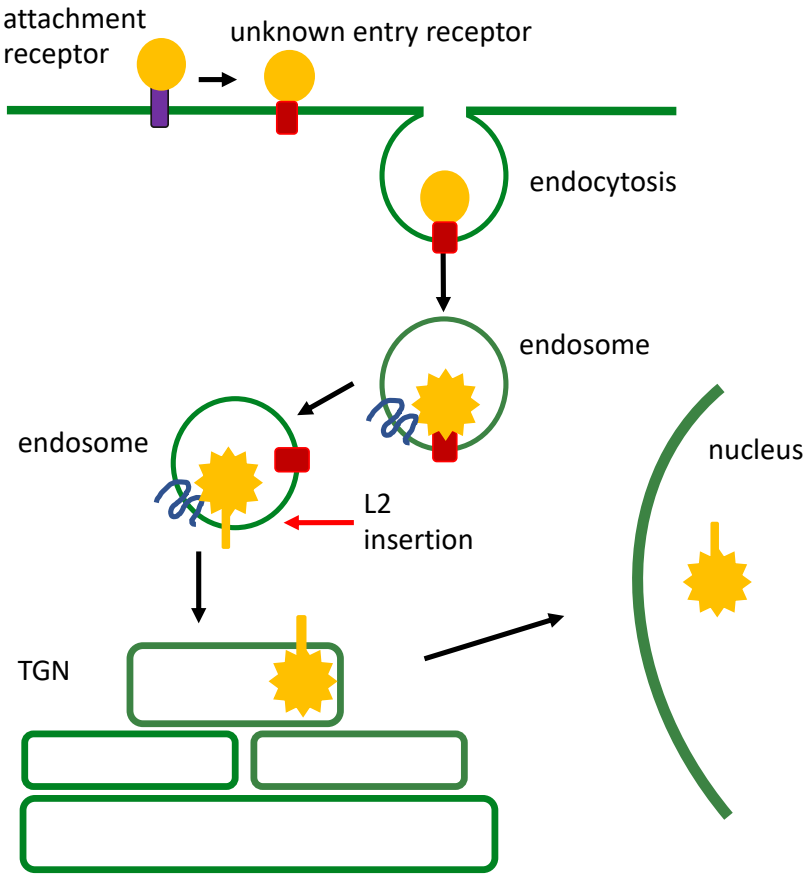
attachment
receptor
unknown entry receptor
endocytosis
endosome
endosome
L2
insertion
nucleus
TGN

Figure 1-2. HPV entry pathway.

To initiate infection, HPV binds HSPG on the plasma membrane. Conformational changes induced by KLK8, cyclophilins, and furin cleavage of L2 induce receptor binding, and promote endocytosis. Once endocytosed, the virus encounters γ-secretase in the endosome, where L2 is inserted into the endosomal membrane. This insertion, and cytosolic exposure of L2 recruits the retromer complex, trafficking the endosomal-L2 complex to the TGN. HPV resides in the TGN until mitosis, during which nuclear envelope breakdown facilitates HPV entry in to the nucleus where viral genome replication occurs.

References:

1) Suomalainen M, Luisoni S, Boucke K, Bianchi S, Engel DA, Greber UF. 2013. A direct and versatile assay measuring membrane penetration of adenovirus in single cells. J Virol 87:12367-12379.

2) Strauss M, Filman DJ, Belnap DM, Cheng N, Noel RT, Hogle JM. 2015. Nectin-like interactions between poliovirus and its receptor trigger conformational changes associated with cell entry. J Virol 89:4143-4157.

3) Gardner, S.D.; Field, A.M.; Coleman, D.V.; Hulme, B. New human papovavirus (B.K.) isolated from urine after renal transplantation. Lancet 1971, 1, 1253–1257.

4) Padgett, B.L.; Walker, D.L.; ZuRhein, G.M.; Eckroade, R.J.; Dessel, B.H. Cultivation of papova-like virus from human brain with progressive multifocal leucoencephalopathy. Lancet 1971, 1, 1257–1260.

5) Moens, U.; Johannessen, M. Human polyomaviruses and cancer: Expanding repertoire. J. Dtsch. Dermatol. Ges. 2008, 6, 704–708.

6) White, M.K.; Gordon, J.; Khalili, K. The rapidly expanding family of human polyomaviruses: Recent developments in understanding their life cycle and role in human pathology PLoS Pathog. 2013, 9, e1003206.

7) DeCaprio, J.A.; Garcea, R.L. A cornucopia of human polyomaviruses. Nat. Rev. Microbiol. 2013, 11, 264–276.

8) Arora, R.; Chang, Y.; Moore, P.S. MCV and Merkel cell carcinoma: A molecular success story. Curr. Opin. Virol. 2012, 2, 489–498.

9) Kean, J.M.; Rao, S.; Wang, M.; Garcea, R.L. Seroepidemiology of human polyomaviruses. PLoS Pathog. 2009,5, e1000363.

10) Bennett, S.M.; Broekema, N.M.; Imperiale, M.J. BK polyomavirus: Emerging pathogen. Microbes Infect. 2012,14, 672–683.

11) Dalianis, T.; Hirsch, H.H. Human polyomaviruses in disease and cancer. Virology 2013, 437, 63–72.

12) Maginnis, M.S.; Nelson, C.D.; Atwood, W.J. JC polyomavirus attachment, entry, and trafficking: Unlocking the keys to a fatal infection. J. Neurovirol. 2015, 21, 601–613.

13) Daniels, R.; Sadowicz, D.; Hebert, D.N. A very late viral protein triggers the lytic release of SV40. PLoS Pathog. 2007, 3, e98.

14) Liddington, R.C.; Yan, Y.; Moulai, J.; Sahli, R.; Benjamin, T.L.; Harrison, S.C. Structure of simian virus 40 at 3.8-A resolution. Nature 1991, 354, 278–284.

15) Stehle, T.; Gamblin, S.J.; Yan, Y.; Harrison, S.C. The structure of simian virus 40 refined at 3.1 A resolution. Structure 1996, 4, 165–182.

16) Chen, X.S.; Stehle, T.; Harrison, S.C. Interaction of polyomavirus internal protein VP2 with the major capsid protein VP1 and implications for participation of VP2 in viral entry. EMBO J. 1998, 17, 3233–3240.

17) Tsai, B.; Gilbert, J.M.; Stehle, T.; Lencer, W.; Benjamin, T.L.; Rapoport, T.A. Gangliosides are receptors for murine polyoma virus and SV40. EMBO J. 2003, 22, 4346–4355.

18) Campanero-Rhodes, M.A.; Smith, A.; Chai, W.; Sonnino, S.; Mauri, L.; Childs, R.A.; Zhang, Y.; Ewers, H.;Helenius, A.; Imberty, A.; et al. N-glycolyl GM1 ganglioside as a receptor for simian virus 40. J. Virol. 2007, 81, 12846–12858.

19) Ewers, H.; Romer, W.; Smith, A.E.; Bacia, K.; Dmitrieff, S.; Chai, W.; Mancini, R.; Kartenbeck, J.; Chambon, V.;Berland, L.; et al. GM1 structure determines SV40-induced membrane invagination and infection.Nat. Cell Biol. 2010, 12, 11–18.

20) Engel, S.; Heger, T.; Mancini, R.; Herzog, F.; Kartenbeck, J.; Hayer, A.; Helenius, A. Role of endosomes in simian virus 40 entry and infection. J. Virol. 2011, 85, 4198-4211.

21)Kartenbeck, J.; Stukenbrok, H.; Helenius, A. Endocytosis of simian virus 40 into the endoplasmic reticulum. J. Cell Biol. 1989, 109, 2721–2729.

22)Qian, M.; Cai, D.; Verhey, K.J.; Tsai, B. A lipid receptor sorts polyomavirus from the endolysosome to the endoplasmic reticulum to cause infection. PLoS Pathog. 2009, 5, e1000465.

23)Nakanishi, A.; Clever, J.; Yamada, M.; Li, P.P.; Kasamatsu, H. Association with capsid proteins promotes nuclear targeting of simian virus 40 DNA. Proc. Natl. Acad. Sci. USA 1996, 93, 96–100.

24)Clever, J.; Yamada, M.; Kasamatsu, H. Import of simian virus 40 virions through nuclear pore complexes. Proc. Natl. Acad. Sci. USA 1991, 88, 7333–7337

25)Ravindran, M.S.; Bagchi, P.; Cunningham, C.N.; Tsai, B. Opportunistic intruders: How viruses orchestrate ER functions to infect cells. Nat. Rev. Microbiol. 2016, 14, 407–420.

26) Brodsky, J.L. Cleaning up: ER-associated degradation to the rescue. Cell 2012, 151, 1163–1167.

27) Schelhaas, M.; Malmstrom, J.; Pelkmans, L.; Haugstetter, J.; Ellgaard, L.; Grunewald, K.; Helenius, A. Simian Virus 40 depends on ER protein folding and quality control factors for entry into host cells. Cell 2007, 131, 516–529.

28) Walczak, C.P.; Tsai, B. A PDI family network acts distinctly and coordinately with ERp29 to facilitate polyomavirus infection. J. Virol. 2011, 85, 2386–2396.

29) Inoue, T.; Dosey, A.; Herbstman, J.F.; Ravindran, M.S.; Skiniotis, G.; Tsai, B. ERdj5 Reductase Cooperates with Protein Disulfide Isomerase To Promote Simian Virus 40 Endoplasmic Reticulum Membrane Translocation. J. Virol. 2015, 89, 8897–8908.

30) Magnuson, B.; Rainey, E.K.; Benjamin, T.; Baryshev, M.; Mkrtchian, S.; Tsai, B. ERp29 triggers a conformational change in polyomavirus to stimulate membrane binding. Mol. Cell 2005, 20, 289–300.

31) Rainey-Barger, E.K.; Mkrtchian, S.; Tsai, B. The C-terminal domain of ERp29 mediates polyomavirus binding, unfolding, and infection. J. Virol. 2009, 83, 1483–1491.

32) Gilbert, J.; Ou, W.; Silver, J.; Benjamin, T. Downregulation of protein disulfide isomerase inhibits infection by the mouse polyomavirus. J. Virol. 2006, 80, 10868–10870.

33) Daniels, R.; Rusan, N.M.; Wadsworth, P.; Hebert, D.N. SV40 VP2 and VP3 insertion into ER membranes is controlled by the capsid protein VP1: Implications for DNA translocation out of the ER. Mol. Cell 2006, 24, 955–966.

34) Kuksin, D.; Norkin, L.C. Disassembly of simian virus 40 during passage through the endoplasmic reticulum and in the cytoplasm. J. Virol. 2012, 86, 1555–1562.

35) Nelson, C.D.; Derdowski, A.; Maginnis, M.S.; O'Hara, B.A.; Atwood, W.J. The VP1 subunit of JC polyomavirus recapitulates early events in viral trafficking and is a novel tool to study polyomavirus entry. Virology 2012, 428, 30–40.

36) Geiger, R.; Andritschke, D.; Friebe, S.; Herzog, F.; Luisoni, S.; Heger, T.; Helenius, A. BAP31 and BiP are essential for dislocation of SV40 from the endoplasmic reticulum to the cytosol. Nat. Cell Biol. 2011, 13,1305–1314.

37) Goodwin, E.C.; Lipovsky, A.; Inoue, T.; Magaldi, T.G.; Edwards, A.P.; Van Goor, K.E.; Paton, A.W.; Paton, J.C.; Atwood, W.J.; Tsai, B.; et al. BiP and multiple DNAJ molecular chaperones in the endoplasmic reticulum are required for efficient simian virus 40 infection. MBio 2011, 2, e00101–e00111.

38) Nishikawa, S.I.; Fewell, S.W.; Kato, Y.; Brodsky, J.L.; Endo, T. Molecular chaperones in the yeast endoplasmic reticulum maintain the solubility of proteins for retrotranslocation and degradation. J. Cell Biol. 2001, 153, 1061–1070.

39) Kampinga, H.H.; Craig, E.A. The HSP70 chaperone machinery: J proteins as drivers of functional specificity. Nat. Rev. Mol. Cell Biol. 2010, 11, 579–592.

40) Inoue, T.; Tsai, B. A nucleotide exchange factor promotes endoplasmic reticulum-to-cytosol membrane penetration of the nonenveloped virus simian virus 40. J. Virol. 2015, 89, 4069–4079.

41) Inoue, T.; Tsai, B. The Grp170 nucleotide exchange factor executes a key role during ERAD of cellular misfolded clients. Mol. Biol. Cell 2016, 27, 1650–1662.

42) Lilley, B.N.; Gilbert, J.M.; Ploegh, H.L.; Benjamin, T.L. Murine polyomavirus requires the endoplasmic reticulum protein Derlin-2 to initiate infection. J. Virol. 2006, 80, 8739–8744.

43) Jiang, M.; Abend, J.R.; Tsai, B.; Imperiale, M.J. Early events during BK virus entry and disassembly. J. Virol.2009, 83, 1350–1358.

44) Yamamoto, Y.H.; Kimura, T.; Momohara, S.; Takeuchi, M.; Tani, T.; Kimata, Y.; Kadokura, H.; Kohno, K. A novel ER J-protein DNAJB12 accelerates ER-associated degradation of membrane proteins including CFTR. Cell Struct. Funct. 2010, 35, 107–116.

45) Grove, D.E.; Fan, C.Y.; Ren, H.Y.; Cyr, D.M. The endoplasmic reticulum-associated Hsp40 DNAJB12 and Hsc70 cooperate to facilitate RMA1 E3-dependent degradation of nascent CFTRDeltaF508. Mol. Biol. Cell 2011, 22, 301–314.

46) Sopha, P.; Kadokura, H.; Yamamoto, Y.H.; Takeuchi, M.; Saito, M.; Tsuru, A.; Kohno, K. A novel mammalian ER-located J-protein, DNAJB14, can accelerate ERAD of misfolded membrane proteins. Cell Struct. Funct. 2012, 37, 177–187.

47) Walczak, C.P.; Ravindran, M.S.; Inoue, T.; Tsai, B. A cytosolic chaperone complexes with dynamic membrane J-proteins and mobilizes a nonenveloped virus out of the endoplasmic reticulum. PLoS Pathog. 2014, 10, e1004007.

48) Bagchi, P.; Walczak, C.P.; Tsai, B. The endoplasmic reticulum membrane J protein C18 executes a distinct role in promoting simian virus 40 membrane penetration. J. Virol. 2015, 89, 4058–4068.

49) Shibata, Y.; Voeltz, G.K.; Rapoport, T.A. Rough sheets and smooth tubules. Cell 2006, 126, 435–439.

50) Ravindran, M.S.; Bagchi, P.; Inoue, T.; Tsai, B. A Non-enveloped Virus Hijacks Host Disaggregation Machinery to Translocate across the Endoplasmic Reticulum Membrane. PLoS Pathog. 2015, 11, e1005086.

51) Ravindran, MS.; Engelke MF.; Verhey, KJ.; Tsai, B. Exploiting the kinesin-1 molecular motor to generate a virus membrane penetration site. Nat Commun. 2017, 8, 15496.

52) Inoue, T.; Tsai, B. A large and intact viral particle penetrates the endoplasmic reticulum membrane to reach the cytosol. PLoS Pathog. 2011, 7, e1002037.

53) Ye, Y.; Meyer, H.H.; Rapoport, T.A. The AAA ATPase Cdc48/p97 and its partners transport proteins from the ER into the cytosol. Nature 2001, 414, 652–656.

54) Dupzyk, A.; Williams, JM.; Bagchi, P.; Inoue, T.; Tsai, B. 2017. SGTA-Dependent Regulation of Hsc70 Promotes Cytosol Entry of Simian Virus 40 from the Endoplasmic Reticulum. J Virol 91.

55) Dupzyk, A.; Tsai, B. 2018. Bag2 Is a Component of a Cytosolic Extraction Machinery That Promotes Membrane Penetration of a Nonenveloped Virus. J Virol 92.

56) Polier, S.; Dragovic, Z.; Hartl, F.U.; Bracher, A. Structural basis for the cooperation of Hsp70 and Hsp110 chaperones in protein folding. Cell 2008, 133, 1068–1079.

57) Mattoo, R.U.; Sharma, S.K.; Priya, S.; Finka, A.; Goloubinoff, P. Hsp110 is a bona fide chaperone using ATP to unfold stable misfolded polypeptides and reciprocally collaborate with Hsp70 to solubilize protein aggregates. J. Biol. Chem. 2013, 288, 21399–21411.

58) Bracher, A.; Verghese, J. GrpE, Hsp110/Grp170, HspBP1/Sil1 and BAG domain proteins: Nucleotide exchange factors for Hsp70 molecular chaperones. Subcell Biochem. 2015, 78:1-33.

59) Xu Z, Page RC, Gomes MM, Kohli E, Nix JC, Herr AB, Patterson C, Misra S. 2008. Structural basis of nucleotide exchange and client binding by the Hsp70 cochaperone Bag2. Nat Struct Mol Biol 15:1309-1317.

60) Angeletti, P.C.; Walker, D.; Panganiban, A.T. Small glutamine-rich protein/viral protein U-binding protein is a novel cochaperone that affects heat shock protein 70 activity. Cell Stress Chaperones 2002, 7, 258–268.

61) Philp, L.K.; Butler, M.S.; Hickey, T.E.; Butler, L.M.; Tilley, W.D.; Day, T.K. SGTA: A new player in the molecular co-chaperone game. Horm. Cancer 2013, 4, 343–357.

62) Chartron, J.W.; Clemons, W.M., Jr.; Suloway, C.J. The complex process of GETting tail-anchored membrane proteins to the ER. Curr. Opin. Struct. Biol. 2012, 22, 217–224.

63) Denic, V.; Dotsch, V.; Sinning, I. Endoplasmic reticulum targeting and insertion of tail-anchored membrane proteins by the GET pathway. Cold Spring Harb. Perspect. Biol. 2013, 5, a013334.

64) Wang, Q.; Liu, Y.; Soetandyo, N.; Baek, K.; Hegde, R.; Ye, Y. A ubiquitin ligase-associated chaperone holdase maintains polypeptides in soluble states for proteasome degradation. Mol. Cell 2011, 42, 758–770.

65) Xu, Y.; Cai, M.; Yang, Y.; Huang, L.; Ye, Y. SGTA recognizes a noncanonical ubiquitin-like domain in the Bag6-Ubl4A-Trc35 complex to promote endoplasmic reticulum-associated degradation. Cell Rep. 2012, 2, 1633–1644.

66) Hrizo, S.L.; Gusarova, V.; Habiel, D.M.; Goeckeler, J.L.; Fisher, E.A.; Brodsky, J.L. The Hsp110 molecular chaperone stabilizes apolipoprotein B from endoplasmic reticulum-associated degradation (ERAD). J. Biol. Chem. 2007, 282, 32665–32675.

67) McBride AA. 2017. Oncogenic human papillomaviruses. Philos Trans R Soc Lond B Biol Sci 372.

68) Forman D, de Martel C, Lacey CJ, Soerjomataram I, Lortet-Tieulent J, Bruni L, Vignat J, Ferlay J, Bray F, Plummer M, Franceschi S. 2012. Global burden of human papillomavirus and related diseases. Vaccine 30 Suppl 5:F12-23.

69) Hildesheim A, Herrero R, Wacholder S, Rodriguez AC, Solomon D, Bratti MC, Schiller JT, Gonzalez P, Dubin G, Porras C, Jimenez SE, Lowy DR, Costa Rican HPVVTG. 2007. Effect of human papillomavirus 16/18 L1 viruslike particle vaccine among young women with preexisting infection: a randomized trial. JAMA 298:743-753.

70) Lee LY, Garland SM. 2017. Human papillomavirus vaccination: the population impact. F1000Res 6:866.

71) Schelhaas M, Shah B, Holzer M, Blattmann P, Kuhling L, Day PM, Schiller JT, Helenius A. 2012. Entry of human papillomavirus type 16 by actin-dependent, clathrin- and lipid raft-independent endocytosis. PLoS Pathog 8:e1002657.

72) Buck CB, Cheng N, Thompson CD, Lowy DR, Steven AC, Schiller JT, Trus BL. 2008. Arrangement of L2 within the papillomavirus capsid. J Virol 82:5190-5197.

73) Mallon RG, Wojciechowicz D, Defendi V. 1987. DNA-binding activity of papillomavirus proteins. J Virol 61:1655-1660.

74) Doorbar J. 2005. The papillomavirus life cycle. J Clin Virol 32 Suppl 1:S7-15.

75) Zhang P, Nouri M, Brandsma JL, Iftner T, Steinberg BM. 1999. Induction of E6/E7 expression in cottontail rabbit papillomavirus latency following UV activation. Virology 263:388-394.

76) Roberts JN, Buck CB, Thompson CD, Kines R, Bernardo M, Choyke PL, Lowy DR, Schiller JT. 2007. Genital transmission of HPV in a mouse model is potentiated by nonoxynol-9 and inhibited by carrageenan. Nat Med 13:857-861.

77) McBride AA. 2008. Replication and partitioning of papillomavirus genomes. Adv Virus Res 72:155-205.

78) Volpers C, Unckell F, Schirmacher P, Streeck RE, Sapp M. 1995. Binding and internalization of human papillomavirus type 33 virus-like particles by eukaryotic cells. J Virol 69:3258-3264.

79) Joyce JG, Tung JS, Przysiecki CT, Cook JC, Lehman ED, Sands JA, Jansen KU, Keller PM. 1999. The L1 major capsid protein of human papillomavirus type 11 recombinant virus-like particles interacts with heparin and cell-surface glycosaminoglycans on human keratinocytes. J Biol Chem 274:5810-5822.

80) Giroglou T, Florin L, Schafer F, Streeck RE, Sapp M. 2001. Human papillomavirus infection requires cell surface heparan sulfate. J Virol 75:1565-1570.

81) Johnson KM, Kines RC, Roberts JN, Lowy DR, Schiller JT, Day PM. 2009. Role of heparan sulfate in attachment to and infection of the murine female genital tract by human papillomavirus. J Virol 83:2067-2074.

82) Cerqueira C, Liu Y, Kuhling L, Chai W, Hafezi W, van Kuppevelt TH, Kuhn JE, Feizi T, Schelhaas M. 2013. Heparin increases the infectivity of Human Papillomavirus type 16 independent of cell surface proteoglycans and induces L1 epitope exposure. Cell Microbiol 15:1818-1836.

83) Cerqueira C, Samperio Ventayol P, Vogeley C, Schelhaas M. 2015. Kallikrein-8 Proteolytically Processes Human Papillomaviruses in the Extracellular Space To Facilitate Entry into Host Cells. J Virol 89:7038-7052.

84) Hanoulle X, Melchior A, Sibille N, Parent B, Denys A, Wieruszeski JM, Horvath D, Allain F, Lippens G, Landrieu I. 2007. Structural and functional characterization of the interaction between cyclophilin B and a heparin-derived oligosaccharide. J Biol Chem 282:34148-34158.

85) Bienkowska-Haba M, Patel HD, Sapp M. 2009. Target cell cyclophilins facilitate human papillomavirus type 16 infection. PLoS Pathog 5:e1000524.

86) Selinka HC, Giroglou T, Nowak T, Christensen ND, Sapp M. 2003. Further evidence that papillomavirus capsids exist in two distinct conformations. J Virol 77:12961-12967.

87) Richards RM, Lowy DR, Schiller JT, Day PM. 2006. Cleavage of the papillomavirus minor capsid protein, L2, at a furin consensus site is necessary for infection. Proc Natl Acad Sci U S A 103:1522-1527.

88) Selinka HC, Florin L, Patel HD, Freitag K, Schmidtke M, Makarov VA, Sapp M. 2007. Inhibition of transfer to secondary receptors by heparan sulfate-binding drug or antibody induces noninfectious uptake of human papillomavirus. J Virol 81:10970-10980.

89) Day PM, Lowy DR, Schiller JT. 2008. Heparan sulfate-independent cell binding and infection with furin-precleaved papillomavirus capsids. J Virol 82:12565-12568.

90) Becker M, Greune L, Schmidt MA, Schelhaas M. 2018. Extracellular conformational changes in the capsid of human papillomaviruses contribute to asynchronous uptake into host cells. J Virol doi:10.1128/JVI.02106-17.

91) Day PM, Lowy DR, Schiller JT. 2003. Papillomaviruses infect cells via a clathrin-dependent pathway. Virology 307:1-11.

92) Smith JL, Campos SK, Wandinger-Ness A, Ozbun MA. 2008. Caveolin-1-dependent infectious entry of human papillomavirus type 31 in human keratinocytes proceeds to the endosomal pathway for pH-dependent uncoating. J Virol 82:9505-9512.

93) Bienkowska-Haba M, Williams C, Kim SM, Garcea RL, Sapp M. 2012. Cyclophilins facilitate dissociation of the human papillomavirus type 16 capsid protein L1 from the L2/DNA complex following virus entry. J Virol 86:9875-9887.

94) DiGiuseppe S, Bienkowska-Haba M, Guion LGM, Keiffer TR, Sapp M. 2017. Human papillomavirus major capsid protein L1 remains associated with the incoming viral genome throughout the entry process. J Virol doi:10.1128/JVI.00537-17.

95) Day PM, Baker CC, Lowy DR, Schiller JT. 2004. Establishment of papillomavirus infection is enhanced by promyelocytic leukemia protein (PML) expression. Proc Natl Acad Sci U S A 101:14252-14257.

96) Huang HS, Buck CB, Lambert PF. 2010. Inhibition of gamma secretase blocks HPV infection. Virology 407:391-396.

97) Karanam B, Peng S, Li T, Buck C, Day PM, Roden RB. 2010. Papillomavirus infection requires gamma secretase. J Virol 84:10661-10670.

98) Zhang W, Kazakov T, Popa A, DiMaio D. 2014. Vesicular trafficking of incoming human papillomavirus 16 to the Golgi apparatus and endoplasmic reticulum requires gamma-secretase activity. MBio 5:e01777-01714.

99) Inoue T, Zhang P, Zhang W, Goodner-Bingham K, Dupzyk A, DiMaio D, Tsai B. 2018. gamma-Secretase promotes membrane insertion of the human papillomavirus L2 capsid protein during virus infection. J Cell Biol 217:3545-3559.

100) Bronnimann MP, Chapman JA, Park CK, Campos SK. 2013. A transmembrane domain and GxxxG motifs within L2 are essential for papillomavirus infection. J Virol 87:464-473.

101) Day PM, Thompson CD, Schowalter RM, Lowy DR, Schiller JT. 2013. Identification of a role for the trans-Golgi network in human papillomavirus 16 pseudovirus infection. J Virol 87:3862-3870.

102) Lipovsky A, Popa A, Pimienta G, Wyler M, Bhan A, Kuruvilla L, Guie MA, Poffenberger AC, Nelson CD, Atwood WJ, DiMaio D. 2013. Genome-wide siRNA screen identifies the retromer as a cellular entry factor for human papillomavirus. Proc Natl Acad Sci U S A 110:7452-7457.

103) Popa A, Zhang W, Harrison MS, Goodner K, Kazakov T, Goodwin EC, Lipovsky A, Burd CG, DiMaio D. 2015. Direct binding of retromer to human papillomavirus type 16 minor capsid protein L2 mediates endosome exit during viral infection. PLoS Pathog 11:e1004699

104) DiGiuseppe S, Bienkowska-Haba M, Hilbig L, Sapp M. 2014. The nuclear retention signal of HPV16 L2 protein is essential for incoming viral genome to transverse the trans-Golgi network. Virology 458-459:93-105.

105) Pyeon D, Pearce SM, Lank SM, Ahlquist P, Lambert PF. 2009. Establishment of human papillomavirus infection requires cell cycle progression. PLoS Pathog 5:e1000318.

106) Aydin I, Weber S, Snijder B, Samperio Ventayol P, Kuhbacher A, Becker M, Day PM, Schiller JT, Kann M, Pelkmans L, Helenius A, Schelhaas M. 2014. Large scale RNAi reveals the requirement of nuclear envelope breakdown for nuclear import of human papillomaviruses. PLoS Pathog 10:e1004162.

107) DiGiuseppe S, Luszczek W, Keiffer TR, Bienkowska-Haba M, Guion LG, Sapp MJ. 2016. Incoming human papillomavirus type 16 genome resides in a vesicular compartment throughout mitosis. Proc Natl Acad Sci U S A 113:6289-6294.

108) Aydin I, Villalonga-Planells R, Greune L, Bronnimann MP, Calton CM, Becker M, Lai KY, Campos SK, Schmidt MA, Schelhaas M. 2017. A central region in the minor capsid protein of papillomaviruses facilitates viral genome tethering and membrane penetration for mitotic nuclear entry. PLoS Pathog 13:e1006308.

109) Calton CM, Bronnimann MP, Manson AR, Li S, Chapman JA, Suarez-Berumen M, Williamson TR, Molugu SK, Bernal RA, Campos SK. 2017. Translocation of the papillomavirus L2/vDNA complex across the limiting membrane requires the onset of mitosis. PLoS Pathog 13:e1006200.

110) Yuan L, Arikkath J. 2017. Functional roles of p120ctn family of proteins in central neurons. Semin Cell Dev Biol 69:70-82.

111) Anastasiadis PZ, Reynolds AB. 2000. The p120 catenin family: complex roles in adhesion, signaling and cancer. J Cell Sci 113 (Pt 8):1319-1334.

112) Reynolds AB, Herbert L, Cleveland JL, Berg ST, Gaut JR. 1992. p120, a novel substrate of protein tyrosine kinase receptors and of p60v-src, is related to cadherin-binding factors beta-catenin, plakoglobin and armadillo. Oncogene 7:2439-2445.

113) Reynolds AB, Daniel J, McCrea PD, Wheelock MJ, Wu J, Zhang Z. 1994. Identification of a new catenin: the tyrosine kinase substrate p120cas associates with E-cadherin complexes. Mol Cell Biol 14:8333-8342.

114) Kiss A, Troyanovsky RB, Troyanovsky SM. 2008. p120-catenin is a key component of the cadherin-gamma-secretase supercomplex. Mol Biol Cell 19:4042-4050.

115) Kouchi Z, Barthet G, Serban G, Georgakopoulos A, Shioi J, Robakis NK. 2009. p120 catenin recruits cadherins to gamma-secretase and inhibits production of Abeta peptide. J Biol Chem 284:1954-1961.

Chapter 2: SGTA-Dependent Regulation of Hsc70 Promotes Cytosol Entry of Simian Virus 40 from the Endoplasmic Reticulum

INTRODUCTION

The molecular basis by which nonenveloped viruses penetrate biological membranes to gain entry into the host cytosol and cause infection remains mysterious (1). For enveloped viruses, fusion between the viral and a host membrane enables the core viral particle to reach the cytosol (2). However, since nonenveloped viruses lack a surrounding lipid bilayer, their membrane transport mechanisms are likely distinct from those of enveloped viruses. Although the precise molecular mechanism remains unclear, a general principle describing nonenveloped membrane translocation has nonetheless emerged. Upon trafficking to the site of membrane penetration, host cues, including cellular proteases, chaperones, reductases, and low pH, act on the viral particle to impart conformational changes. As a consequence, the conformationally altered virus becomes hydrophobic, enabling it to engage and disrupt the limiting membrane. Alternatively, the structural change may release a lytic peptide previously hidden in the native virus, which in turn integrates into and impairs the integrity of the membrane. Regardless of the mechanism, these reactions prime the viral (or subviral) particle for transfer across the host membrane. An outstanding question is whether cytosolic components are recruited to “pull” the virus into the cytosol to complete the membrane penetration process.

In the case of the nonenveloped polyomavirus simian virus 40 (SV40), penetration across the endoplasmic reticulum (ER) membrane to reach the cytosol represents the decisive infection step. Structurally, SV40 is composed of 72 pentamers of the coat protein VP1, with each pentamer harboring either the underlying internal hydrophobic protein VP2 or VP3 (3-6). These pentamers in turn encapsulate the viral DNA genome. VP1 C-terminal arms emanating from a pentamer invade adjacent pentamers and stabilize the overall viral architecture through a network of disulfide bonds and noncovalent interactions (3,4). To infect cells, SV40 binds to the ganglioside GM1 receptor on the host plasma membrane (7-10). After receptor-mediated endocytosis, the virus traffics to the endolysosomes (11,12) before being sorted to the ER (11-13). Here, SV40 penetrates the ER membrane to gain entry into the cytosol (14) and is further transported into the nucleus (15), where ensuing transcription and replication of the viral genome lead to lytic infection or cellular transformation. Although ER-to-cytosol membrane transport of SV40 remains enigmatic, aspects of this step are slowly being revealed.

In the ER, redox enzymes reduce and isomerize the SV40 disulfide bonds (16-18), while molecular chaperones locally unfold the VP1 C-terminal arms (17,19,20) to expose the internal proteins VP2 and VP3 (21,22). These events generate a hydrophobic virus that integrates into the ER membrane. To clarify how membrane-embedded SV40 is ejected into the cytosol, we previously identified a cytosolic chaperone complex comprised of Hsc70, Hsp105, and SGTA that is tethered to the ER membrane by association with the membrane J-protein B14 (23-35). A J-protein typically stimulates Hsc70 (and Hsp70) chaperones to capture a substrate (26). In the

context of the Hsc70-Hsp105-SGTA protein complex, our analyses further unveiled important roles of Hsp105 and SGTA in extracting SV40 from the ER and transporting the virus to the cytosol (24, 25). Although our previous results also suggested that Hsc70 may be involved in this step (24,25), direct evidence demonstrating Hsc70's participation in the viral extraction step is lacking. Moreover, how Hsc70 might act in concert with Hsp105 or SGTA is also unclear.

Using cell-based approaches, our study demonstrates that Hsc70 executes a key role in promoting cytosol entry of SV40 from the ER in a step that is regulated by SGTA. While SGTA's ability to interact with Hsc70 via its central tetratricopeptide repeat (TPR) domain is important during SV40's ER-to-cytosol transport, SGTA's N-terminal domain, which normally mediates homodimerization and recruits various cellular adapters, is not essential in this step. Instead, this domain appears to play an unanticipated post-ER membrane transport role during viral infection. Our results thus further illuminate the mechanistic basis by which a nonenveloped virus penetrates a host membrane.

MATERIALS AND METHODS

Antibodies

Monoclonal SV40 large T antigen, Hsp90, and Hsp105 antibodies were purchased from Santa Cruz Biotechnology (Santa Cruz, CA). Monoclonal VP1 antibody was provided by Walter Scott (University of Miami). Anti S-tag and anti-PDI (RL90) antibodies were purchased from Abcam (Cambridge, MA). DNAJB14 and SGTA antibodies were purchased from Proteintech Group (Chicago, IL). Monoclonal BAP31 and Hsc70 antibodies were purchased from Pierce (Rockford, IL), and anti-FLAG antibody was

purchased from Sigma (St. Louis, MO). Anti-UBL4A antibody was kindly provided by the Protein Folding Disease Initiative at the University of Michigan and was purchased from Proteintech Group (Chicago, IL). Hsp27 antibody was purchased from Stressgen (San Diego, CA). Actin antibody was purchased from Cell Signaling (Danvers, MA). Polyclonal CTA antibody was produced against denatured CTA purchased from EMD Biosciences (San Diego, CA).

Reagents

FLAG M2 antibody-conjugated agarose beads, Triton X-100, and *N*-ethylmaleimide (NEM) were purchased from Sigma-Aldrich (St. Louis, MO). S-protein-conjugated beads were purchased from EMD Millipore Chemicals (San Diego, CA). Digitonin was purchased from EMD Millipore Chemicals (San Diego, CA). Opti-MEM and 0.25% trypsin were purchased from Invitrogen (Carlsbad, CA). DTT, dithiobis succinimidyl propionate (DSP), and phenylmethylsulfonyl fluoride (PMSF) were purchased from Sigma. The mounting reagent was Life Technologies ProLong Diamond antifade mountant with DAPI (4′,6′-diamidino-2-phenylindole) from Thermo Fisher (Carlsbad, CA).

Cells

CV-1, COS-7, and HEK293T cells (ATCC) were cultured in complete Dulbecco's modified Eagle medium (cDMEM) containing 10% fetal bovine serum, 10 U/ml penicillin, and 10 µg/ml streptomycin from Gibco (Grand Island, NY).

DNA plasmids and siRNA transfection

The siRNAs used were as follows: Hsc70 siRNA 1 (j-017609-02; Dharmacon), Hsc70 siRNA 2 (5′-GACCUUCACUACCUAUUCU-3′; Dharmacon), SGTA siRNA 1 (5′-

CAGCCUACAGCAAACUCGGCAACUA-3′; Invitrogen), SGTA siRNA 2 (5′-CCAACCUCAAGAUAGCGGAGCUGAA-3′; Invitrogen), and scrambled control (all-star negative; Qiagen). WT SGTA-Myc/FLAG-containing plasmid was purchased from Origene (Rockville, MD). The amino acid positions defining the boundaries of SGTA's N- and Hsc70-binding TPR domains were defined based on UniProt. The ΔN SGTA construct was generated by deleting residues 1 to 90, the D3 mutant was created by using point mutagenesis that targets L15, A35, and L39, and the K160E/R164E mutant was generated using point mutagenesis targeting residues K160 and R164, as reported previously (24). All SGTA mutants contain a pcDNA3.1(−) vector backbone and harbor a C-terminal Myc/FLAG tag. In addition, all siRNA and DNA transfections were incubated for a minimum of 24 h.

Preparation of SV40

WT SV40 was prepared as described previously (14) using an OptiPrep gradient system (Sigma).

Semipermeabilized, ER-to-cytosol membrane transport assay

This assay has been previously described by Inoue and Tsai (14). Briefly, SV40-infected CV-1 cells were trypsinized, washed in phosphate-buffered saline (PBS), and pelleted. The cell pellet was semipermeabilized in 0.1% digitonin in a physiological buffer (50 mM HEPES [pH 7.4], 150 mM NaCl, and PMSF). For infected COS-7 cells, 0.025% digitonin was used. The cells were then centrifuged at 4°C at 16,000 × *g* to generate two fractions: a supernatant fraction that represents the cytosol fraction and a pellet fraction that represents the membrane fraction. Samples were subjected to either reducing (in the case of CV-1-infected cells) or nonreducing (in the case of COS-7-

infected cells) SDS-PAGE. To isolate ER-localized SV40, the membrane fraction was further lysed in a physiological buffer containing 1% Triton X-100. The extracted material represents the ER-localized fraction.

SV40 infection

Monitoring of SV40 large T antigen expression in the host nucleus has been previously described by Ravindran et al. (25). All images provided were taken with an inverted epifluorescence microscope (Eclipse TE2000-E; Nikon, Melville, NY). A standard 40× lens objective was used, along with blue (DAPI), fluorescein isothiocyanate (green), and TRITC (tetramethyl rhodamine isothiocyanate; red) filter cubes. Images were analyzed using ImageJ software. Cell counting was done using ImageJ software (Plugin cell counter). In the SGTA knockdown-rescue experiments, only cells expressing the FLAG-tagged protein were counted.

ER-to-cytosol transport of cholera toxin

ER-to-cytosol transport of cholera toxin was performed as previously described by Williams et al. (29), except that cells were transfected with 30 nM Hsc70 siRNA 1 or control siRNA.

ER transmembrane protein BAP31 focus-tracking assay

The ER transmembrane protein BAP31 focus-tracking assay was carried out as previously described by Ravindran et al. (25). Briefly, CV-1 cells were seeded on sterile glass coverslips and transfected with 30 nM control or Hsc70 siRNA (siRNA 1 or siRNA 2). After 24 h of transfection, the cells were infected with SV40 (MOI of ~4 to 5) for 16 h. The cells were washed in PBS, fixed in 1% paraformaldehyde (PFA) in PBS for 15 min at 25°C, and permeabilized with 0.2% Triton X-100 for 5 min at 25°C. After

permeabilization, the cells were incubated with anti-BAP31 and anti-VP1 antibodies for 1 h at 25°C. Following primary antibody incubation, the cells were washed in 5% milk (in PBS and 0.02% Tween 20) and then incubated with anti-mouse (Alexa Fluor 488) and anti-rat (rhodamine) secondary antibodies for 30 min in the dark at 25°C. After incubation, the cells were washed, and the coverslips were dried and mounted on slides. At least 100 cells were counted per biological replicate, and at least three biological replicates were performed. Merge (3× zoom) was done using PowerPoint software.

Hsc70 immunoprecipitation

In the case of SGTA knockdown, CV-1 cells were transfected with 20 nM SGTA siRNA or 20 nM scrambled siRNA using RNAiMAX for 24 h in 10-cm plates. The cells were then transfected with 3 μg of plasmid containing Hsc70-S for 32 h. In the case of SGTA overexpression, COS-7 cells were transfected with 8 μg of either WT SGTA-Myc/FLAG- or GFP-FLAG-containing plasmids in addition to 3 μg of Hsc70-S-containing plasmids for 32 h. After DNA transfection, the cells were infected with SV40 (MOI of ~4 to 5) for 16 h. The cells were then lysed in a lysis buffer (50 mM HEPES [pH 7.4], 150 mM NaCl, and PMSF) containing 1% Triton X-100 at 4°C for 10 min. Cells were then centrifuged at 16,000 × *g* at 4°C for 10 min. The resulting cell extract was incubated with S-protein-conjugated beads for 2 h, washed with the lysis buffer, and boiled in 2× SDS sample buffer with 5% β-mercaptoethanol (BME). The samples were subjected to SDS-PAGE and immunoblotting.

Coimmunoprecipitation

HEK293T cells were seeded in 6-cm plates. After 24 h, the cells were transfected with plasmids encoding GFP-FLAG or with SGTA constructs containing Myc/FLAG tags using polyethyleneimine (PEI) and Opti-MEM. For SGTA dimerization analyses, cells were transfected with plasmids containing WT SGTA-S and the indicated SGTA-Myc/FLAG or GFP-FLAG constructs. After 48 h, the cells were washed in PBS and lysed in 1% Deoxy Big CHAP (DBC) (G-Biosciences) in physiological buffer. Lysed cells were centrifuged at 16,000 × *g* for 10 min at 4°C. The resulting extract was incubated with FLAG M2 antibody-conjugated agarose beads and rotated at 4°C for 2 h. The precipitated material was washed in a buffer containing 0.01% Deoxy Big CHAP. Then 5× SDS sample buffer with 5% BME was added to the beads, followed by boiling for 10 min. Samples were subjected to SDS-PAGE and immunoblotting with the indicated antibodies.

ΔN SGTA immunoprecipitation

COS-7 cells were transfected with 12.5 nM SGTA siRNA 1 using RNAiMAX for 24 h. The cells were then transfected with 3 µg of GFP-FLAG or 4 µg of ΔN SGTA-Myc/FLAG using PEI and Opti-MEM for 24 h. Twenty-four h after DNA transfection, the cells were infected with SV40 (MOI of ~3 to 4) for 16 h. At 16 hpi, the cells were cross-linked in 2 mM DSP at 4°C for 30 min and quenched with 10 mM Tris at 4°C for 10 min. The cells were then lysed in 1% Deoxy Big CHAP in 50 mM Tris, 150 mM NaCl, 1 mM EDTA, 20 mM NEM, and PMSF at 4°C for 10 min. Lysed cells were centrifuged at 16,000 × *g* at 4°C for 10 min. The supernatant was incubated with FLAG M2 antibody-conjugated agarose beads for 2 h and rotated at 4°C. After 2 h, the beads were washed with lysis

buffer and boiled in 5× SDS sample buffer with 5% BME for 10 min. The samples were subjected to SDS-PAGE and immunoblotting with the indicated antibodies.

In vitro SV40-Hsc70 coimmunoprecipitation

A 100-ng portion of SV40 was treated with 3 mM DTT and 10 mM EGTA in PBS for 45 min at 37°C. After 45 min, 1 μg of GFP-FLAG or Hsc70-His was added to the virus, followed by incubation for 1 h at 25°C. VP1 antibody specific for the VP1 protein was added and rotated overnight at 4°C. After 18 h, protein A/G beads were added and rotated for 2 h at 4°C. After an additional 2 h, the beads were washed with 0.1% Deoxy Big Chap in physiological buffer. Next, 5× SDS sample buffer with 5% BME was added to the beads, followed by boiling for 10 min. The samples were subjected to SDS-PAGE and immunoblotting with the specified antibodies.

Statistics

Graphs represent the mean value of at least three independent experiments, and paired Student two-tailed *t* tests were used to determine the *P* values.

RESULTS

Hsc70 depletion impairs SV40 cytosol entry from the ER.

Based on an RNA interference (RNAi) screen, DNAJ B14 (B14) was identified as an ER membrane J-protein that promotes ER-to-cytosol membrane penetration of SV40 (23). Subsequent binding analyses identified a cytosolic complex composed of Hsc70, Hsp105, and SGTA that associates with B14 (24, 25). Importantly, loss- and gain-of-function strategies revealed that Hsp105 and SGTA have a central function in extracting SV40 from the ER and transporting the virus to the cytosol (24, 25). Whether Hsc70

directly exerts a role in this process is unknown. To test this, we used a well-characterized cell-based, semipermeabilized ER-to-cytosol transport assay. In this assay, simian CV-1 cells transfected with a control small interfering RNA (siRNA) (scrambled) or either of two specific siRNAs directed against Hsc70 (Hsc70 siRNA 1 or siRNA 2) were infected with SV40. CV-1 cells were used because they are a naturally permissive cell line commonly used to study SV40 infection. The cells were then harvested, treated with a low concentration of digitonin to permeabilize the plasma membrane without damaging internal membranes, and centrifuged. This procedure generates two fractions: (i) a supernatant fraction that contains cytosolic proteins and virus that reaches the cytosol ("cytosol") and (ii) a pellet fraction that harbors membranes, including the ER, as well as virus associated with membranes ("membrane"). The integrity of the fractionation procedure can be monitored in the pelleting of the ER-resident protein disulfide isomerase (PDI) to the membrane fraction without significant release of this protein into the cytosolic fraction (Fig. 2-1A, compare the seventh to the third panel). In contrast, the majority of actin partitions to the cytosolic fraction with a lower level found in the membrane fraction that likely represents nuclear-associated actin (Fig. 2-1A, compare the second to the sixth panel). Using this assay, we found that even a moderate knockdown of Hsc70 (Fig. 2-1A, fourth panel, compare lanes 2 and 3 to lane 1) is sufficient to potently reduce the SV40 VP1 level in the cytosol (Fig. 2-1A, first panel, compare lanes 2 and 3 to lane 1; the VP1 band intensity is quantified in Fig. 2-1B). We intentionally kept the level of Hsc70 knockdown modest by using the lowest siRNA concentration for a minimal time to achieve protein knockdown

because a significant depletion of this chaperone is likely to compromise overall cellular integrity due to Hsc70's role as a general housekeeping protein.

When ER-localized SV40 was isolated from the membrane fraction using a previously established biochemical fractionation protocol (14) (see Materials and Methods), we found that depleting Hsc70 did not decrease the VP1 level (Fig. 2-1A, eighth panel, compare lanes 2 and 3 to lane 1; the VP1 band intensity is quantified in Fig. 2-1C); in fact, Hsc70 siRNA 1 may have caused a slight increase in the ER-localized SV40 level. Together, these findings suggest that Hsc70 promotes the release of SV40 into the cytosol from the ER. Because Hsc70 is an important housekeeping protein and its depletion may globally perturb cellular proteostasis, we assessed whether our results were specific to SV40 ER-to-cytosol transport or due to a general disruption of cellular processes. To this end, we used cholera toxin (CT), another toxic agent that also undergoes ER-to-cytosol membrane transport to cause disease (27-29), to evaluate whether the knockdown of Hsc70 affects its membrane transport process using the same semipermeabilized assay. To intoxicate cells, CT traffics from the cell surface to the ER, where its cholera toxin A (CTA) subunit is reduced to generate the catalytic CTA1 peptide which in turn transports across the ER membrane to reach the cytosol; in the cytosol, CTA1 induces cytotoxicity. When Hsc70 is depleted, neither the formation of CTA1 (Fig. 2-1D, fourth panel, compare lane 2 to lane 1) nor the arrival of CTA1 to the cytosol (Fig. 2-1D, first panel, compare lane 2 to lane 1) was affected. These results demonstrate that Hsc70 is unlikely to play a role in promoting either cell surface-to-ER or ER-to-cytosol transport of the toxin. Since Hsc70 knockdown does not

globally impair all ER-to-cytosol membrane transport processes, we conclude that Hsc70 selectively exerts a role during SV40's ER membrane penetration event.

Knockdown of Hsc70 or SGTA enhances SV40-induced focus formation.

We used an independent assay to further evaluate the idea that Hsc70 executes an important role in extracting SV40 from the ER and transporting the virus to the cytosol. When SV40 reaches the ER from the cell surface, it induces the reorganization of several ER membrane proteins (including BAP31) to distinct puncta called “foci” that act as cytosol entry sites for the virus (24, 25, 30); not surprisingly, SV40 itself is also concentrated in the foci. We reasoned that if Hsc70 extracts focus-localized SV40 from the ER and is necessary for cytosol arrival, depleting Hsc70 should trap the virus in the foci, thereby enhancing the focus structure. In fact, when Hsp105 of the Hsc70-Hsp105-SGTA complex was depleted, the virus-induced focus structure increased (25). Indeed, we now find that when Hsc70 was knocked down, the number of cells containing at least one BAP31-positive focus increased (Fig. 2-2A, compare the top to the bottom row; quantified in Fig. 2-2B). These findings strengthen the notion that Hsc70 plays a key role in promoting SV40 release into the cytosol from the ER.

We previously demonstrated that SGTA is part of the Hsc70-Hsp105-SGTA complex that facilitates SV40 ER-to-cytosol membrane transport (24). Not surprisingly, knocking down SGTA (using SGTA siRNA 1 and siRNA 2) also increased virus-induced focus formation (Fig. 2-2C, compare the top to the bottom row; quantified in Fig. 2-2D), similar to the effect of depleting Hsp105 (25) and Hsc70 (Fig. 2-2A and 2-2B). The similar phenotype (i.e., enhanced focus formation) observed when any single component of the Hsc70-Hsp105-SGTA complex is depleted suggests that these

individual components all contribute to the virus extraction event. We note that when a much higher SV40 concentration was used (multiplicity of infection [MOI] of ~50), SGTA knockdown did not increase the formation of the virus-induced foci (24), likely because all the cells already displayed focus formation under the control condition.

SGTA regulates SV40-Hsc70 interaction.

As a cochaperone of Hsc70, SGTA has been previously shown to control Hsc70's intrinsic ATPase activity (31, 32). We therefore sought to determine whether SGTA within the Hsc70-Hsp105-SGTA complex might regulate Hsc70's function during the viral membrane extraction process. Binding analyses revealed that in SV40-infected CV-1 cells expressing S-tagged Hsc70 (Hsc70-S), affinity purification of Hsc70-S pulled down more SV40 in SGTA-depleted cells than in the control (Fig. 2-3A, first panel, compare lane 2 to lane 1; the VP1 band intensity is quantified in Fig. 2-3B). When the reverse experiment was conducted, we found that in comparison to cells expressing the control green fluorescent protein (GFP)-FLAG, overexpressing wild-type (WT) SGTA containing a Myc/FLAG tag at the C terminus (WT SGTA-Myc/FLAG) decreased the level of Hsc70-SV40 interaction (Fig. 2-3C, first panel, compare lane 2 to lane 1; quantified in Fig. 2-3C); this experiment was performed using (CV-1-derived) COS-7 cells because they afford a higher transfection efficiency than CV-1 cells, which facilitated the experiment. When purified His-tagged Hsc70 (Hsc70-His) or GFP-FLAG (Fig 2-3E) was incubated with partially disassembled SV40 (due to dithiothreitol [DTT] and EGTA treatment), precipitation of SV40 pulled down Hsc70 but not GFP (Fig. 2-3F, first and second panels, compare lane 4 to lane 3). This finding demonstrates that Hsc70 interacts with SV40 directly. We note that the difference in SV40's ability to bind

to Hsc70 when SGTA's level is altered is likely not due to a simple competition between SGTA and Hsc70 for binding to the same SV40 substrate. This is because we previously used a purified system and found that purified WT SGTA containing copurified Hsc70 in fact binds more to SV40 than a SGTA mutant (see below) that does not copurify Hsc70 (24). Hence, our data demonstrate that SGTA regulates the SV40-Hsc70 interaction (see Discussion).

Structure-function analyses of SGTA.

Because SGTA impacts the virus-Hsc70 interaction, we sought to determine whether SGTA's ability to associate with Hsc70 via SGTA's central TPR domain (Fig. 2-4A) (32-34), as well as SGTA's N-terminal domain, which mediates homodimerization and the recruitment cellular adapters, including the Ubl4A-Tric35-Bag6 complex (33-36), is important during ER extraction and cytosol arrival of the virus. Since SGTA's C-terminal domain is limited to substrate binding (31, 37, 38) and unlikely to control Hsc70's function, we did not characterize this domain in this study. Accordingly, in addition to WT SGTA-Myc/FLAG, we used a SGTA construct lacking its N-terminal domain (ΔN SGTA-Myc/FLAG, which lacks the first 90 amino acids of SGTA), a dimerization-defective mutant in which three residues (L15, A35, and L39) postulated to reside at the dimerization interface are simultaneously mutated to aspartic acid (D3 SGTA-Myc/FLAG) and a TPR mutant that cannot bind to Hsc70 (K160E/R164E SGTA-Myc/FLAG [24]).

To test these constructs' behavior in our system, we first cotransfected WT SGTA containing an S-tag (WT SGTA-S) with either GFP-FLAG, WT SGTA-Myc/FLAG, ΔN SGTA-Myc/FLAG, or D3 SGTA-Myc/FLAG in cells. Immunoprecipitation using FLAG

antibody-conjugated agarose beads, followed by subjecting the precipitated material to SDS-PAGE and immunoblotting, revealed that precipitating WT SGTA-Myc/FLAG, but not GFP-FLAG, ΔN SGTA-Myc/FLAG, or D3 SGTA-Myc/FLAG, pulled down WT SGTA-S (Fig. 2-4B, first panel, compare lane 2 to lanes 1, 3, and 4). These results confirm that SGTA's N-terminal domain is essential for dimerization (34). Moreover, by demonstrating that D3 SGTA does not dimerize, our data specifically pinpoint three critical residues lying at the SGTA dimerization interface (34) as essential for mediating this oligomerization process.

When GFP-FLAG or WT SGTA-Myc/FLAG was individually transfected into the cells, precipitating WT SGTA-Myc/FLAG but not GFP-FLAG pulled down endogenous B14, Hsp105, Hsc70, and Ubl4A as expected (Fig. 2-4B, compare lane 6 to lane 5). In cells transfected with ΔN SGTA-Myc/FLAG, pulldown of this protein also coprecipitated endogenous B14, Hsp105, and Hsc70 but did not precipitate Ubl4A due to the absence of the N-terminal domain (Fig. 2-4B, lane 7). In addition, in cells expressing the dimerization-defective D3 SGTA-Myc/FLAG mutant, precipitating this mutant pulled down B14, Hsp105, and (with higher affinity) Hsc70 (Fig. 2-4B, lane 8). Why D3 SGTA binds to Hsc70 with greater efficiency is unclear, but the observation that D3 SGTA did not bind to Ubl4A suggests that SGTA dimerization may be required to engage Ubl4A.

When a similar binding study was performed using K160E/R164E SGTA-Myc/FLAG, precipitation analyses showed this Hsc70-binding-defective construct interacts with Ubl4A, but not B14, Hsp105, or Hsc70 (Fig. 2-4C, lane 3). K160E/R164E SGTA's inability to bind to Hsc70 confirms previous observations (32, 37, 39) and is likely the reason it cannot bind to B14, indicating the SGTA-B14 binding is likely indirect

and mediated by Hsc70. This SGTA mutant's failure to bind to Hsp105 could also be due to its inability to bind to Hsc70, again suggesting that Hsc70 mediates the SGTA-Hsp105 interaction.

SGTA's ability to bind to Hsc70 is crucial in SV40 ER-to-cytosol transport.

We tested if SGTA's N terminus or its ability to dimerize is crucial to support SV40 cytosol entry from the ER using the cell-based semipermeabilized assay. We found that in SGTA-depleted cells, SV40's arrival to the cytosol was significantly impaired compared to that in control cells (Fig. 2-5A, first panel, compare lane 2 to lane 1; the VP1 band intensity is quantified in Fig. 2-5C), as reported previously (24). Under the SGTA-knockdown condition, expressing a WT SGTA-Myc/FLAG construct that is resistant to the SGTA siRNA at a level similar to that of endogenous SGTA (Fig. 2-5A, second panel, lane 3) partially restored SV40's arrival to the cytosol (Fig. 2-5A, first panel, compare lane 3 to lane 2; quantified in Fig. 2-5C). Likewise, expressing either ΔN SGTA-Myc/FLAG or D3 SGTA-Myc/FLAG under the SGTA-depleted condition (Fig. 2-5A, second panel, lanes 4 and 5) also partially restored the arrival of SV40 to the cytosol (Fig. 2-5A, first panel, compare lanes 4 and 5 to lane 3; quantified in Fig. 2-5C). These data suggest that SGTA's N-terminal domain and ability to dimerize are dispensable for supporting SV40's ER membrane transport.

However, our results demonstrate that expressing K160E/R164E SGTA-Myc/FLAG in cells depleted of SGTA (Fig. 2-5B, second panel, compare lane 3 to lane 2) did not restore the block in SV40 cytosol entry due to depletion of SGTA (Fig. 2-5B, first panel, compare lane 3 to lane 2; quantified in Fig. 2-5C). This finding strengthens the idea that SGTA must engage Hsc70 in order to regulate the viral ER membrane

transport event, a view consistent with our data that SGTA regulates the Hsc70-SV40 interaction (Fig. 2-3).

SGTA's N-terminal domain and Hsc70-binding are essential to promote SV40 infection.

We used the same “knockdown-rescue” approach to evaluate structural features of SGTA that are necessary in supporting SV40 infection. Cells transfected with either scrambled or SGTA siRNA were cotransfected with the indicated FLAG construct, and virus infection was assessed by monitoring for the expression of viral large T antigen in the host nucleus. Only cells expressing the FLAG-containing protein were scored. Using this strategy, we found that expressing WT SGTA or D3 SGTA but not K160E/R164E or ΔN SGTA in SGTA-knockdown cells rescued the infection block caused by depleting SGTA (Fig. 2-6A). The finding that K160E/R164E SGTA cannot rescue infection under the SGTA knocked-down condition is in line with this construct's inability to restore cytosol entry of the virus from the ER in SGTA-depleted cells (Fig. 2-5B and 2-5C). However, the observation that ΔN SGTA fails to rescue infection despite the fact that it can restore cytosol entry of SV40 from the ER (Fig. 2-5A and 2-5C) raises the strong possibility that SGTA's N terminus exerts a post-ER membrane penetration role during entry. This SGTA mutant's inability to restore infection is not due to lack of virus binding, since our data revealed that ΔN SGTA coimmunoprecipitates with SV40 at 16 h postinfection (hpi; Fig. 2-6B, first panel, compare lane 2 to lane 1), when a significant portion of the virus has reached the cytosol from the ER. Moreover, during the postulated post-ER membrane penetration event, SGTA's N terminus appears to

function in a dimerization-independent fashion since the dimerization-defective D3 SGTA is capable of restoring virus infection in SGTA-knockdown cells.

DISCUSSION

One of the least understood steps during membrane penetration of nonenveloped viruses is the events on the cytosolic side of the limiting membrane that impact the viral membrane translocation process. In the case of ER-to-cytosol membrane transport of SV40, the molecular basis by which host factors extract the virus from the ER and facilitate cytosol arrival is not completely understood. We previously identified a cytosolic protein complex composed of Hsc70, Hsp105, and SGTA that is tethered to the ER membrane through binding to the membrane J-protein B14 (24, 25). Although Hsp105 and SGTA within this complex was demonstrated to participate in extracting membrane-embedded SV40 from the ER and transporting the virus to the cytosol (24, 25), direct evidence demonstrating a function of Hsc70 in supporting viral extraction has yet to be firmly established.

In this report, we used two independent approaches to determine the role of Hsc70 in stimulating cytosol release of SV40 from the ER (Fig. 2-6C). First, we used a cell-based, semipermeabilized transport assay and found that modestly knocking down Hsc70 is sufficient to robustly impair SV40 entry into the cytosol. This strongly supports the idea that Hsc70 exerts a role in the cytosol arrival of SV40. Second, we relied on an imaging strategy based on visualizing a suborganellar punctate structure called a focus that represents the virus cytosol entry site from the ER. In this case, we found that depleting Hsc70 enhances the formation of this structure, similar to the depletion of Hsp105 (25)

or SGTA (this study). Enhanced focus formation likely reflects the entrapment of SV40 at the site of cytosol entry when the extraction machinery is impaired. This finding thus strengthens results using the semipermeabilized assay, furthering the hypothesis that Hsc70 directly participates in the extraction event.

Our previous experiments hinted at a role for Hsc70 in mediating SV40 ER membrane penetration essential for virus infection. Specifically, we found that WT B14, but not an Hsc70-binding-defective B14 mutant, rescues SV40 infection in B14-depleted cells (24), suggesting that Hsc70 is involved in infectious SV40 entry. Likewise, for Hsp105, which can serve as a nucleotide exchange factor (NEF) against Hsc70 (40, 41), our results indicated that WT Hsp105, but not a NEF-defective Hsp105, restores the block in SV40 infection in Hsp105-knockdown cells (25), again implicating a function of Hsc70 during SV40 entry.

Another major point in this study is that SGTA controls SV40's ability to bind to Hsc70. Specifically, we found that depleting SGTA increased SV40 binding to Hsc70. Such an enhanced interaction might reflect preferential binding of SV40 to Hsc70 that is associated with the ER membrane. This would prevent efficient SV40 release into the cytosol and explain why SGTA depletion impairs SV40 extraction from the ER and cytosol arrival (24). In addition, we found that overexpressing SGTA decreased the virus-Hsc70 interaction. The SGTA depletion and overexpression data together suggest that SGTA favors the transition of Hsc70 from the high-affinity ADP-Hsc70 substrate-binding state to the low-affinity ATP-Hsc70 state (Fig. 2-6C, zoomed panel). Although how SGTA precisely accomplishes this feat remains unclear, we envision two distinct possibilities.

In one scenario, SGTA disrupts Hsc70's intrinsic ATPase activity, which normally converts ATP-Hsc70 to ADP-Hsc70. This scenario would agree with a previous report demonstrating that SGTA inhibits Hsc70's ATPase activity (32) but differs from another study, where SGTA was shown to increase Hsc70's ATPase activity (31). The reason for these opposite observations is unclear, but it could be due to the use of different substrates and experimental conditions. In the second scenario, SGTA enhances the nucleotide exchange reaction to favor ATP-Hsc70 formation, perhaps by assisting the action of the Hsp105 NEF. Regardless of the mechanism, SGTA's ability to engage Hsc70 via its central TPR domain, but not SGTA's N-terminal domain, which is responsible for homodimerization and recruitment of cellular factors, is important in facilitating ER extraction and cytosol arrival of SV40.

Finally, our data reveal a potential post-ER membrane penetration role of SGTA during SV40 infection. This is based on the observation that SGTA's N terminus, despite not being important in stimulating virus ER-to-cytosol membrane transport, is nonetheless critical for promoting infection. One possibility is that SGTA directly participates in delivering the virus from the cytosol into the nucleus. In fact, our laboratory has shown that SGTA binds to SV40 (24), and others have demonstrated that SGTA localizes to the nucleus (42,43). In this context, it should be noted that SGTA's N terminus does not contain a canonical nuclear localization sequence. Another possibility is that SGTA, via its N terminus, recruits a cellular component which in turn targets the virus into the nucleus. Clearly, future experiments are needed to clarify this intriguing observation. In summary, in the present study we furthered our understanding of how a nonenveloped virus penetrates a biological membrane during infection by

demonstrating that as part of the cytosolic Hsc70-Hsp105-SGTA complex, Hsc70 plays an essential role in ejecting the nonenveloped SV40 from the ER membrane and transporting the virus to the cytosol in a reaction controlled by SGTA.

Chapter 2 Figures:

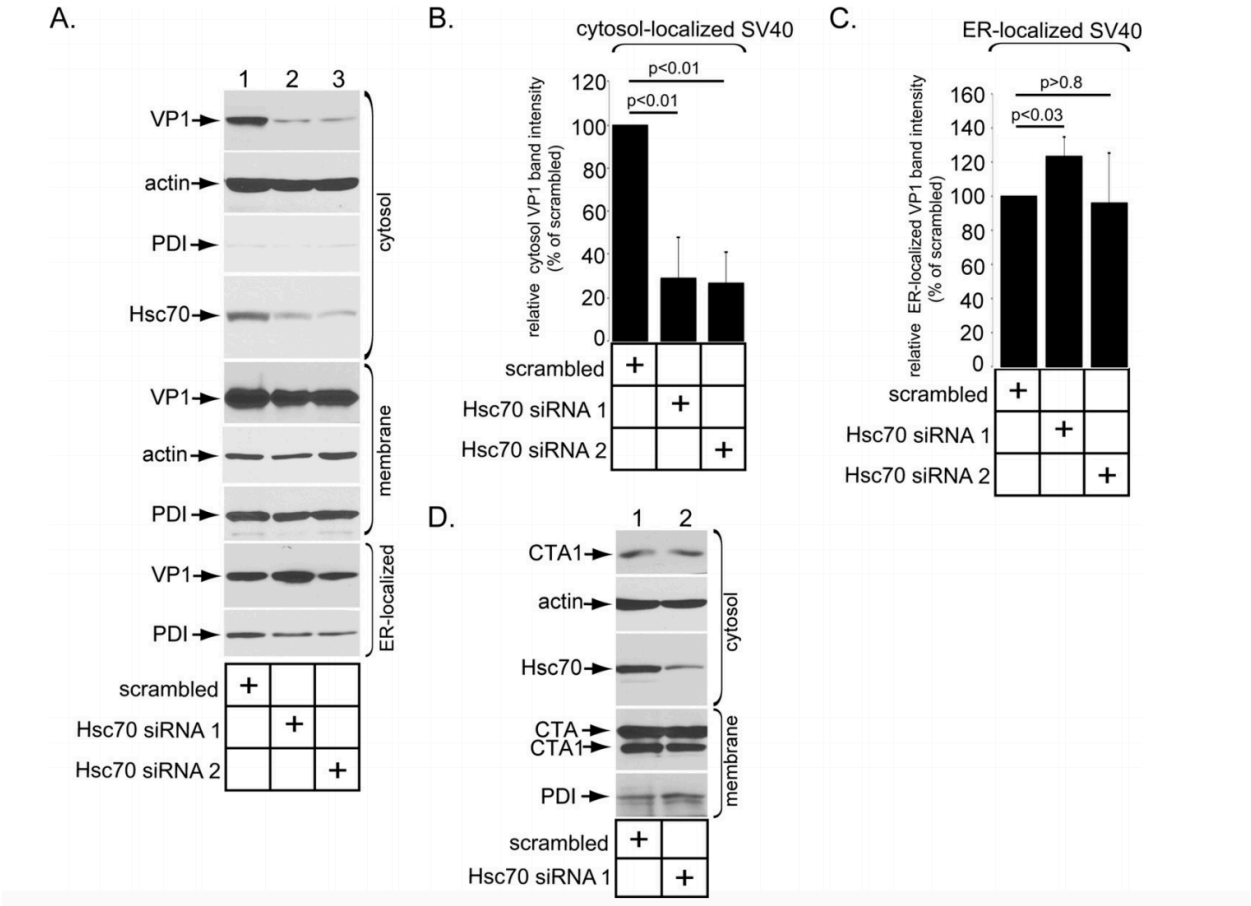

FIG. 2-1 Hsc70 depletion impairs SV40 cytosol arrival from the ER.

(A) CV-1 cells transfected with Hsc70 siRNA 1, Hsc70 siRNA 2, or scrambled siRNA were infected with purified SV40 for 16 h and subjected to the semipermeabilized, ER-to-cytosol transport assay. Cytosol-, membrane-, and ER-localized fractions (see Materials and Methods) were analyzed by SDS-PAGE and immunoblotting.
(B) The VP1 band intensity in the cytosol fraction in panel A was quantified by using ImageJ (National Institutes of Health) and plotted as a percentage of the VP1 band intensity in the scrambled siRNA-treated condition. The graph represents the means the SD from three biological replicates.
(C) Same as in panel B, except quantification is of the VP1 band intensity in the ER-localized fraction.
(D) CV-1 cells transfected with Hsc70 siRNA 1 or scrambled siRNA were intoxicated with cholera toxin for 90 min. The cells were lysed in 0.1% digitonin and fractionated as in panel A. Both the cytosol and the membrane fractions were subjected to SDS-PAGE and immunoblotting.

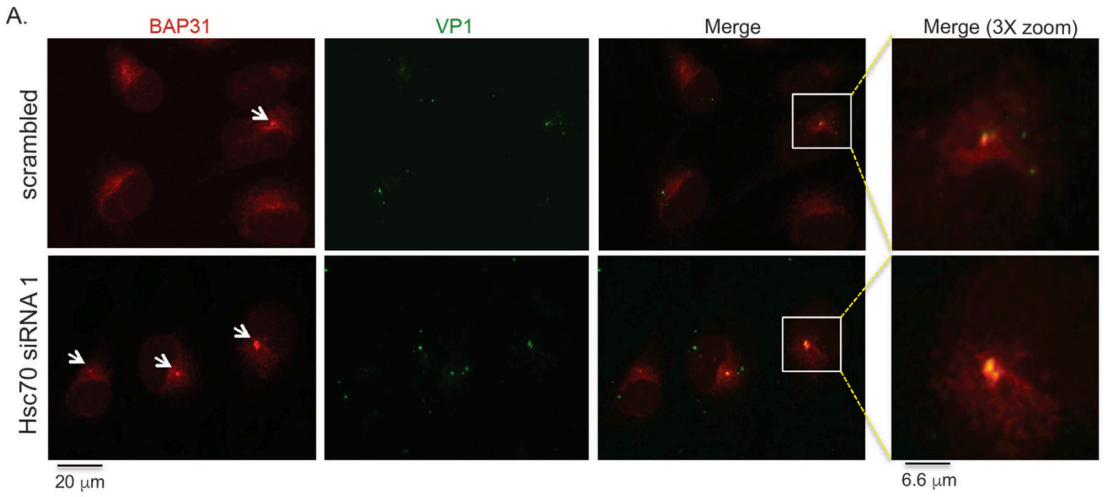
A.
BAP31
VP1
Merge
Merge (3X zoom)
scrambled
Hsc70 siRNA 1
20 μm
6.6 μm

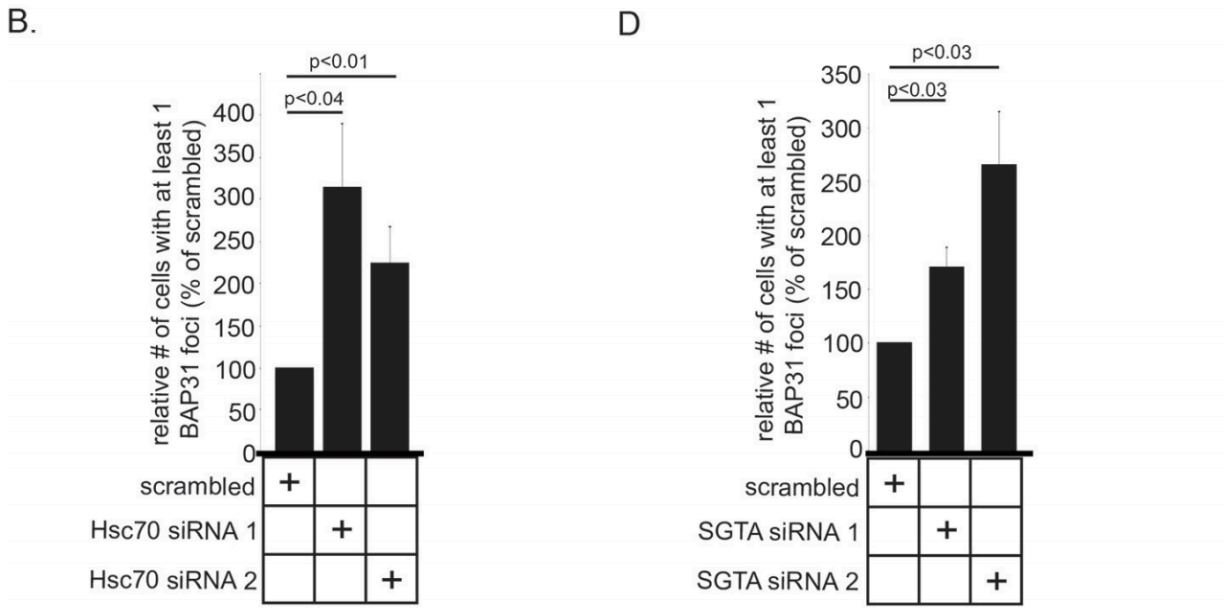
B.
p<0.01
p<0.04
relative # of cells with at least 1 BAP31 foci (% of scrambled)
400
350
300
250
200
150
100
50
0
scrambled
Hsc70 siRNA 1
Hsc70 siRNA 2
D
p<0.03
p<0.03
relative # of cells with at least 1 BAP31 foci (% of scrambled)
350
300
250
200
150
100
50
0
scrambled
SGTA siRNA 1
SGTA siRNA 2

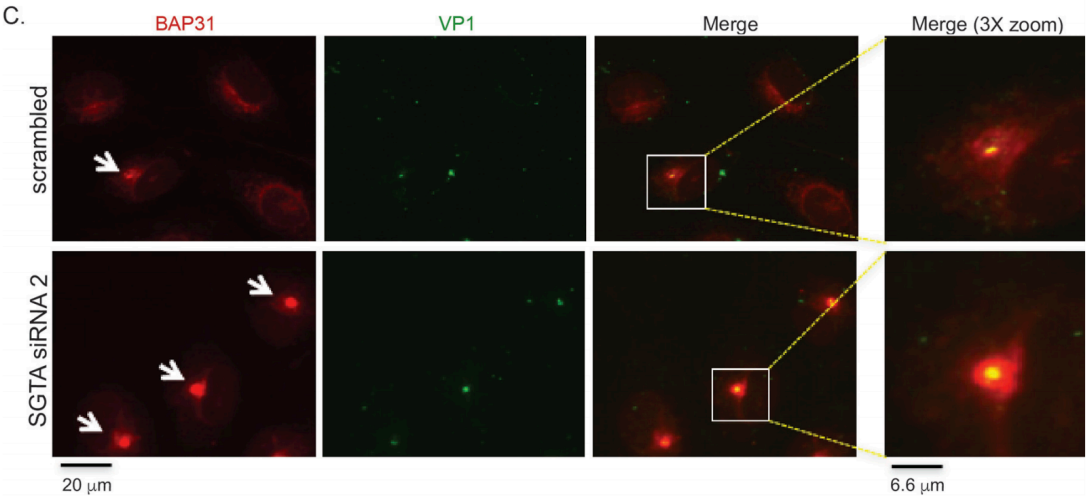
C.
BAP31
VP1
Merge
Merge (3X zoom)
scrambled
SGTA siRNA 2
20 μm
6.6 μm

FIG. 2-2 Knockdown of Hsc70 or SGTA enhances SV40-induced focus formation.

(A) CV-1 cells were seeded on glass coverslips and simultaneously transfected with Hsc70 siRNA 1 (bottom row) or scrambled siRNA (top row). After 24 h of siRNA transfection, the cells were infected with SV40 (MOI of 4 to 5) for 16 h. At 16 hpi, the cells were fixed and stained for BAP31 (red) and VP1 (green) and imaged using fluorescence microscopy. Zoomed images (3X) of the white boxed area in the merged images are shown.
(B) Data are plotted as the number of cells containing at least one BAP31 focus as a percentage of the scrambled siRNA-treated condition. The graph represents the means the SD from three biological replicates.
(C) Same as in panel A, except that images derived from cells treated with SGTA siRNA 2 are shown.
(D) Same as in panel B, except the focus formation in panel C is quantified based on results derived from SGTA siRNA 1 and siRNA 2.

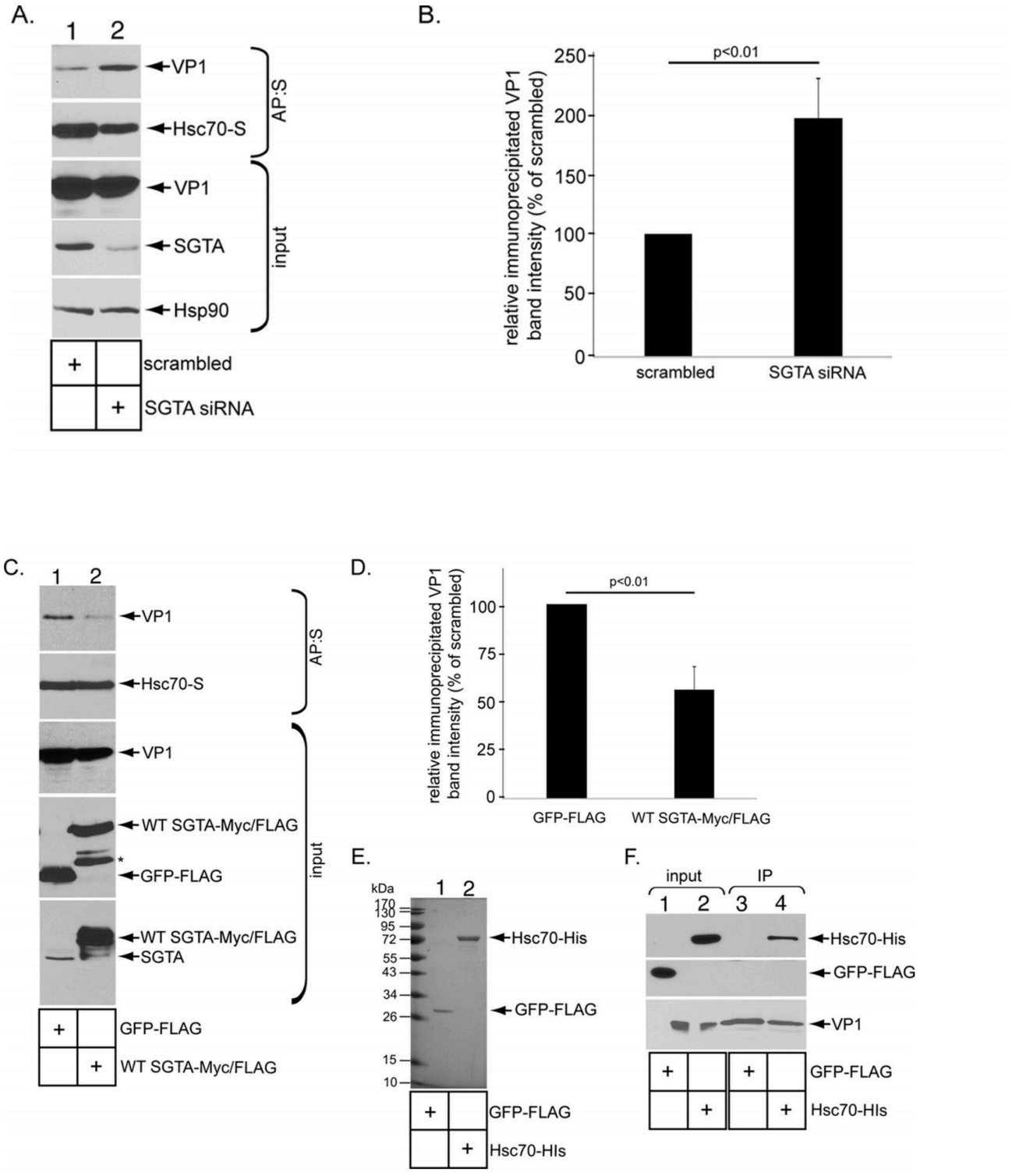
A.
1 2
VP1
Hsc70-S
AP:S
VP1
SGTA
Hsp90
input
+
scrambled
SGTA siRNA
B.
p<0.01
relative immunoprecipitated VP1 band intensity (% of scrambled)
250
200
150
100
50
0
scrambled
SGTA siRNA
C.
1 2
VP1
Hsc70-S
AP:S
VP1
WT SGTA-Myc/FLAG
*
GFP-FLAG
WT SGTA-Myc/FLAG
SGTA
input
+
GFP-FLAG
WT SGTA-Myc/FLAG
D.
p<0.01
relative immunoprecipitated VP1 band intensity (% of scrambled)
100
75
50
25
0
GFP-FLAG
WT SGTA-Myc/FLAG
E.
kDa
1 2
170
130
95
72
55
43
34
26
15
10
Hsc70-His
GFP-FLAG
+
GFP-FLAG
Hsc70-HIs
F.
input
IP
1 2 3 4
Hsc70-His
GFP-FLAG
VP1
+
GFP-FLAG
Hsc70-HIs

FIG. 2-3 SGTA regulates SV40-Hsc70 interaction.

(A) CV-1 cells transfected with scrambled or SGTA siRNA 1 were cotransfected with Hsc70-S for 24 h, followed by 16 h of SV40 infection. Hsc70-S was affinity purified from the resulting whole-cell lysate, and the isolated sample was subjected to SDS-PAGE and immunoblotting.
(B) Quantification of the VP1 band intensity in panel A as a percentage of the scrambled siRNA-treated cells. The graph represents the means the SD from three biological replicates.
(C) Same as in panel A, except COS-7 cells transfected with Hsc70-S were cotransfected with GFP-FLAG or WT SGTA-Myc/FLAG. *, Degraded WT SGTA-Myc/FLAG.
(D) Quantification of the VP1 band intensity in panel C as a percentage of cells expressing GFP-FLAG. The graph represents the means the SD from three biological replicates.
(E) Purified GFP-FLAG and Hsc70-His subjected to Coomassie blue staining.
(F) Hsc70-His and GFP-FLAG were incubated with DTT-EGTA-treated SV40, followed by incubation with a VP1 specific antibody. The precipitated samples were subjected to SDS-PAGE and immunoblotting.

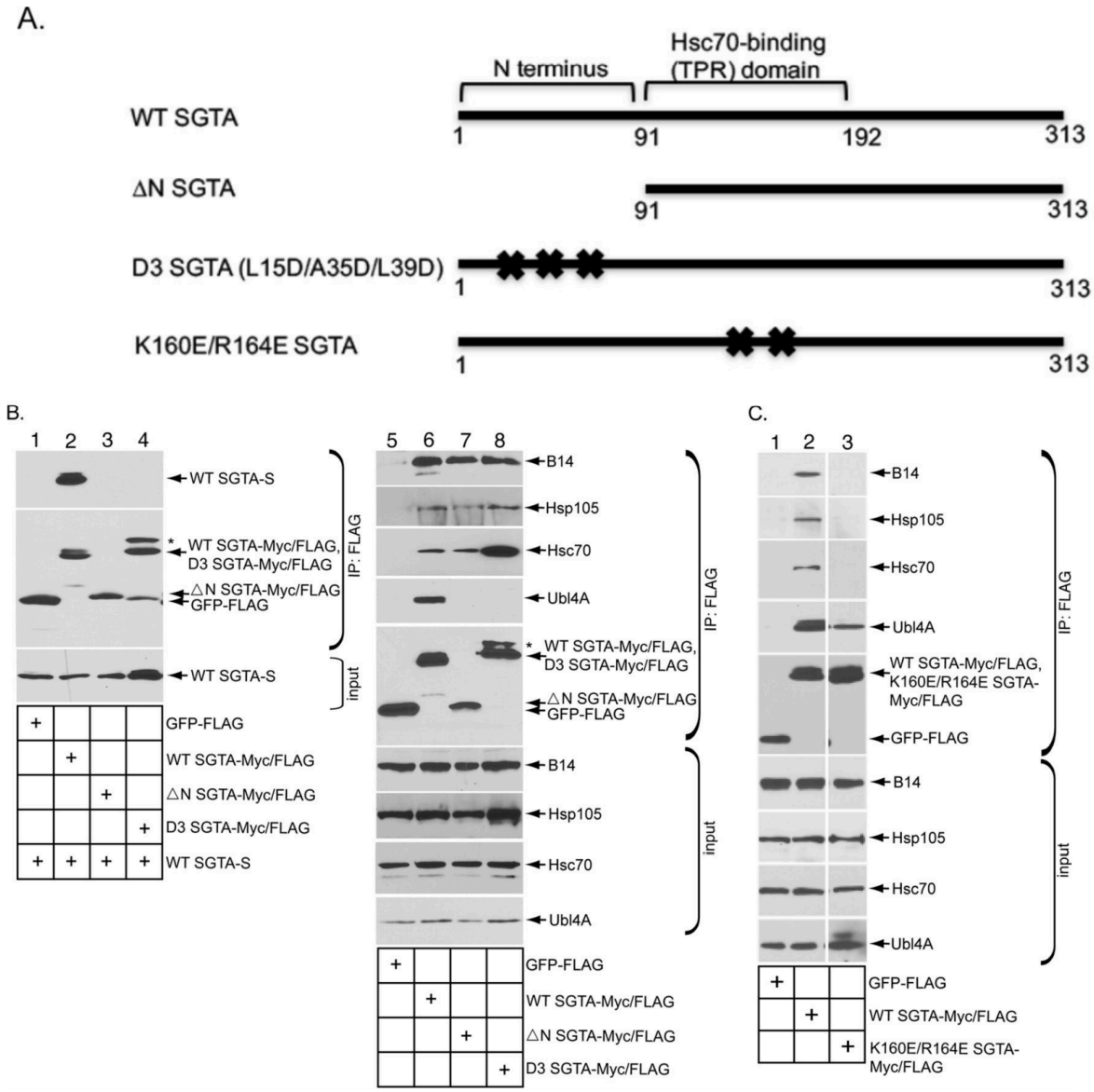
A.
N terminus
Hsc70-binding (TPR) domain
WT SGTA
1
91
192
313
ΔN SGTA
91
313
D3 SGTA (L15D/A35D/L39D)
1
313
K160E/R164E SGTA
1
313
B.
1 2 3 4
WT SGTA-S
* WT SGTA-Myc/FLAG, D3 SGTA-Myc/FLAG
△N SGTA-Myc/FLAG
GFP-FLAG
WT SGTA-S
IP: FLAG
input
GFP-FLAG
WT SGTA-Myc/FLAG
△N SGTA-Myc/FLAG
D3 SGTA-Myc/FLAG
WT SGTA-S
5 6 7 8
B14
Hsp105
Hsc70
Ubl4A
* WT SGTA-Myc/FLAG, D3 SGTA-Myc/FLAG
△N SGTA-Myc/FLAG
GFP-FLAG
IP: FLAG
B14
Hsp105
Hsc70
Ubl4A
input
GFP-FLAG
WT SGTA-Myc/FLAG
△N SGTA-Myc/FLAG
D3 SGTA-Myc/FLAG
C.
1 2 3
B14
Hsp105
Hsc70
Ubl4A
WT SGTA-Myc/FLAG, K160E/R164E SGTA-Myc/FLAG
GFP-FLAG
IP: FLAG
B14
Hsp105
Hsc70
Ubl4A
input
GFP-FLAG
WT SGTA-Myc/FLAG
K160E/R164E SGTA-Myc/FLAG

FIG. 2-4 Characterization of SGTA mutants.

(A) Structures of WT and SGTA mutants used in this figure.
(B) Cell lysates derived from HEK293T cells transfected with the indicated constructs were subjected to immunoprecipitation using FLAG antibody-conjugated agarose beads. The precipitated materials were subjected to SDS-PAGE and immunoblotting.
(C) Same as in panel B, except the indicated constructs were used. The white intervening space indicates that the lanes were spliced from the same immunoblot.

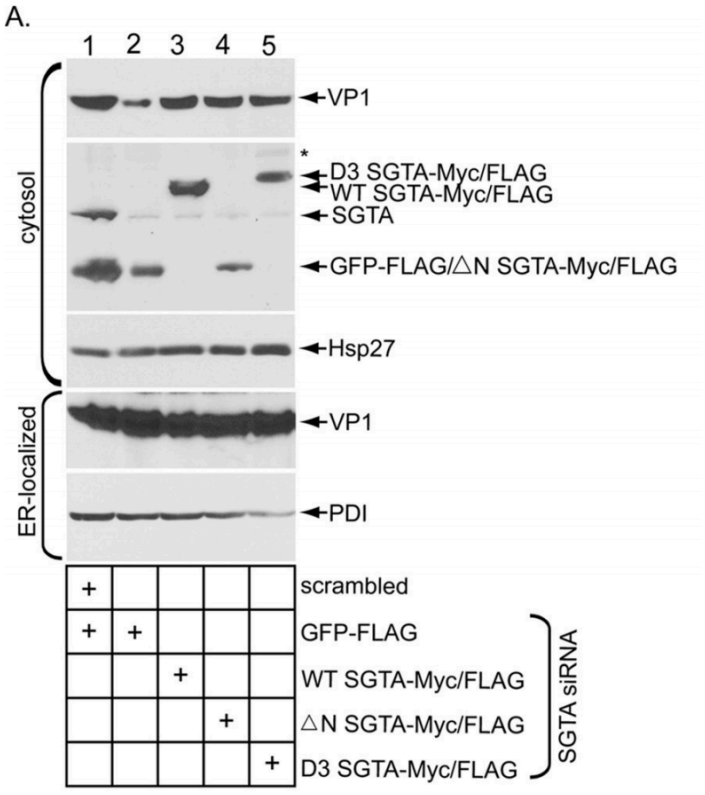
A.
1 2 3 4 5
cytosol
ER-localized
VP1
*
D3 SGTA-Myc/FLAG
WT SGTA-Myc/FLAG
SGTA
GFP-FLAG/△N SGTA-Myc/FLAG
Hsp27
VP1
PDI
scrambled
GFP-FLAG
WT SGTA-Myc/FLAG
△N SGTA-Myc/FLAG
D3 SGTA-Myc/FLAG
SGTA siRNA

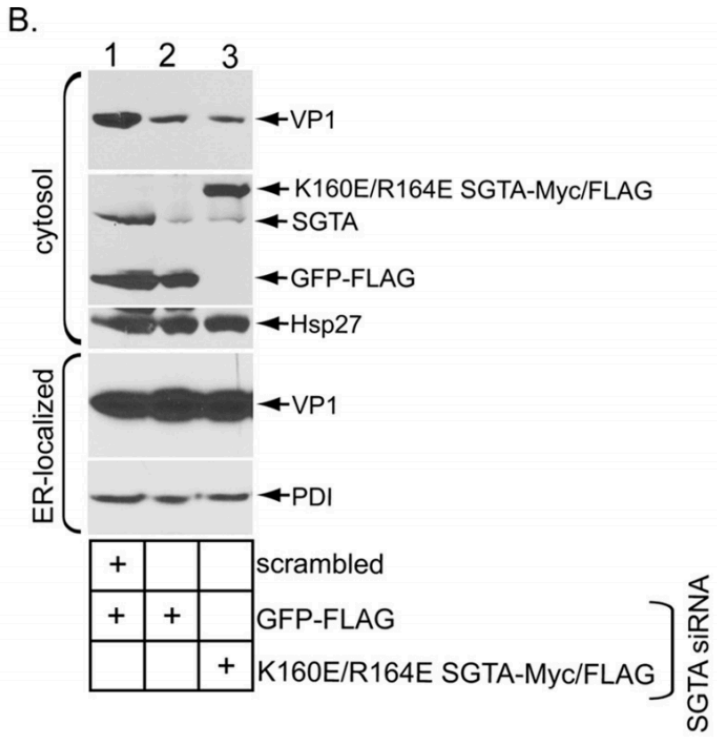
B.
1 2 3
cytosol
ER-localized
VP1
K160E/R164E SGTA-Myc/FLAG
SGTA
GFP-FLAG
Hsp27
VP1
PDI
scrambled
GFP-FLAG
K160E/R164E SGTA-Myc/FLAG
SGTA siRNA

C.

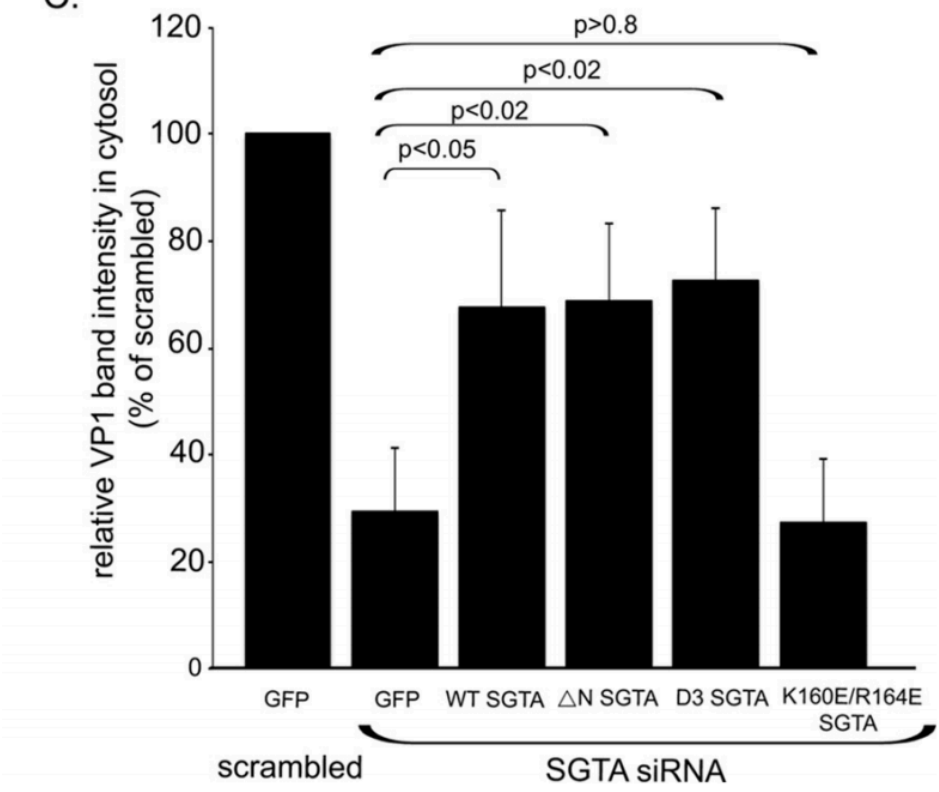
p>0.8
p<0.02
p<0.02
p<0.05
relative VP1 band intensity in cytosol
(% of scrambled)
120
100
80
60
40
20
0
GFP
GFP
WT SGTA
△N SGTA
D3 SGTA
K160E/R164E
SGTA
scrambled
SGTA siRNA

FIG. 2-5 SGTA's ability to bind to Hsc70 is important in promoting SV40 ER-to-cytosol transport.

(A) COS-7 cells transfected with scrambled or SGTA siRNA 1 for 24 h were cotransfected with the indicated construct. The cells were then infected with SV40 for 16 h, lysed, and fractionated as in Fig. 1A. Cytosol- and ER-localized fractions were subjected to nonreducing SDS-PAGE and immunoblotting.
(B) Same as in panel A, except the indicated constructs were used.
(C) Quantification of the VP1 band intensity in the cytosol fraction in panels A and B. The VP1 band intensity was quantified as a percentage of the scramble siRNA-treated condition. The data represent the means the SD of at least three biological replicates.

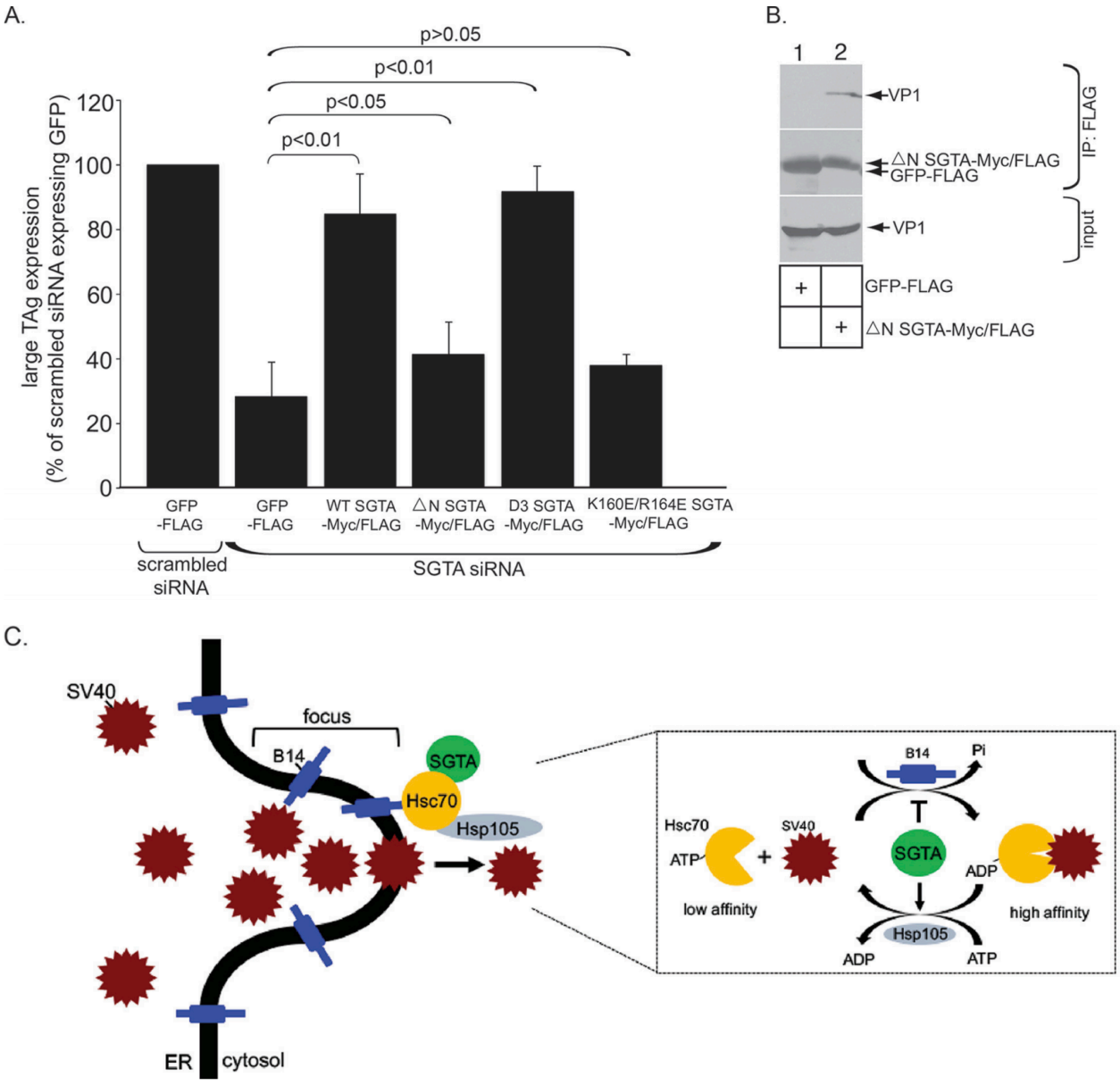
A.
p>0.05
p<0.01
p<0.05
p<0.01
large TAg expression
(% of scrambled siRNA expressing GFP)
120
100
80
60
40
20
0
GFP -FLAG
GFP -FLAG
WT SGTA -Myc/FLAG
△N SGTA -Myc/FLAG
D3 SGTA -Myc/FLAG
K160E/R164E SGTA -Myc/FLAG
scrambled siRNA
SGTA siRNA
B.
1 2
VP1
△N SGTA-Myc/FLAG
GFP-FLAG
IP: FLAG
VP1
input
+
GFP-FLAG
+
△N SGTA-Myc/FLAG
C.
SV40
focus
B14
SGTA
Hsc70
Hsp105
ER
cytosol
Hsc70
ATP
low affinity
SV40
B14
Pi
SGTA
ADP
high affinity
Hsp105
ADP
ATP

FIG. 2-6 SGTA's N-terminal domain and Hsc70-binding are essential to promote SV40 infection.

(A) CV-1 cells transfected with GFP-FLAG, WT SGTA-Myc/FLAG, or mutant SGTA-Myc/FLAG for 24 h were seeded on glass coverslips and transfected with scrambled or SGTA siRNA 1. Following 24 h of siRNA transfection, cells were infected with SV40 (MOI of 1) for 20 h. Cells were then fixed, stained, and counted. Only cells expressing the FLAG protein were scored. At least 100 cells were counted per biological replicate. The graph represents means SD of at least three biological replicates.
(B) COS-7 cells were transfected with SGTA siRNA 1 for 24 h and then transfected with GFP-FLAG or ΔN SGTA-Myc/FLAG for 24 h. Following 24 h of DNA transfection, cells were infected with SV40 (MOI of 3 to 4) for 16 h. At 16 hpi, cells were cross-linked with DSP, lysed in 1% DBC, and immunoprecipitated. Samples were subjected to SDS-PAGE and immunoblotted with the indicated antibodies.
(C) A model depicting a role of SGTA-dependent regulation of Hsc70 during ER extraction and cytosol arrival of the virus. The focus represents the postulated cytosol entry site for the virus. The inset shows two possible mechanisms by which SGTA controls SV40-Hsc70 interaction. See Discussion for more detail.

References:

1. Tsai B. 2007. Penetration of nonenveloped viruses into the cytoplasm. Annu Rev Cell Dev Biol 23:23–43. doi:10.1146/annurev.cellbio.23.090506.123454.

2. Poranen MM, Daugelavicius R, Bamford DH. 2002. Common principles in viral entry. Annu Rev Microbiol 56:521–538. doi:10.1146/annurev.micro.56.012302.160643.

3. Liddington RC, Yan Y, Moulai J, Sahli R, Benjamin TL, Harrison SC. 1991. Structure of simian virus 40 at 3.8-Å resolution. Nature 354:278–284. doi:10.1038/354278a0.

4. Stehle T, Yan Y, Benjamin TL, Harrison SC. 1994. Structure of murine polyomavirus complexed with an oligosaccharide receptor fragment. Nature 369:160–163. doi:10.1038/369160a0.

5. Stehle T, Harrison SC. 1996. Crystal structures of murine polyomavirus in complex with straight-chain and branched-chain sialyloligosaccharide receptor fragments. Structure 4:183–194. doi:10.1016/S0969-2126(96)00021-4.

6. Chen XS, Stehle T, Harrison SC. 1998. Interaction of polyomavirus internal protein VP2 with the major capsid protein VP1 and implications for participation of VP2 in viral entry. EMBO J 17:3233–3240. doi:10.1093/emboj/17.12.3233.

7. Smith AE, Lilie H, Helenius A. 2003. Ganglioside-dependent cell attachment and endocytosis of murine polyomavirus-like particles. FEBS Lett 555:199–203. doi:10.1016/S0014-5793(03)01220-1.

8. Tsai B, Gilbert JM, Stehle T, Lencer W, Benjamin TL, Rapoport TA. 2003. Gangliosides are receptors for murine polyoma virus and SV40. EMBO J 22:4346–4355. doi:10.1093/emboj/cdg439.

9. Low JA, Magnuson B, Tsai B, Imperiale MJ. 2006. Identification of gangliosides GD1b and GT1b as receptors for BK virus. J Virol 80:1361–1366. doi:10.1128/JVI.80.3.1361-1366.2006.

10. Campanero-Rhodes MA, Smith A, Chai W, Sonnino S, Mauri L, Childs RA, Zhang Y, Ewers H, Helenius A, Imberty A, Feizi T. 2007. N-glycolyl GM1 ganglioside as a receptor for simian virus 40. J Virol 81:12846–12858. doi:10.1128/JVI.01311-07.

11. Qian M, Cai D, Verhey KJ, Tsai B. 2009. A lipid receptor sorts polyomavirus from the endolysosome to the endoplasmic reticulum to cause infection. PLoS Pathog 5:e1000465. doi:10.1371/journal.ppat.1000465

12. Engel S, Heger T, Mancini R, Herzog F, Kartenbeck J, Hayer A, Helenius A. 2011. Role of endosomes in simian virus 40 entry and infection. J Virol 85:4198–4211. doi:10.1128/JVI.02179-10.

13. Kartenbeck J, Stukenbrok H, Helenius A. 1989. Endocytosis of simian virus 40 into the endoplasmic reticulum. J Cell Biol 109:2721–2729. doi:10.1083/jcb.109.6.2721.

14. Inoue T, Tsai B. 2011. A large and intact viral particle penetrates the endoplasmic reticulum membrane to reach the cytosol. PLoS Pathog 7:e1002037. doi:10.1371/journal.ppat.1002037.

15. Nakanishi A, Clever J, Yamada M, Li PP, Kasamatsu H. 1996. Association with capsid proteins promotes nuclear targeting of simian virus 40 DNA. Proc Natl Acad Sci U S A 93:96–100. doi:10.1073/pnas.93.1.96.

16. Schelhaas M, Malmstrom J, Pelkmans L, Haugstetter J, Ellgaard L, Grunewald K, Helenius A. 2007.Simian virus 40 depends on ER protein folding and quality control factors for entry into host cells. Cell131:516–529. doi:10.1016/j.cell.2007.09.038.

17. Walczak CP, Tsai B. 2011. A PDI family network acts distinctly and coordinately with ERp29 to facilitate polyomavirus infection. J Virol 85:2386–2396. doi:10.1128/JVI.01855-10.

18. Inoue T, Dosey A, Herbstman JF, Ravindran MS, Skiniotis G, Tsai B. 2015. ERdj5 reductase cooperates with protein disulfide isomerase to promote simian virus 40 endoplasmic reticulum membrane translocation. J Virol 89:8897–8908. doi:10.1128/JVI.00941-15.

19. Magnuson B, Rainey EK, Benjamin T, Baryshev M, Mkrtchian S, Tsai B. 2005. ERp29 triggers a conformational change in polyomavirus to stimulate membrane binding. Mol Cell 20:289–300. doi:10.1016/j.molcel.2005.08.034.

20. Gilbert J, Ou W, Silver J, Benjamin T. 2006. Downregulation of protein disulfide isomerase inhibits infection by the mouse polyomavirus. J Virol 80:10868–10870. doi:10.1128/JVI.01117-06.

21. Daniels R, Rusan NM, Wadsworth P, Hebert DN. 2006. SV40 VP2 and VP3 insertion into ER membranes is controlled by the capsid protein VP1: implications for DNA translocation out of the ER. Mol Cell 24:955–966. doi:10.1016/j.molcel.2006.11.001.

22. Kuksin D, Norkin LC. 2012. Disassembly of simian virus 40 during passage through the endoplasmic reticulum and in the cytoplasm. J Virol 86:1555–1562. doi:10.1128/JVI.05753-11.

23. Goodwin EC, Lipovsky A, Inoue T, Magaldi TG, Edwards AP, Van Goor KE, Paton AW, Paton JC, Atwood WJ, Tsai B, DiMaio D. 2011. BiP and multiple DNAJ molecular chaperones in the endoplasmic reticulum are required for efficient simian virus 40 infection. mBio 2:e00101–00111. doi:10.1128/mBio.00101-11.

24. Walczak CP, Ravindran MS, Inoue T, Tsai B. 2014. A cytosolic chaperone complexes with dynamic membrane J-proteins and mobilizes a nonenveloped virus out of the endoplasmic reticulum. PLoS Pathog10:e1004007. doi:10.1371/journal.ppat.1004007.

25. Ravindran MS, Bagchi P, Inoue T, Tsai B. 2015. A nonenveloped virus hijacks host disaggregation machinery to translocate across the endoplasmic reticulum membrane. PLoS Pathog 11:e1005086. doi:10.1371/journal.ppat.1005086.

26. Kampinga HH, Craig EA. 2010. The HSP70 chaperone machinery: J proteins as drivers of functional specificity. Nat Rev Mol Cell Biol 11:579–592. doi:10.1038/nrm2941.

27. Lencer WI, Tsai B. 2003. The intracellular voyage of cholera toxin: going retro. Trends Biochem Sci28:639–645. doi:10.1016/j.tibs.2003.10.002.

28. Bernardi KM, Forster ML, Lencer WI, Tsai B. 2008. Derlin-1 facilitates the retro-translocation of cholera toxin. Mol Biol Cell 19:877–884. doi:10.1091/mbc.E07-08-0755.

29. Williams JM, Inoue T, Chen G, Tsai B. 2015. The nucleotide exchange factors Grp170 and Sil1 induce cholera toxin release from BiP to enable retrotranslocation. Mol Biol Cell 26:2181–2189. doi:10.1091/mbc.E15-01-0014.

30. Bagchi P, Walczak CP, Tsai B. 2015. The endoplasmic reticulum membrane J protein C18 executes a distinct role in promoting simian virus 40 membrane penetration. J Virol 89:4058–4068. doi:10.1128/JVI.03574-14.

31. Tobaben S, Thakur P, Fernandez-Chacon R, Sudhof TC, Rettig J, Stahl B. 2001. A trimeric protein complex functions as a synaptic chaperone machine. Neuron 31:987–999. doi:10.1016/S0896-6273(01)00427-5.

32. Angeletti PC, Walker D, Panganiban AT. 2002. Small glutamine-rich protein/viral protein U-binding protein is a novel cochaperone that affects heat shock protein 70 activity. Cell Stress Chaperones 7:258–268. doi:10.1379/1466-1268(2002)007<0258:SGRPVP>2.0.CO;2.

33. Chartron JW, Gonzalez GM, Clemons WM Jr. 2011. A structural model of the Sgt2 protein and its interactions with chaperones and the Get4/Get5 complex. J Biol Chem 286:34325–34334. doi:10.1074/jbc.M111.277798.

34. Chartron JW, VanderVelde DG, Clemons WM Jr. 2012. Structures of the Sgt2/SGTA dimerization domain with the Get5/UBL4A UBL domain reveal an interaction that forms a conserved dynamic interface. Cell Rep 2:1620–1632. doi:10.1016/j.celrep.2012.10.010.

35. Xu Y, Cai M, Yang Y, Huang L, Ye Y. 2012. SGTA recognizes a noncanonical ubiquitin-like domain in the Bag6-Ubl4A-Trc35 complex to promote endoplasmic reticulum-associated degradation. Cell Rep2:1633–1644 doi:10.1016/j.celrep.2012.11.010.

36. Darby JF, Krysztofinska EM, Simpson PJ, Simon AC, Leznicki P, Sriskandarajah N, Bishop DS, Hale LR, Alfano C, Conte MR, Martinez-Lumbreras S, Thapaliya A, High S, Isaacson RL. 2014. Solution structure of the SGTA dimerization domain and investigation of its interactions with the ubiquitin-like domains of BAG6 and UBL4A. PLoS One 9:e113281. doi:10.1371/journal.pone.0113281.

37. Liou ST, Wang C. 2005. Small glutamine-rich tetratricopeptide repeat-containing protein is composed of three structural units with distinct functions. Arch Biochem Biophys 435:253–263. doi:10.1016/j.abb.2004.12.020.

38. Roberts JD, Thapaliya A, Martinez-Lumbreras S, Krysztofinska EM, Isaacson RL. 2015. Structural and functional insights into small, glutamine-rich, tetratricopeptide repeat protein alpha. Front Mol Biosci 2:71. doi:10.3389/fmolb.2015.00071.

39. Wu SJ, Liu FH, Hu SM, Wang C. 2001. Different combinations of the heat-shock cognate protein 70 (hsc70) C-terminal functional groups are utilized to interact with distinct tetratricopeptide repeat-containing proteins. Biochem J 359:419–426. doi:10.1042/bj3590419.

40. Dragovic Z, Broadley SA, Shomura Y, Bracher A, Hartl FU. 2006. Molecular chaperones of the Hsp110 family act as nucleotide exchange factors of Hsp70s. EMBO J 25:2519–2528. doi:10.1038/sj.emboj.7601138.

41. Raviol H, Bukau B, Mayer MP. 2006. Human and yeast Hsp110 chaperones exhibit functional differences. FEBS Lett 580:168–174. doi:10.1016/j.febslet.2005.11.069.

42. Cziepluch C, Kordes E, Poirey R, Grewenig A, Rommelaere J, Jauniaux JC. 1998. Identification of a novel cellular TPR-containing protein, SGT, that interacts with the nonstructural protein NS1 of parvovirus H-1. J Virol 72:4149–4156.

43. Yin H, Wang H, Zong H, Chen X, Wang Y, Yun X, Wu Y, Wang J, Gu J. 2006. SGT, a Hsp90β binding partner, is accumulated in the nucleus during cell apoptosis. Biochem Biophys Res Commun 343:1153–1158. doi:10.1016/j.bbrc.2006.03.090.

Chapter 3: Bag2 is a Component of the Cytosolic Extraction Machinery That Promotes Membrane Penetration of a Nonenveloped Virus

Introduction

Enveloped and nonenveloped viruses must devise strategies to penetrate a host membrane in order to cause infection. However, this process is likely intrinsically different between the two. For an enveloped virus, encasement in a lipid bilayer allows membrane fusion between viral and host membranes (1). In contrast, a nonenveloped virus, which lacks a surrounding lipid bilayer, must mount an alternative strategy for membrane penetration (1,2). Although this process is poorly understood, key strategies are becoming clearer. To prime the membrane transport process, a nonenveloped virus undergoes conformational changes induced by host factors (proteases, chaperones, and reductases) or the environment (low pH) at the membrane penetration site. These conformational changes can generate a hydrophobic viral particle that enables the virus to bind to and integrate into the limiting membrane. To complete membrane penetration, recent studies suggest a new strategy in which host factors are in fact exploited to "pull" a nonenveloped virus across the membrane (3,4), but this last step of nonenveloped virus membrane transport remains enigmatic.

The nonenveloped polyomaviruses (PyVs) are highly prevalent and cause significant diseases in immunocompromised individuals (5,6). Due to its structural and genetic similarities to human PyV, studies on the simian PyV simian virus 40 (SV40) have provided significant insights into the cellular infection pathway of its human

counterparts. Structurally, SV40 is composed of 72 VP1pentamers that encase the viral DNA genome (7-9). To maintain stability, these pentamers are linked by disulfide bonds, as well as noncovalent interactions established when the VP1 C-terminal arm extends from one pentamer to an adjacent pentamer (7,8). Each VP1 pentamer harbors a hydrophobic VP2 or VP3 protein (7,8,10). SV40 infection is initiated when the virus binds to the ganglioside GM1 receptor at the plasma membrane (11-13). Upon endocytosis, the virus is delivered in a retrograde manner to endosomal compartments (14) and then to the endoplasmic reticulum (ER), where it penetrates the ER membrane in order to reach the cytosol (14-17). From the cytosol, the virus continues into the nucleus, where replication and transcription of the viral genome occur (18,19). In the ER, SV40 and other PyV family members experience conformational changes resulting from interactions with ER-resident chaperones that unfold the VP1 capsid and redox enzymes that reduce and isomerize the capsid disulfide bonds (20-24). These events render the virus hydrophobic by exposing underlying VP2 and VP3, allowing insertion of the virus into the ER membrane (25-27). Our laboratory previously identified the fact that ER membrane J proteins (B12, B14, and C18) act as docking sites to recruit a cytosolic chaperone complex that functions to extract SV40 from the ER into the cytosol (3, 4, 28). To date, the established components of this protein complex are Hsc70, SGTA, and Hsp105 (3, 4, 28).

In one model describing the extraction process, Hsc70 binds to the membrane-embedded SV40 when the ER membrane J proteins convert ATP-Hsc70 to ADP-Hsc70, which displays a high substrate-binding affinity. Once ADP-Hsc70 has reverted to ATP-Hsc70 via the action of a nucleotide exchange factor (NEF), ATP-Hsc70 releases SV40

due to its low affinity for the substrate. Iterative cycles of binding to and release from Hsc70 eject the virus into the cytosol. In the context of this reaction, SGTA regulates Hsc70's ability to engage SV40 (28) and binds directly to SV40 (3), while Hsp105 promotes SV40 disassembly, which likely facilitates the virus extraction process (4).

Here, we report that the Bag2 NEF is a novel component of the cytosolic virus extraction machinery. Using both cell-based and *in vitro* assays performed under loss-of-function conditions, our findings reveal that Bag2 is necessary for SV40 extraction from the ER into the cytosol because it acts as a NEF to trigger SV40 release from Hsc70, thereby enabling the virus to successfully reach the cytosol. These findings underscore the importance of host NEF activity during SV40 infection and reveal additional insights into the molecular mechanism of nonenveloped virus membrane penetration.

Materials and Methods

Antibodies

Endogenous Bag2, PDI, anti-VP1, and anti-S antibodies were purchased from Abcam (Cambridge, MA). Hsc70 and BAP31 antibodies were purchased from Invitrogen (Carlsbad, CA). Actin antibody was purchased from Cell Signaling (Danvers, MA). Anti-FLAG antibody was purchased from Sigma (St. Louis, MO). Monoclonal large T antigen Hsp90, and Hsp105 antibodies were purchased from Santa Cruz Biotechnology (Santa Cruz, CA). Anti-B12 antibody was purchased from Proteintech Group (Chicago, IL).

Reagents

FLAG M2 antibody-conjugated beads, phenylmethylsulfonyl fluoride (PMSF), and Triton X-100 were purchased from Sigma-Aldrich (St. Louis, MO). S protein-conjugated beads

and digitonin were purchased from EMD Millipore Chemicals (San Diego, CA). Opti-MEM and 0.25% trypsin were purchased from Invitrogen (Carlsbad, CA). Prolong Diamond antifade mount with DAPI (4′,6-diamidino-2-phenylindole) mounting reagent was purchased from Thermo Fisher (Carlsbad, CA). Phosphate-buffered saline (PBS) (1×) was purchased from Gibco (Carlsbad, CA). Purified Hsc70 was purchased from StressMarq Biosciences (Victoria, British Columbia, Canada), and purified Bag2 was purchased from Fitzgerald Industries International (Acton, MA). Magnetic protein G-conjugated Dynabeads were purchased from ThermoFisher (Carlsbad, CA).

Cells

CV-1, COS-7, and HEK 293T (ATCC) cells were cultured in complete Dulbecco's modified Eagle medium (cDMEM) supplemented with 10% fetal bovine serum (FBS), 10 U/ml penicillin, and 10 μg/ml streptomycin from Gibco (Carlsbad, CA).

DNA plasmid and siRNA transfection

To generate a Bag2 expression construct, Bag2 was cloned from a 293T cDNA library and amplified by PCR. PCR fragments were then inserted into a pcDNA3.1(−) backbone. To generate an siRNA-resistant Bag2 construct, overlapping PCR was performed using the following primers: forward, CTCCGTGGAGACTATCAGGAATCCCCAGCAGCAAGAATCCCT, and reverse, ATTCCTGATAGTCTCCACGGAGACTTCAACGGTGAGAGTTCT.

The amplified Bag2 fragment generates the following silent mutations (underlined): GTC TCC GTG GAGACT ATC AGG AAT. The I160A Bag2 mutant was generated using point mutagenesis at residue I160, as previously reported (32). All the Bag2 constructs were inserted into the pcDNA3.1(−) backbone harboring a C-terminal FLAG

tag and subjected to DNA sequencing to confirm the sequence. The Bag2 siRNA sequence is 5′-GUUGGCUUUAGCGUUGAUCUUCGCCUG-3′ (Life Technologies), and the scrambled siRNA sequence is that of the “all-star negative” siRNA from Qiagen. All DNA and siRNA transfections were incubated for at least 24 h.

Preparation of SV40

Purified SV40 preparation using the OptiPrep gradient system (Sigma) has been described previously (33).

Immunoprecipitation

For affinity purification of S-tagged J proteins, HEK 293T cells were seeded in 6-cm plates. The cells were transfected or not with B12-S, B14-S, C18-S, or GFP-S for 24 h in polyethyleneimine (PEI) and Opti-MEM and lysed in 1% Triton X-100 in physiological buffer (50 mM HEPES, pH 7.4, 150 mM NaCl, and phenylmethylsulfonyl fluoride [PMSF]) at 4°C. Postlysis, the cells were centrifuged at 16,000 rpm at 4°C for 10 min. The supernatant was collected and rotated at 4°C for 2 h with S protein-conjugated beads. The beads were washed three times and boiled in 5× SDS sample buffer before being subjected to SDS-PAGE and immunoblotting. For immunoprecipitation of endogenous B12, cells were lysed, and the resulting lysate was incubated with an antibody against B12 (or a nonspecific IgG control antibody). The lysates were then incubated with protein A agarose beads for 2 h. The precipitated materials were processed as described above. For immunoprecipitation of FLAG-tagged proteins, HEK 293T cells were seeded in 6-cm plates and transfected with FLAG-tagged constructs in PEI and Opti-MEM for 24 h. The cells were lysed in 1% Triton X-100 in a physiological buffer at 4°C for 10 min and centrifuged at 16,000 rpm at 4°C for 10 min. The

supernatant was collected and rotated at 4°C for 2 h with M2 FLAG-conjugated beads. The precipitated materials were processed as described above. To examine the interaction between SV40 and Hsc70 under Bag2 knockdown conditions, COS-7 cells were seeded in 6-cm plates and treated with either 50 nM Bag2 siRNA or a scrambled siRNA. After 24 h, the cells were transfected with Hsc70-S for 24 h. The cells were then infected with SV40 (multiplicity of infection [MOI], ~20 to 30) for 16 h before being lysed in 1% Triton X-100 in a physiological buffer at 4°C for 10 min. The cells were then centrifuged at 16,000 rpm for 10 min at 4°C. The supernatant was collected and rotated with S protein-conjugated beads for 2 h at 4°C. After 2 h, the beads were washed three times in lysis buffer. The beads were then treated with 5× SDS sample buffer and subjected to SDS-PAGE and immunoblotting. The graph in Fig. 3-5B represents three biological replicates, and the VP1 band was quantified using Image J software (National Institutes of Health) and normalized to affinity-purified Hsc70-S.

SV40 infection

CV-1 cells (3×10^5) were seeded and transfected with 50 nM Bag2 siRNA, 25 nM Hsp105 siRNA, or 50 nM scrambled siRNA (along with Opti-MEM and RNAiMax) onto glass coverslips in 6-well plates. The cells were incubated at 37°C for 48 h. For knockdown-rescue experiments, 1.5×10^5CV-1 cells were seeded and transfected using siRNA as described above. After 24 h of siRNA transfection, the cells were washed and transfected with the indicated FLAG-tagged constructs using Fugene and Opti-MEM, totaling 48 h of siRNA knockdown before infection. After 48 h, cells were infected with purified SV40 (MOI, ~0.5 to 1.5) for 24 h. After 24 h, the cells were fixed in 1% paraformaldehyde (PFA) for 15 min, permeabilized in 0.2% Triton X-100 for 5 min, and

incubated with rabbit anti-FLAG and mouse anti-large T antigen antibodies for 1 h at 25°C. The cells were then washed and incubated with anti-rabbit (Alexa Fluor 488) and anti-mouse (Alexa Fluor 594) antibodies in the dark at 25°C for 30 min. The cells were washed, dried, and mounted on slides using Prolong Diamond antifade mount with DAPI (Invitrogen). For evaluating SV40 infection in cells without DNA transfection, at least 1,000 cells were counted per condition. To assess SV40 infection in cells transfected with DNA, at least 100 cells were counted per condition. The graphs in Fig. 3-2B, 3-2C and 3-6A represent the mean and standard deviation (SD) of at least 3 biological replicates, with paired Student two-tailed *t* tests used to determine the *P* values.

ER-to-cytosol transport assay

The protocol for the ER-to-cytosol transport assay has been described previously (33). Briefly, CV-1 cells were seeded in 6-cm plates and transfected with 50 nM Bag2 siRNA, 50 nM scrambled siRNA, or 25 nM Hsp105 siRNA for 24 h. After 24 h, the cells were infected with purified SV40 (MOI, ~1 to 5) for 16 h. The cells were then treated with 0.1% digitonin and centrifuged. The resulting supernatant fraction represented the cytosol fraction, while the pellet fraction represented the membrane fraction. When the membrane fraction was treated with 1% Triton X-100 and the extracted material was isolated, the fraction then contained ER-localized SV40. The VP1 band intensity was quantified using Image J software (National Institutes of Health) and normalized to Hsp90 loading control bands.

Focus formation assay

The focus formation assay method has been described previously (3, 4, 30). Briefly, control or knocked-down cells were fixed 16 h postinfection (hpi) (MOI, ~1 to 5) and stained with anti-rat BAP31 and anti-mouse VP1 antibodies for 1 h at 25°C. The cells were then washed and incubated with anti-mouse (Alexa Fluor 488) and anti-rat (Alexa Fluor 594) antibodies in the dark at 25°C for 30 min. For the knockdown-rescue focus formation assay, cells were transfected with siRNA as described above for 24 h, followed by DNA transfection of the indicated constructs for 24 h. The cells were fixed as described above and stained with anti-rat BAP31 and anti-rabbit FLAG and S antibodies. The cells were washed and incubated with anti-rat (Alexa Fluor 594) and anti-rabbit (Alexa Fluor 488) antibodies as described above. At least 100 cells were counted per condition, and 3 biological replicates were completed. The graphs in Fig. 3-4C and 3-6B represent the means and standard deviations of at least 3 biological replicates, with paired Student two-tailed *t* tests used to determine *P* values. Using Image J (National Institutes of Health), the VP1 focus size was measured by transforming images to 8 bits, adjusting the threshold, and processing the images as binary with watershed. The focus size was then quantified in pixels squared.

Bag2-dependent release of Hsc70 from SV40

To isolate the Hsc70-SV40 complex, 1 µg of Hsc70, 250 ng of SV40, 1 mM $MgCl_2$, 2 mM ATP, and 1 mM DTT were incubated at 37°C in 0.1% Triton X-100 in PBS for 30 min. Anti-VP1 antibody was added to the samples for 30 min at 25°C, followed by addition of magnetic protein G Dynabeads for 30 min at 25°C. The beads were then washed 2 times in PBS. The beads then harbored the Hsc70-SV40 complex. To induce release of Hsc70 from SV40, purified Bag2 was added to samples at the indicated

concentrations in the presence of 1 mM $MgCl_2$, 1 mM KCl, and 2 mM ATP at 25°C for 10 min. The beads were subsequently washed 2 times in PBS, boiled in 5× SDS running buffer for 10 min, and subjected to silver staining.

Results

Bag2 binds to ER membrane J proteins.

Through a previously reported unbiased RNA interference (RNAi) screen, the ER membrane J proteins DNAJB12 (B12), DNAJB14 (B14), and DNAJC18 (C18) were found to be essential in promoting ER-to-cytosol membrane transport of SV40 (29). Using a biochemical protein-protein interaction strategy, the components of a cytosolic protein complex composed of Hsc70, SGTA, and Hsp105 were subsequently identified as binding partners of these three ER membrane J proteins that function to extract SV40 from the ER into the cytosol (3, 4, 28, 30). Whether additional cytosolic components play a role in this virus membrane transport process is unknown.

In this context, we previously reported that when 3×FLAG-tagged B12 (3×FLAG-B12) stably expressed in a 293T cell line was immunoprecipitated and the precipitated material was subjected to mass spectrometry analysis, peptides corresponding to the cytosolic NEF Bag2 were identified (31) (Fig. 3-1A). Likewise, when 3×FLAG-C18 stably expressed in a 293T cell line was immunoprecipitated and the precipitated sample was analyzed by mass spectrometry, Bag2-derived peptides were also found (Fig. 3-1A). A similar analysis for 3×FLAG-B14 was not performed. These findings raise the possibility that Bag2 represents a novel binding partner of B12/C18. To test this, S-tagged B12 (B12-S), B14 (B14-S), C18 (C18-S), and the control green fluorescent protein (GFP)

(GFP-S) were transiently transfected in 293T cells; the S-tagged protein was affinity purified (AP); and the AP sample was subjected to SDS-PAGE, followed by immunoblotting. We found that endogenous Bag2 coprecipitated with B12-S, B14-S, and C18-S but minimally with GFP-S (Fig. 3-1B, top row), suggesting that Bag2 interacts with the ER membrane J proteins. Moreover, endogenous Bag2 can also bind to endogenous B12 (Fig. 3-1C, top row), indicating that this interaction is not an overexpression artifact. These results demonstrate that the ER membrane J proteins interact with Bag2.

A J protein binds to and stimulates the ATPase activity of Hsc70 to generate ADP-Hsc70, while a NEF associates with Hsc70, converting ADP-Hsc70 to ATP-Hsc70. In this scenario, Hsc70 bridges the interaction between a J protein and a NEF. Accordingly, we asked if B12's interaction with Bag2 depends on Hsc70. To test this, we transfected 293T cells with either a FLAG-tagged B12 mutant that cannot bind to Hsc70 (QPD B12-FLAG), wild-type B12 (WT B12-FLAG), or the control GFP (GFP-FLAG) construct. When the FLAG-tagged proteins were immunoprecipitated, endogenous Hsc70 was found in the WT B12-FLAG- but not the QPD B12-FLAG-precipitated sample (Fig. 3-1D, second row from top), indicating that WT B12, but not QPD B12, binds to Hsc70, as previously reported (31). Importantly, endogenous Bag2 was observed in the WT B12-FLAG-precipitated but minimally in the QPD B12-FLAG-precipitated material (Fig. 3-1D, top row). These results suggest that B12's interaction with Bag2 depends on Hsc70.

To corroborate these data, we performed the reverse experiment in which a Bag2 mutant previously shown to lack Hsc70 binding (I160A Bag2*) (32) (the asterisk in

the Bag2 constructs indicates that the backbone Bag2 sequence was modified, rendering it resistant to a Bag2-specific small interfering RNA [siRNA] [see Materials and Methods]) was tested for its ability to associate with B12. Indeed, endogenous B12 and Hsc70 were pulled down when transfected FLAG-tagged WT Bag2 (WT Bag2*-FLAG), but not I160A Bag2 (I160A Bag2*-FLAG), was precipitated (Fig. 3-1E, top and second panels). Collectively, these findings demonstrate that the B12-Bag2 interaction is mediated by Hsc70.

Bag2 promotes SV40 infection.

As B12 and Hsc70 are both necessary host factors for SV40 entry, we asked if Bag2 plays a role in SV40 infection. Successful SV40 infection can be monitored by expression of the virus-encoded large T antigen in the host nucleus. Accordingly, simian CV-1 cells (used classically to study SV40 infection) were transfected with either the control siRNA (scrambled), an siRNA targeting Bag2, Hsp105 (a positive control), or both Bag2 and Hsp105 siRNAs. The levels of Bag2 and Hsp105 proteins under the knockdown conditions are shown in Fig. 3-2A. When these cells were incubated with SV40 and analyzed by immunofluorescence microscopy, we found that SV40 infection robustly decreased in Bag2-depleted cells (Fig. 3-2B), similar to the extent observed when Hsp105 was knocked down, as previously reported (4). Simultaneous depletion of Bag2 and Hsp105 potently impaired virus infection, although it did not appear to exacerbate the single-knockdown phenotype. This finding suggests that neither NEF is sufficient to support SV40 infection.

To ensure that the block in SV40 infection in Bag2 siRNA-treated cells is specifically a result of depleting Bag2 and is not due to unintended off-target effects, we performed a knockdown-rescue experiment. To this end, cells transfected with either scrambled or Bag2 siRNA were cotransfected with either GFP-FLAG, WT Bag2*-FLAG, or I160A Bag2*-FLAG. The cells were incubated with SV40, and large T antigen expression was assessed in FLAG-expressing cells. Using this approach, we found that expressing WT, but not I160A, Bag2 largely restored SV40 infection in Bag2-depleted cells (Fig. 3-2C), indicating that the decrease in SV40 infection resulting from the Bag2 siRNA is due to the loss of Bag2. These data demonstrate that Bag2 promotes SV40 infection, and this is dependent on Bag2's ability to interact with Hsc70.

Bag2 is important for ER-to-cytosol transport of SV40.

As Bag2 is recruited to the ER membrane J proteins via Hsc70 (Fig. 3-1), we envision that Bag 2 is strategically localized to promote cytosol entry of SV40 from the ER membrane. To test this, we employed a cell-based, semipermeabilization assay that detects SV40 arrival in the cytosol from the ER. This assay, developed in our laboratory, is routinely used to characterize ER-to-cytosol membrane transport of PyV family members (33). In the assay, cells are treated with the gentle detergent digitonin, which permeabilizes the plasma membrane while maintaining the membrane integrity of intracellular organelles. Centrifugation of the semipermeabilized cells generates two fractions, a supernatant fraction that contains cytosolic proteins and virus that successfully reached the cytosol from the ER (cytosol), and a pellet fraction that harbors membranes, including the ER and virus that is trapped in the ER (membrane). Using

this method, cytosolic Hsp90 largely partitioned to the cytosol fraction (Fig. 3-3A, compare 2nd row to 7th row), while ER-resident PDI remained in the membrane fraction (Fig 3-3A compare 8th row to 3rd row), verifying the integrity of the fractionation protocol. Importantly, under these conditions, we found that the level of SV40 VP1 in the cytosol decreased markedly when Bag2 was knocked down (Fig. 3-3A, top row; the VP1 band intensity in the cytosol fraction is quantified in panel B), similar to the effect observed when Hsp105 is depleted, as previously reported (4). Using a biochemical extraction approach designed to isolate ER-localized SV40 from the membrane fraction (see Materials and Methods), we found that knockdown of neither Bag2 nor Hsp105 significantly affected the level of ER-localized SV40 (Fig. 3-3A, 9th row), indicating that these cytosolic factors do not facilitate ER arrival of the virus from the cell surface. Hence, Bag2 plays an important role in promoting cytosol entry of SV40 from the ER, consistent with its function in supporting SV40 infection (Fig. 3-2).

Depletion of Bag2 traps SV40 in the ER-to-cytosol membrane penetration site.

As an independent approach to evaluate whether Bag2 promotes extraction of SV40 from the ER into the cytosol, we used a microscopy-based strategy. We and others previously demonstrated that upon reaching the ER, SV40 reorganizes selective ER membrane proteins (including the membrane J proteins and the BAP31 ER membrane protein) to distinct punctate structures in the ER harboring the virus, called foci (3, 4, 17, 30). Our findings further suggest that these virus-induced foci act as cytosol entry sites (3, 4, 30). We therefore reasoned that if Bag2 extracts SV40 from the ER into the cytosol, depletion of Bag2 should trap the virus in the foci, consequently

augmenting this virus-containing structure. To test this, CV-1 cells transfected with either the scrambled or Bag2 siRNA were infected with SV40 and stained for SV40 VP1 and BAP31. Indeed, we found that depletion of Bag2 increased the number of cells containing at least one BAP31$^+$ focus (Fig. 3-4A, compare bottom and top rows); the relative size of VP1 harbored in the BAP31$^+$ focus also increased when Bag2 was depleted(Fig. 3-4B). These findings are consistent with the idea that Bag2 plays an important role in extracting SV40 from the ER into the cytosol.

We further asked whether reexpression of WT Bag2, I160A Bag2, or HspBP1, a cytosolic NEF previously shown to be dispensable during SV40 infection (4), in Bag2-depleted cells affected focus formation. For this, CV-1 cells transfected with either the scrambled or Bag2 siRNA were cotransfected with GFP-FLAG, WT Bag2*-FLAG, I160A Bag2*-FLAG, or HspBP1-S. The cells were then infected with SV40 and stained for BAP31. Only cells expressing the FLAG-tagged (or S-tagged) protein were assessed. Again, we found that depleting Bag2 increased the number of cells containing at least one BAP31$^+$ focus (the extent of focus formation is quantified in Fig. 3-4C; representative images are shown in panel D). Importantly, add-back of WT Bag2*-FLAG, but not I160A Bag2*-FLAG or HspBP1-S, in the Bag2-depleted cells reduced the number of cells harboring at least one BAP31$^+$ focus to control levels (the extent of focus formation is quantified in Fig. 3-4C; see representative images in Fig. 3-4D). These results indicate that restoring Bag2 expression in Bag2-depleted cells can promote cytosol entry of the virus from the ER, thereby decreasing the focus structures. Thus, our microscopy-based analyses are in agreement with data from the

semipermeabilization assay, strengthening the hypothesis that Bag2 plays a decisive role in extracting SV40 from the ER into the cytosol.

Bag2 triggers release of SV40 from Hsc70.

Our data indicate that Bag2 binds to B12 via Hsc70. Because Bag2 functions as a NEF to induce substrate release from Hsc70 (32, 34), we hypothesized that Bag2 induces release of SV40 from Hsc70 to promote cytosol entry. To test this, we transfected (CV-1-derived) COS-7 cells expressing Hsc70-S with scrambled or Bag2 siRNA and precipitated Hsc70-S. (COS-7 cells were used because they support higher transfection efficiency than CV-1 cells). Importantly, under the Bag2 knockdown condition, Hsc70-S precipitated significantly more VP1 than cells treated with scrambled siRNA (Fig. 3-5A, top row; the VP1 band intensity is quantified in panel B), indicating that SV40 is trapped on Hsc70 in the absence of Bag2. This result is consistent with the hypothesis that Bag2 stimulates SV40 release from Hsc70.

To strengthen this finding, we reconstituted the virus release reaction using purified components, including Hsc70, SV40, and Bag2 (Fig. 3-5C). In the ER, SV40 undergoes disulfide bond reduction, priming it for insertion into the ER membrane (22, 23). The reductant dithiothreitol (DTT) was therefore added to purified SV40 to partially mimic this reduced viral conformation. The reduced SV40 was incubated with Hsc70, followed by pulldown of SV40 in order to isolate the SV40-Hsc70 complex. Importantly, when this complex was subsequently incubated with increasing concentrations of Bag2 in the presence of ATP and the SV40 was reisolated, the level of bound Hsc70 decreased compared to addition of a control buffer containing only ATP (Fig. 3-5D, top

row, compare lanes 2 and 3 to lane 1). These findings demonstrate that Bag2 can promote disengagement of SV40 from Hsc70 *in vitro*, in agreement with the premise that Bag2 induces the release of SV40 from Hsc70 in the intact cell.

Bag2 and Hsp105 play overlapping roles.

Our results show that depleting either Bag2 or Hsp105 inhibits SV40 infection (Fig. 3-2B). Because Hsp105 is also a NEF of Hsc70 (35-37), we asked if Bag2 and Hsp105 perform overlapping roles. To test this, we transfected cells with scrambled, Bag2, or Hsp105 siRNA and cotransfected the cells with either GFP-FLAG, WT Bag2*-FLAG, or Hsp105*-FLAG (Hsp105*-FLAG is a construct that is resistant to the Hsp105 siRNA). Only FLAG-expressing cells were assessed for large T antigen expression in order to evaluate SV40 infection. We found that add-back of Bag2 largely restored the decrease in SV40 infection in Bag2-depleted cells (Fig. 3-6A, compare columns 3 and 1, and 2C), while add-back of Hsp105 rescued the block in SV40 infection in Hsp105-depleted cells (Fgi. 3-6A, compare 6th and 1st columns from left), which is consistent with our previous report (4). Strikingly, expression of Hsp105 fully restored SV40 infection in Bag2-depleted cells (Fig. 3-6A, compare 4th and 1st columns from left), and likewise, expression of Bag2 rescued SV40 infection in Hsp105-depleted cells (Fig. 3-6A, compare 7th and 1st columns from left). These results indicate that Bag2 and Hsp105 display overlapping functions.

As both Bag2 (this study) and Hsp105 (4) promote the arrival of SV40 in the cytosol from the ER, we assessed if Bag2 and Hsp105 play overlapping roles at this step. To this end, cells transfected with scrambled or Bag2 siRNA were cotransfected

with GFP-FLAG, WT Bag2*-FLAG, or Hsp105*-FLAG. The cells were then infected with SV40 and stained for BAP31 and VP1 to detect formation of virus-induced focus structures that represent the virus' cytosol entry sites (Fig. 3-4A). We found that the enhanced focus formation observed in Bag2-depleted cells could be decreased to control levels by add-back of either WT Bag2*-FLAG or Hsp105*-FLAG (the extent of focus formation is quantified in Fig. 3-6B, with representative images in panel C), suggesting that SV40 trapped in the focus structure due to the absence of Bag2 can be released into the cytosol (thereby decreasing the focus structure) when Bag2 or Hsp105 is added back. These results corroborate the infection data, suggesting that the two cytosolic NEFs have overlapping functions.

Although Bag2 and Hsp105 must bind to Hsc70 to induce substrate release, whether they engage the same Hsc70 complex is unknown. We postulate that if Bag2 and Hsp105 in fact interact with the same Hsc70 complex, precipitation of Bag2 should correspondingly pull down Hsp105, and vice versa. To test this, Hsp105*-FLAG, WT Bag2*-FLAG, and the control GFP-FLAG were immunoprecipitated, and the precipitated material was subjected to immunoblotting. We found that precipitation of Hsp105*-FLAG (but not GFP-FLAG) pulled down endogenous (and transfected) Hsp105 and Hsc70, but not endogenous Bag2 (Fig. 3-6D, top three rows, lanes 2). Similarly, precipitation of WT Bag2*-FLAG coprecipitated endogenous (and transfected) Bag2 and Hsc70, but not endogenous Hsp105 (Fig. 3-6D, top three rows, lanes 3). These results suggest that Bag2 and Hsp105 may form separate Hsc70 complexes.

Discussion

Host membrane penetration is essential for successful virus infection. For a nonenveloped virus, this process remains enigmatic. In the case of the nonenveloped PyV SV40, penetration of the virus across the ER membrane to reach the cytosol represents a decisive infection step. However, the molecular basis by which host factors are exploited to extract the virus from the ER into the cytosol has yet to be fully clarified. We previously demonstrated that Hsc70, SGTA, and Hsp105 form a cytosolic chaperone-cochaperone complex that promotes cytosol entry of the virus from the ER (3, 4, 28); whether Hsp70 or additional cytosolic components participate in this virus extraction process is unknown. Here, we pinpoint the cytosolic NEF Bag2 as a novel cellular component that promotes SV40 infection by supporting viral ER-to-cytosol membrane transport. Our results indicate that Bag2 associates with Hsc70 and ER membrane J proteins to generate a protein complex that is likely distinct from the Hsp105-Hsc70-J protein complex (Fig. 3-7). Importantly, during SV40 entry, Bag2 acts as a NEF to stimulate virus release from Hsc70 in order to support cytosol entry of the virus (Fig. 3-7, inset).

Our previous mass spectrometry data raised the possibility that Bag2 interacts with the ER membrane J protein B12 (31); a similar mass spectrometry approach also suggested that C18 engages Bag2. By immunoprecipitation and affinity purification, we confirmed that Bag2 indeed binds to B12 and C18, as well as the J protein B14, demonstrating that Bag2 is a bona fide binding partner of the J proteins. Using established Hsc70 binding-defective mutants of either Bag2 or B12, our results further indicate that the Bag2-B12 interaction occurs via an Hsc70 intermediate, revealing that this interaction is coupled through the Hsc70 chaperone.

Through knockdown-rescue experiments, we found that Bag2 executes an important Hsc70-dependent function to promote SV40 infection. We then took advantage of two independent strategies—a semipermeabilized fractionation method and a microscopy-based focus-tracking assay—to demonstrate that Bag2 promotes virus extraction from the ER to the cytosol to support virus infection. Hence, by strategic positioning at the ER membrane (via engaging the Hsc70-J protein complex), Bag2 triggers cytosol entry of SV40 from the ER. Whether Bag2 impacts ER-to-cytosol membrane transport of endogenous misfolded substrates is a critical question that needs to be addressed by future experiments. In this context, it is worth noting that ER-to-cytosol membrane transport is central to a major ER-associated degradation pathway designed to remove misfolded ER-resident proteins to the cytosol for degradation by the proteasome (38). In fact, Hsc70, the J proteins, and Bag2 have already been implicated in proteasomal degradation of misfolded substrates (39-42).

Mechanistically, we demonstrated via cell-based and *in vitro* approaches that Bag2 triggers SV40 release from Hsc70, thereby promoting arrival of SV40 in the cytosol. This result is in line with Bag2's established NEF activity, which normally converts ADP-Hsc70 to ATP-Hsc70 to trigger substrate release (32). Our data thus support the hypothesis that release of SV40 from Hsc70 is necessary for successful SV40 arrival in the cytosol.

We previously found that Hsp105 is a crucial factor that stimulates cytosol entry of SV40 from the ER (4). Because Hsp105 can also act as a NEF of Hsc70 (35-37), we asked if Hsp105 and Bag2 displayed overlapping functions and found that they did. However, it is clear that neither NEF is sufficient to support SV40 infection or ER-to-

cytosol transport of the virus. Why might ER-to-cytosol transport of SV40 require two distinct NEFs that display overlapping functions? One possibility is that a threshold level of NEFs beyond what is normally provided by Bag2 or Hsp105 alone is necessary for efficient ER-to-cytosol membrane extraction of SV40. Having both Bag2 and Hsp105 thus provides a sufficiently high level of NEF to carry out the substrate release reaction. However, the observation that the HspBP1 NEF is not involved in SV40 ER membrane penetration (4) suggests that only selective cytosolic NEFs that are membrane associated are strategically positioned to extract the virus from the ER into the cytosol. Another possibility is that the different cell types infected by SV40 may harbor only one of the two NEFs, and thus, having multiple NEFs capable of regulating the same SV40 entry step would ensure successful infection. The simultaneous use of two NEFs to cross the ER membrane is not unprecedented. In fact, cholera toxin requires both ER-resident NEFs, Sil1 and Grp170, to penetrate the ER membrane during the toxin's cellular-intoxication process (43).

Single knockdown of either Bag2 or Hsp105 robustly impaired SV40 infection, indicating that both Bag2 and Hsp105 play critical roles during SV40 infection. Double knockdown of Bag2 and Hsp105 did not cause a more severe block in infection than the single-knockdown condition, although this may reflect the sensitivity of the infection assay. Regardless, this finding suggests that Bag2 and Hsp105 operate within the same pathway during SV40 entry. Because each Hsc70 interacts with only one NEF (through its single ATPase domain) at any one point and Bag2 and Hsp105 engage different Hsc70 complexes (this study), the simplest model for these data is that an individual SV40 particle simultaneously recruits multiple Bag2-Hsc70 and Hsp105-Hsc70 protein

complexes, as depicted in Fig. 3-7; the inclusion of SGTA in this model is based on our previous findings (3). We envision that iterative cycles of binding to and release from these Hsc70-dependent complexes provide the energy to extract SV40 from the ER into the cytosol. In sum, our work here identifies a novel member of a cytosolic protein complex that extracts a nonenveloped virus across a host membrane, which enables its cytosolic entry to cause infection, and provides further insights into this largely enigmatic process.

Chapter 3 Figures

A.

bait	total number of peptides corresponding to: B12	C18	Bag2
3xFLAG-B12	120	1	20
3xFLAG-C18	6	62	11

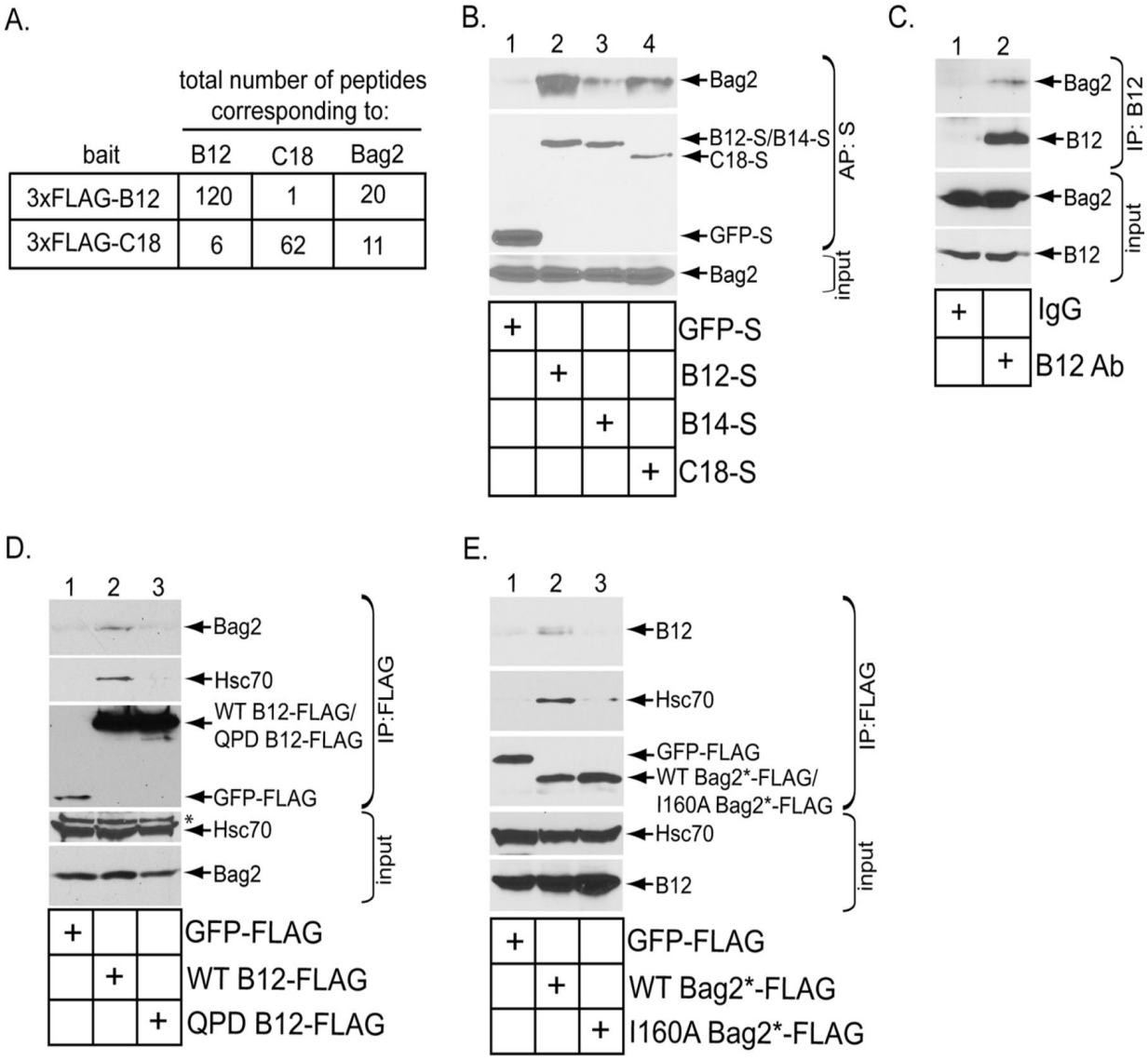

FIG 3-1 Bag2 binds to ER membrane J proteins.

(A) Total numbers of peptides corresponding to B12, C18, and Bag2 identified by mass spectrometry using 3FLAG-B12- or 3FLAG-C18-immunoprecipitated material from HEK 293T cells.
(B) HEK 293T cells were transfected with either GFP-S, B12-S, B14-S, or C18-S. The cells were lysed, and the resulting cell extracts were subjected to affinity purification and SDS-PAGE, followed by immunoblotting using the indicated antibodies. Input represents 8% of the total sample used for affinity purification.
(C) HEK 293T cell extracts were incubated with an anti-B12 or a control IgG antibody. The immunoprecipitated (IP) materials were subjected to SDS-PAGE, followed by immunoblotting using the indicated antibodies.
(D) As for panel C, except that HEK 293T cells were transfected with GFP-FLAG, B12-FLAG, or QPD B12-FLAG, and the cell extracts were incubated with FLAG antibody-conjugated agarose beads. The asterisk indicates an unidentified protein that cross-reacted with the Hsc70 antibody.
(E) As for panel C, except that HEK 293T cells were transfected with GFP-FLAG, WT Bag2*-FLAG, or I160A Bag2*-FLAG, and the cell extracts were incubated with FLAG antibody-conjugated agarose beads.

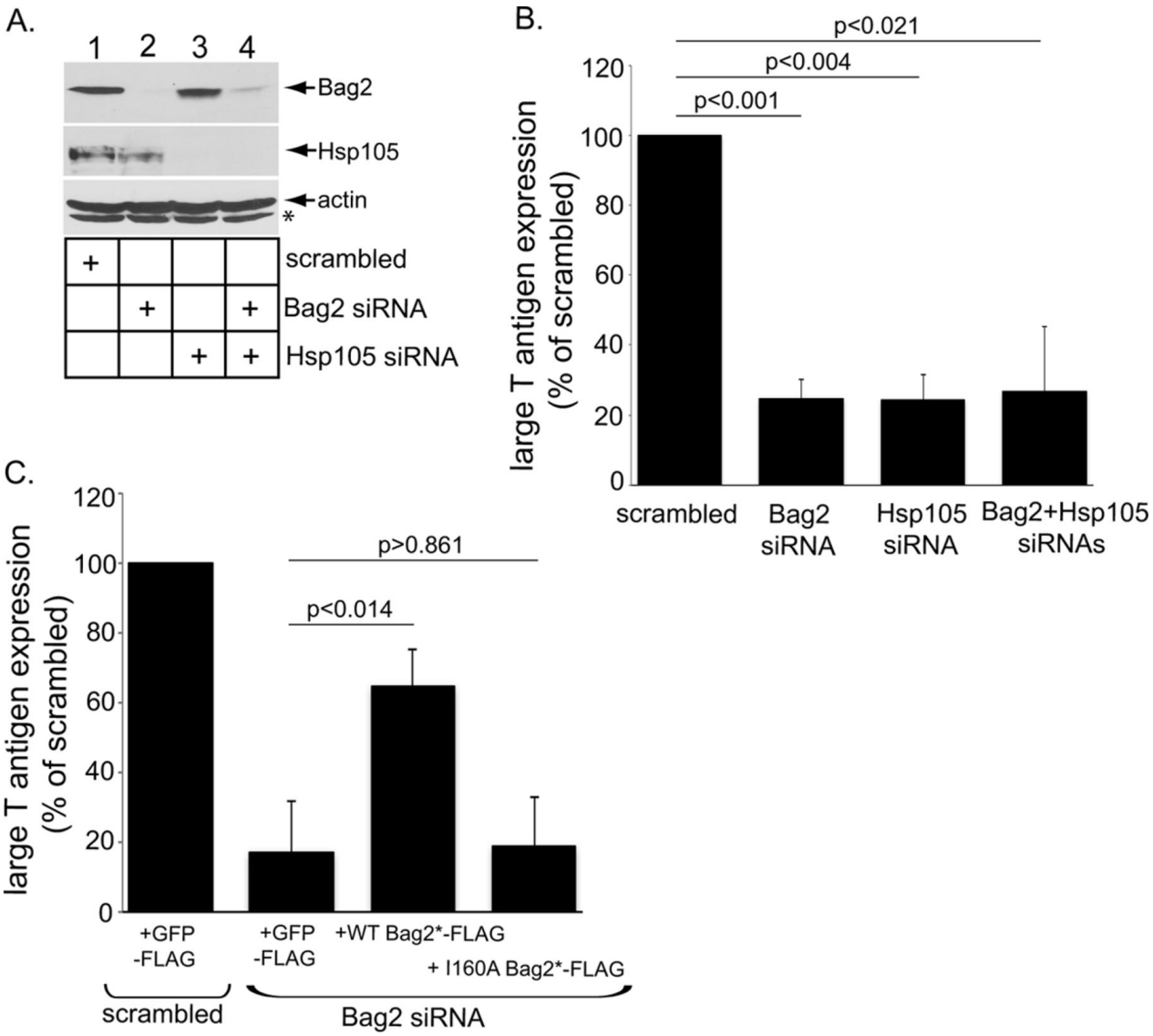
A.
1 2 3 4
Bag2
Hsp105
actin
*
scrambled
Bag2 siRNA
Hsp105 siRNA
B.
p<0.021
p<0.004
p<0.001
large T antigen expression (% of scrambled)
scrambled
Bag2 siRNA
Hsp105 siRNA
Bag2+Hsp105 siRNAs
C.
p>0.861
p<0.014
large T antigen expression (% of scrambled)
+GFP -FLAG
+GFP -FLAG
+WT Bag2*-FLAG
+ I160A Bag2*-FLAG
scrambled
Bag2 siRNA

FIG 3-2 Bag2 promotes SV40 infection.

(A) siRNA knockdown of Bag2 and Hsp105. Cell extracts derived from CV-1 cells transfected with the indicated siRNA(s) were subjected to SDS-PAGE and immunoblotting with the indicated antibodies. The asterisk indicates an unidentified protein that cross-reacted with the actin antibody.
(B) CV-1 cells transfected with the indicated siRNAs were infected with SV40; 24 hpi, the cells were permeabilized, fixed, and stained for large T antigen. At least 300 cells were counted per condition over three biological replicates. The graph represents means and SD. Student's two-tailed t test was used to determine statistical significance.
(C) As for panel B, except cells were transfected with the indicated constructs 24 h prior to infection with SV40. The cells were then fixed, permeabilized, and stained for large T antigen and FLAG. Only cells expressing the FLAG construct were counted. At least 100 cells were counted per condition over three biological replicates. The graph represents means and SD. Student's two-tailed t test was used to determine statistical significance.

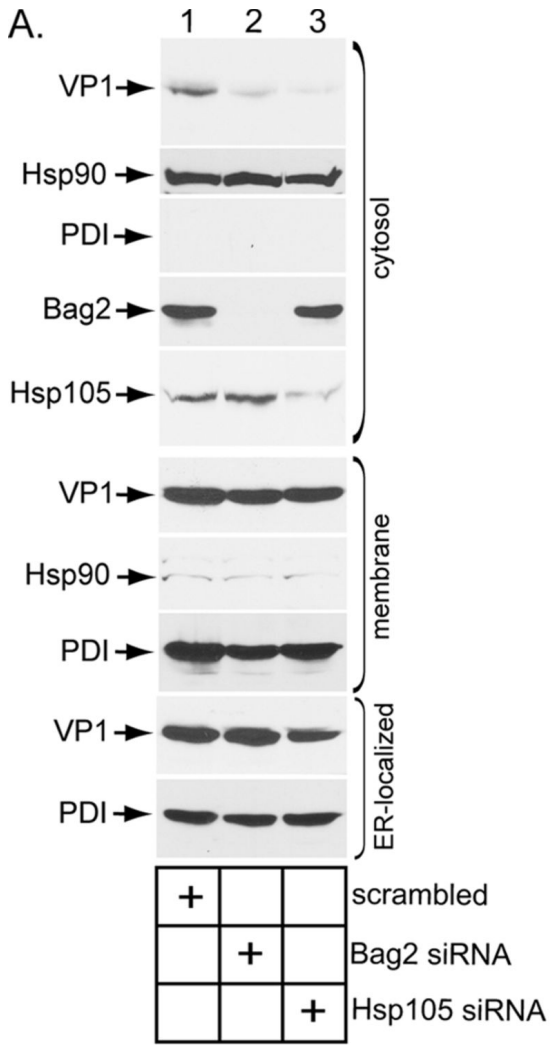
A.
1
2
3
VP1
Hsp90
PDI
Bag2
Hsp105
cytosol
VP1
Hsp90
PDI
membrane
VP1
PDI
ER-localized
+
scrambled
Bag2 siRNA
Hsp105 siRNA

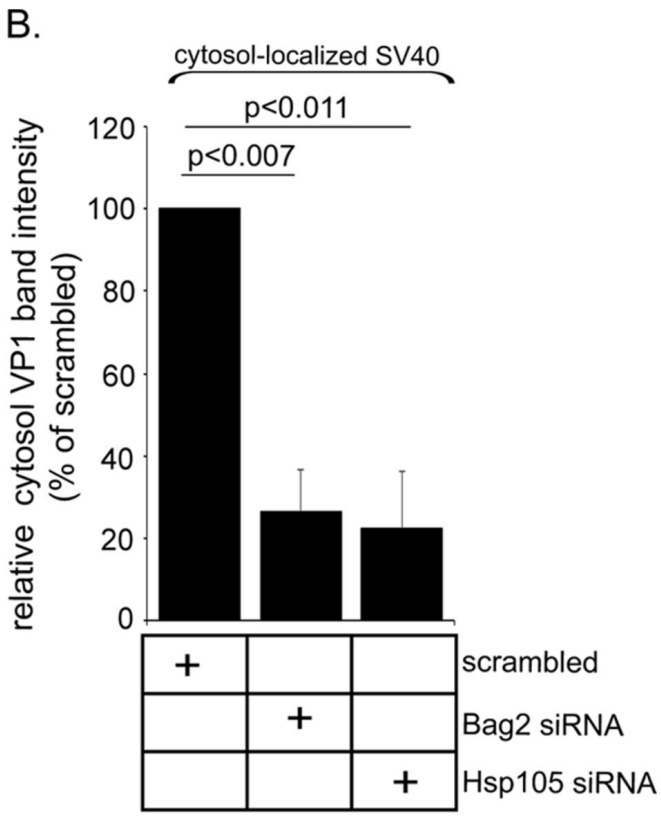
B.
cytosol-localized SV40
p<0.011
p<0.007
relative cytosol VP1 band intensity
(% of scrambled)
120
100
80
60
40
20
0
+
scrambled
Bag2 siRNA
Hsp105 siRNA

FIG 3-3 Bag2 is important for ER-to-cytosol transport of SV40.

(A) CV-1 cells transfected with the indicated siRNAs were infected with SV40 and subjected to semipermeabilization. The resulting cytosol-, membrane-, and ER-localized fractions were subjected to SDS-PAGE and immunoblotting with the indicated antibodies. The amount loaded for the cytosol was 50% of the total cytosol fraction, whereas the amount loaded for the membrane was 20% of the total membrane fraction. Hsp90 and PDI acted as both loading and fractionation controls.
(B) The VP1 band intensity in the cytosol fraction from panel A was quantified with Image J software (National Institutes of Health), normalized relative to the Hsp90 loading control bands, and graphed as a percentage of the VP1 band intensity in the scrambled-siRNAtreated sample. The graph represents the means and SD from at least 3 biological replicates. Student's two-tailed t test was used to determine statistical significance.

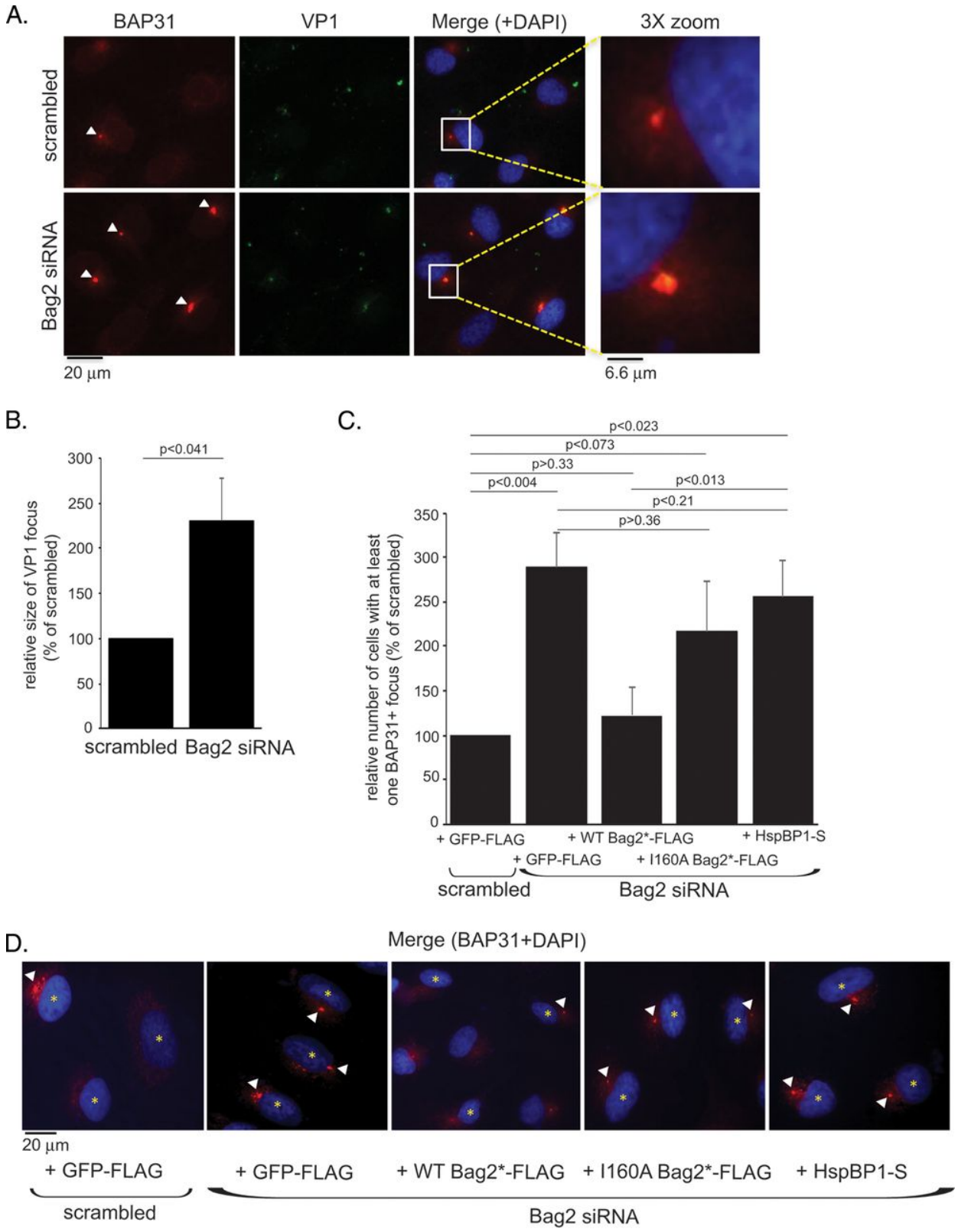
A.
BAP31
VP1
Merge (+DAPI)
3X zoom
scrambled
Bag2 siRNA
20 µm
6.6 µm
B.
p<0.041
relative size of VP1 focus (% of scrambled)
300
250
200
150
100
50
0
scrambled
Bag2 siRNA
C.
p<0.023
p<0.073
p>0.33
p<0.004
p<0.013
p<0.21
p>0.36
relative number of cells with at least one BAP31+ focus (% of scrambled)
350
300
250
200
150
100
50
0
+ GFP-FLAG
+ WT Bag2*-FLAG
+ HspBP1-S
+ GFP-FLAG
+ I160A Bag2*-FLAG
scrambled
Bag2 siRNA
D.
Merge (BAP31+DAPI)
20 µm
+ GFP-FLAG
+ GFP-FLAG
+ WT Bag2*-FLAG
+ I160A Bag2*-FLAG
+ HspBP1-S
scrambled
Bag2 siRNA

FIG 3-4 Depletion of Bag2 traps SV40 in the ER-to-cytosol membrane penetration site.

(A) CV-1 cells were transfected with the indicated siRNAs for 48 h, followed by 16 h of SV40 infection. The cells were fixed, permeabilized, stained using anti-BAP31 and anti-VP1 antibodies, and imaged by fluorescence microscopy. The enlarged images (3 zoom) correspond to the boxed areas in the merged images. The arrowheads indicate BAP31 foci.
(B) The size of the VP1 focus was quantified based on the measured area (in pixels) using Image J software. The graph represents the means and SD of at least 30 cells counted in at least three biological replicates. Student's two-tailed t test was used to determine statistical significance.
(C) As for panel A, except cells were transfected with the indicated constructs 24 h prior to infection with SV40. The cells were then fixed, permeabilized, and stained using anti-BAP31, anti-FLAG, or anti-S antibodies. Only cells expressing the indicated FLAG- or S-tagged constructs were counted. The data plotted are the numbers of cells with at least one BAP31 focus, graphed as a percentage of the scrambled siRNA-treated sample. The graph represents the means and SD of at least 100 cells counted in at least three biological replicates. Student's two-tailed t test was used to determine statistical significance.
(D) Representative images of the data in panel C. The arrowheads indicate BAP31 foci. The asterisks indicate cells expressing the indicated constructs.

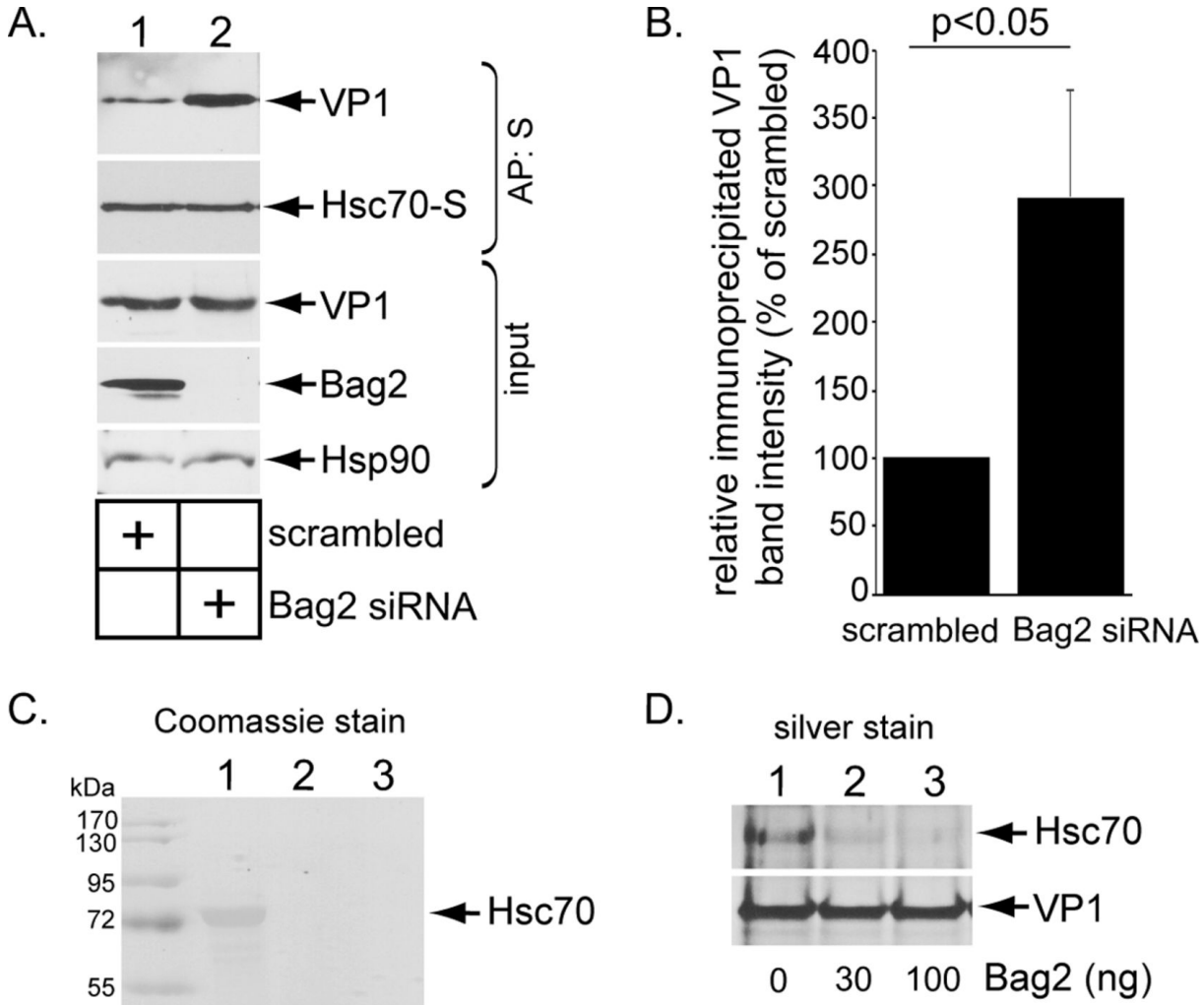
A.
1
2
VP1
Hsc70-S
AP: S
VP1
Bag2
Hsp90
input
+
scrambled
Bag2 siRNA
B.
p<0.05
relative immunoprecipitated VP1 band intensity (% of scrambled)
400
350
300
250
200
150
100
50
0
scrambled
Bag2 siRNA
C.
Coomassie stain
1
2
3
kDa
170
130
95
72
55
43
34
24
Hsc70
VP1
VP3
Bag2
D.
silver stain
1
2
3
Hsc70
VP1
0
30
100
Bag2 (ng)

FIG 3-5 Bag2 releases SV40 from Hsc70.

(A) COS-7 cells were treated with the indicated siRNAs for 24 h, followed by transfection of the Hsc70-S construct. After 24 h, the cells were infected with SV40 for 16 h, and the resulting cell extracts were subjected to affinity purification, SDS-PAGE, and immunoblotting with the indicated antibodies.
(B) The VP1 band intensity from panel A was quantified with Image J software (National Institutes of Health), normalized relative to the affinity-purified Hsc70-S level, and graphed as a percentage of the VP1 band intensity in the scrambled-siRNA-treated sample. The graph represents the means and SD from three biological replicates. Student's two-tailed t test was used to determine statistical significance.
(C) Coomassie staining of commercially available Hsc70 and Bag2, along with purified SV40. Note that the level of VP2 in the SV40 preparation is below the threshold of detection.
(D) After SV40 was incubated with Hsc70 (in the presence of 1 mM DTT), precipitation of SV40 VP1 coprecipitated Hsc70. The SV40-Hsc70 complex was incubated with a control buffer containing only ATP, or the indicated amount of Bag2 with ATP, followed by reimmunoprecipitation of SV40 VP1. The reimmunoprecipitated material was subjected to SDS-PAGE followed by silver staining.

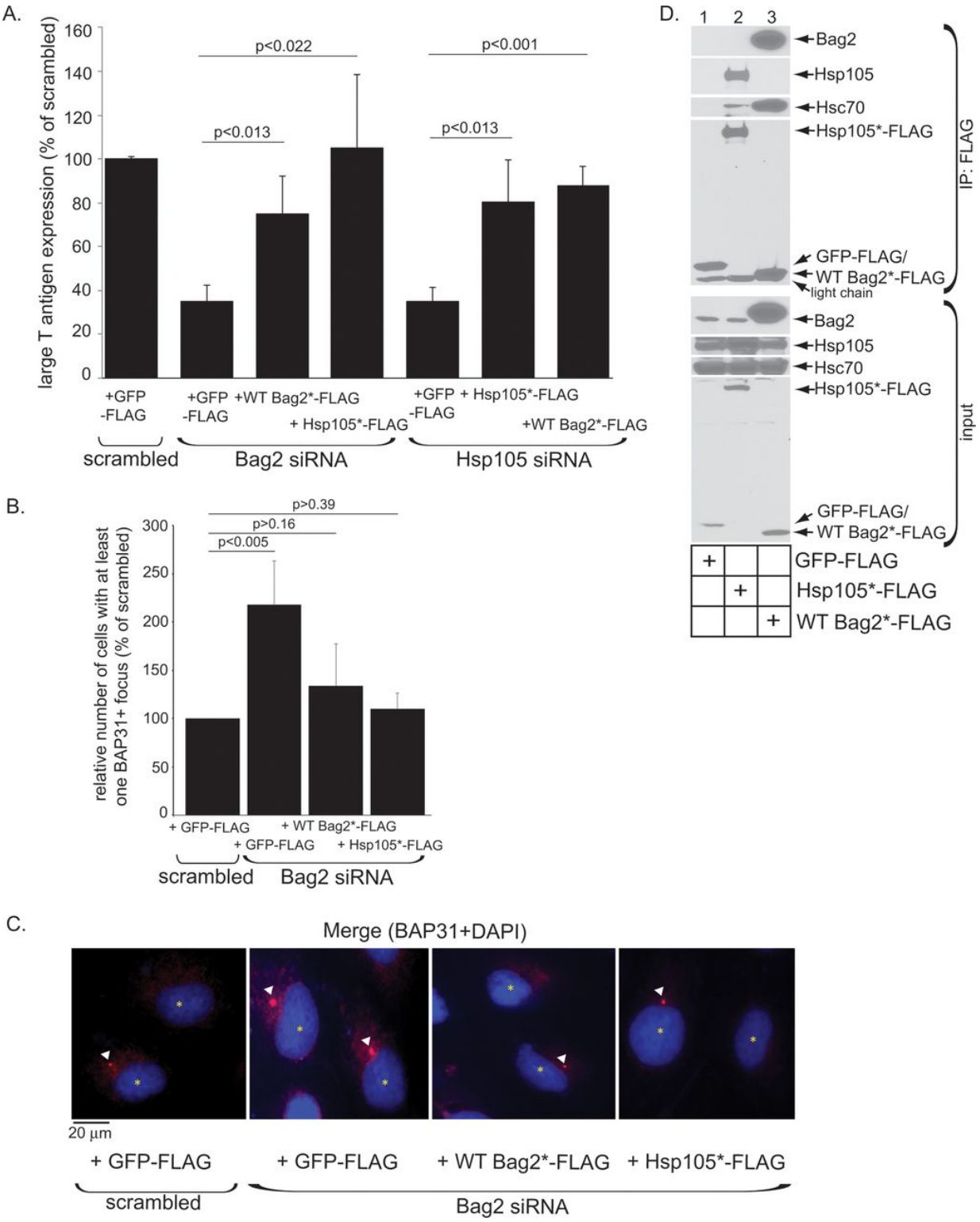
A.
large T antigen expression (% of scrambled)
160
140
120
100
80
60
40
20
0
p<0.022
p<0.001
p<0.013
p<0.013
+GFP -FLAG
+GFP -FLAG
+WT Bag2*-FLAG
+ Hsp105*-FLAG
+GFP -FLAG
+ Hsp105*-FLAG
+WT Bag2*-FLAG
scrambled
Bag2 siRNA
Hsp105 siRNA
D.
1 2 3
Bag2
Hsp105
Hsc70
Hsp105*-FLAG
GFP-FLAG/
WT Bag2*-FLAG
light chain
IP: FLAG
Bag2
Hsp105
Hsc70
Hsp105*-FLAG
GFP-FLAG/
WT Bag2*-FLAG
input
+ GFP-FLAG
+ Hsp105*-FLAG
+ WT Bag2*-FLAG
B.
relative number of cells with at least one BAP31+ focus (% of scrambled)
300
250
200
150
100
50
0
p>0.39
p>0.16
p<0.005
+ GFP-FLAG
+ WT Bag2*-FLAG
+ GFP-FLAG
+ Hsp105*-FLAG
scrambled
Bag2 siRNA
C.
Merge (BAP31+DAPI)
20 µm
+ GFP-FLAG
+ GFP-FLAG
+ WT Bag2*-FLAG
+ Hsp105*-FLAG
scrambled
Bag2 siRNA

FIG 3-6 Bag2 and Hsp105 play overlapping roles.

(A) CV-1 cells were transfected with the indicated siRNAs for 24 h, followed by DNA transfection of the indicated FLAG constructs. After 24 additional hours, the cells were infected with SV40 for 24 h, fixed, permeabilized, and stained for FLAG and large T antigen. Only cells expressing the indicated FLAG constructs were counted. At least 100 cells were counted per condition over three biological replicates. The graph represents means and SD. Student's two-tailed t test was used to determine statistical significance.
(B) As for panel A, except cells were infected with SV40 for 16 h prior to being fixed, permeabilized, and stained for FLAG and BAP31. Only cells expressing the indicated FLAG constructs were counted. The graph represents the means and SD of at least 100 cells counted in at least three biological replicates.
(C) Representative images of the data in panel B. The arrowheads indicate BAP31 foci. The asterisks indicate cells expressing the indicated constructs.
(D) HEK 293T cells were transfected with the indicated FLAG-tagged constructs and lysed, and the resulting cell extract was subjected to immunoprecipitation, SDS-PAGE, and immunoblotting with the indicated antibodies.

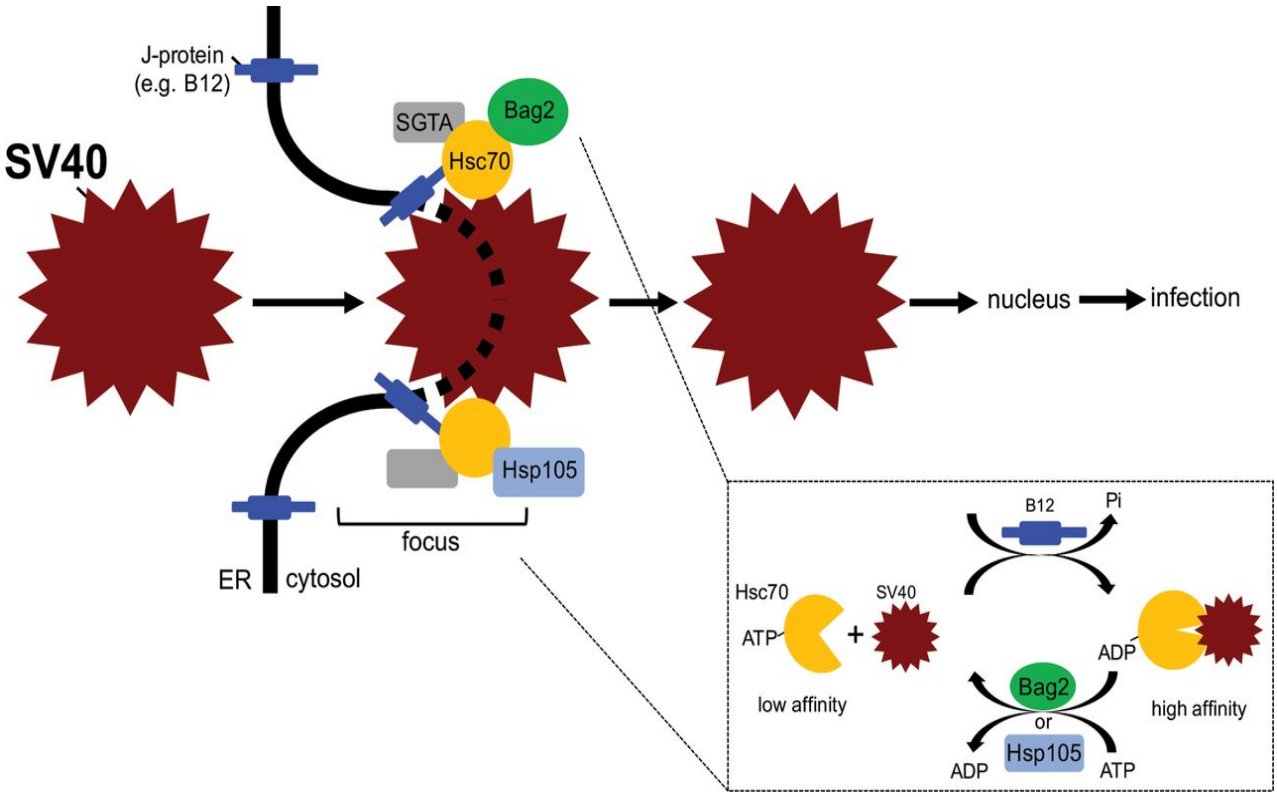
J-protein
(e.g. B12)
SV40
SGTA
Bag2
Hsc70
Hsp105
focus
ER
cytosol
nucleus
infection
B12
Pi
Hsc70
ATP
SV40
low affinity
ADP
high affinity
Bag2
or
Hsp105
ADP
ATP

FIG 3-7 The Hsc70-SGTA-Bag2 complex docks on an ER membrane J protein and promotes SV40 cytosol entry.

In our model, Hsc70-containing protein complexes dock on an ER membrane J protein, such as B12. In association with its cochaperone, SGTA, an Hsc70 molecule recruits Bag2 or Hsp105, forming either the Hsc70-SGTA-Bag2 or Hsc70-SGTA-Hsp105 cytosolic extraction complex. During the final step of SV40's ER-to-cytosol membrane transport, a single membrane-embedded viral particle recruits many copies of either the Hsc70-SGTA-Bag2 or Hsc70-SGTA-Hsp105 protein complex. Iterative cycles of SV40 binding to and release from Hsc70 in turn provide the energy to extract the virus into the cytosol. (Inset) Importantly, Bag2 functions to trigger SV40 release from Hsc70 in this cycle. Bag2 does this by promoting ADP release from Hsc70, generating ATP-Hsc70, which displays low affinity for its substrate, such as SV40. "Focus" refers to the SV40 cytosol entry site in the ER membrane, where the cytosolic extraction machinery is recruited to the ER membrane J protein.

References:

1. Poranen MM, Daugelavicius R, Bamford DH. 2002. Common principles in viral entry. Annu Rev Microbiol 56:521–538. doi:10.1146/annurev.micro.56.012302.160643.

2. Tsai B. 2007. Penetration of nonenveloped viruses into the cytoplasm. Annu Rev Cell Dev Biol 23:23–43. doi:10.1146/annurev.cellbio.23.090506.123454.

3. Walczak CP, Ravindran MS, Inoue T, Tsai B. 2014. A cytosolic chaperone complexes with dynamic membrane J-proteins and mobilizes a nonenveloped virus out of the endoplasmic reticulum. PLoS Pathog 10:e1004007. doi:10.1371/journal.ppat.1004007.

4. Ravindran MS, Bagchi P, Inoue T, Tsai B. 2015. A non-enveloped virus hijacks host disaggregation machinery to translocate across the endoplasmic reticulum membrane. PLoS Pathog 11:e1005086. doi:10.1371/journal.ppat.1005086.

5. Dalianis T, Hirsch HH. 2013. Human polyomaviruses in disease and cancer. Virology 437:63–72. doi:10.1016/j.virol.2012.12.015.

6. DeCaprio JA, Garcea RL. 2013. A cornucopia of human polyomaviruses. Nat Rev Microbiol 11:264–276. doi:10.1038/nrmicro2992.

7. Liddington RC, Yan Y, Moulai J, Sahli R, Benjamin TL, Harrison SC. 1991. Structure of simian virus 40 at 3.8-A resolution. Nature 354:278–284. doi:10.1038/354278a0.

8. Stehle T, Yan Y, Benjamin TL, Harrison SC. 1994. Structure of murine polyomavirus complexed with an oligosaccharide receptor fragment. Nature 369:160–163. doi:10.1038/369160a0.

9. Stehle T, Gamblin SJ, Yan Y, Harrison SC. 1996. The structure of simian virus 40 refined at 3.1 A resolution. Structure 4:165–182. doi:10.1016/S0969-2126(96)00020-2.

10. Chen XS, Stehle T, Harrison SC. 1998. Interaction of polyomavirus internal protein VP2 with the major capsid protein VP1 and implications for participation of VP2 in viral entry. EMBO J 17:3233–3240. doi:10.1093/emboj/17.12.3233.

11. Smith AE, Lilie H, Helenius A. 2003. Ganglioside-dependent cell attachment and endocytosis of murine polyomavirus-like particles. FEBS Lett 555:199–203. doi:10.1016/S0014-5793(03)01220-1.

12. Tsai B, Gilbert JM, Stehle T, Lencer W, Benjamin TL, Rapoport TA. 2003. Gangliosides are receptors for murine polyoma virus and SV40. EMBO J 22:4346–4355. doi:10.1093/emboj/cdg439.

13. Campanero-Rhodes MA, Smith A, Chai W, Sonnino S, Mauri L, Childs RA, Zhang Y, Ewers H, Helenius A, Imberty A, Feizi T. 2007. N-glycolyl GM1 ganglioside as a receptor for simian virus 40. J Virol 81:12846–12858. doi:10.1128/JVI.01311-07.

14. Engel S, Heger T, Mancini R, Herzog F, Kartenbeck J, Hayer A, Helenius A. 2011. Role of endosomes in simian virus 40 entry and infection. J Virol 85:4198–4211. doi:10.1128/JVI.02179-10.

15. Qian M, Cai D, Verhey KJ, Tsai B. 2009. A lipid receptor sorts polyomavirus from the endolysosome to the endoplasmic reticulum to cause infection. PLoS Pathog 5:e1000465. doi:10.1371/journal.ppat.1000465.

16. Kartenbeck J, Stukenbrok H, Helenius A. 1989. Endocytosis of simian virus 40 into the endoplasmic reticulum. J Cell Biol 109:2721–2729.

17. Geiger R, Andritschke D, Friebe S, Herzog F, Luisoni S, Heger T, Helenius A. 2011. BAP31 and BiP are essential for dislocation of SV40 from the endoplasmic reticulum to the cytosol. Nat Cell Biol 13:1305–1314. doi:10.1038/ncb2339.

18. Clever J, Yamada M, Kasamatsu H. 1991. Import of simian virus 40 virions through nuclear pore complexes. Proc Natl Acad Sci U S A 88:7333–7337. doi:10.1073/pnas.88.16.7333.

19. Nakanishi A, Clever J, Yamada M, Li PP, Kasamatsu H. 1996. Association with capsid proteins promotes nuclear targeting of simian virus 40 DNA. Proc Natl Acad Sci U S A 93:96–100. doi:10.1073/pnas.93.1.96.

20. Magnuson B, Rainey EK, Benjamin T, Baryshev M, Mkrtchian S, Tsai B. 2005. ERp29 triggers a conformational change in polyomavirus to stimulate membrane binding. Mol Cell 20:289–300. doi:10.1016/j.molcel.2005.08.034.

21. Gilbert J, Ou W, Silver J, Benjamin T. 2006. Downregulation of protein disulfide isomerase inhibits infection by the mouse polyomavirus. J Virol 80:10868–10870. doi:10.1128/JVI.01117-06.

22. Schelhaas M, Malmstrom J, Pelkmans L, Haugstetter J, Ellgaard L, Grunewald K, Helenius A. 2007. Simian virus 40 depends on ER protein folding and quality control factors for entry into host cells. Cell 131:516–529. doi:10.1016/j.cell.2007.09.038.

23. Walczak CP, Tsai B. 2011. A PDI family network acts distinctly and coordinately with ERp29 to facilitate polyomavirus infection. J Virol 85:2386–2396. doi:10.1128/JVI.01855-10.

24. Inoue T, Dosey A, Herbstman JF, Ravindran MS, Skiniotis G, Tsai B. 2015. ERdj5 reductase cooperates with protein disulfide isomerase to promote simian virus 40 endoplasmic reticulum membrane translocation. J Virol 89:8897–8908. doi:10.1128/JVI.00941-15.

25. Daniels R, Rusan NM, Wadsworth P, Hebert DN. 2006. SV40 VP2 and VP3 insertion into ER membranes is controlled by the capsid protein VP1: implications for DNA translocation out of the ER. Mol Cell 24:955–966. doi:10.1016/j.molcel.2006.11.001.

26. Rainey-Barger EK, Magnuson B, Tsai B. 2007. A chaperone-activated nonenveloped virus perforates the physiologically relevant endoplasmic reticulum membrane. J Virol 81:12996–13004. doi:10.1128/JVI.01037-07.

27. Kuksin D, Norkin LC. 2012. Disassembly of simian virus 40 during passage through the endoplasmic reticulum and in the cytoplasm. J Virol 86:1555–1562. doi:10.1128/JVI.05753-11.

28. Dupzyk A, Williams JM, Bagchi P, Inoue T, Tsai B. 2017. SGTA-dependent regulation of Hsc70 promotes cytosol entry of Simian Virus 40 from the endoplasmic reticulum. J Virol 12:e00232-17. doi:10.1128/JVI.00232-17.

29. Goodwin EC, Lipovsky A, Inoue T, Magaldi TG, Edwards AP, Van Goor KE, Paton AW, Paton JC, Atwood WJ, Tsai B, DiMaio D. 2011. BiP and multiple DNAJ molecular chaperones in the endoplasmic reticulum are required for efficient simian virus 40 infection. mBio 2:e00101-11. doi:10.1128/mBio.00101-11.

30. Bagchi P, Walczak CP, Tsai B. 2015. The endoplasmic reticulum membrane J protein C18 executes a distinct role in promoting simian virus 40 membrane penetration. J Virol 89:4058–4068. doi:10.1128/JVI.03574-14.

31. Inoue T, Tsai B. 2017. Regulated Erlin-dependent release of the B12 transmembrane J-protein promotes ER membrane penetration of a non-enveloped virus. PLoS Pathog 13:e1006439. doi:10.1371/journal.ppat.1006439.

32. Xu Z, Page RC, Gomes MM, Kohli E, Nix JC, Herr AB, Patterson C, Misra S. 2008. Structural basis of nucleotide exchange and client binding by the Hsp70 cochaperone Bag2. Nat Struct Mol Biol 15:1309–1317. doi:10.1038/nsmb.1518.

33. Inoue T, Tsai B. 2011. A large and intact viral particle penetrates the endoplasmic reticulum membrane to reach the cytosol. PLoS Pathog 7:e1002037. doi:10.1371/journal.ppat.1002037.

34. Rauch JN, Gestwicki JE. 2014. Binding of human nucleotide exchange factors to heat shock protein 70 (Hsp70) generates functionally distinct complexes in vitro. J Biol Chem 289:1402–1414. doi:10.1074/jbc.M113.521997.

35. Dragovic Z, Broadley SA, Shomura Y, Bracher A, Hartl FU. 2006. Molecular chaperones of the Hsp110 family act as nucleotide exchange factors of Hsp70s. EMBO J 25:2519–2528. doi:10.1038/sj.emboj.7601138.

36. Raviol H, Bukau B, Mayer MP. 2006. Human and yeast Hsp110 chaperones exhibit functional differences. FEBS Lett 580:168–174. doi:10.1016/j.febslet.2005.11.069.

37. Mattoo RU, Sharma SK, Priya S, Finka A, Goloubinoff P. 2013. Hsp110 is a bona fide chaperone using ATP to unfold stable misfolded polypeptides and reciprocally collaborate with Hsp70 to solubilize protein aggregates. J Biol Chem 288:21399–21411. doi:10.1074/jbc.M113.479253..

38. Berner N, Reutter KR, Wolf DH. 2 February 2018. Protein quality control of the endoplasmic reticulum and ubiquitin-proteasome-triggered degradation of aberrant proteins: yeast pioneers the path. Annu Rev Biochem. doi:10.1146/annurev-biochem-062917-012749.

39. Arndt V, Daniel C, Nastainczyk W, Alberti S, Hohfeld J. 2005. BAG-2 acts as an inhibitor of the chaperone-associated ubiquitin ligase CHIP. Mol Biol Cell 16:5891–5900. doi:10.1091/mbc.e05-07-0660.

40. de Paula CA, Santiago FE, de Oliveira AS, Oliveira FA, Almeida MC, Carrettiero DC. 2016. The co-chaperone BAG2 mediates cold-induced accumulation of phosphorylated tau in SH-SY5Y cells. Cell Mol Neurobiol 36:593–602. doi:10.1007/s10571-015-0239-x.

41. Qin L, Guo J, Zheng Q, Zhang H. 2016. BAG2 structure, function and involvement in disease. Cell Mol Biol Lett 21:18. doi:10.1186/s11658-016-0020-2.

42. Schonbuhler B, Schmitt V, Huesmann H, Kern A, Gamerdinger M, Behl C. 2016. BAG2 interferes with CHIP-mediated ubiquitination of HSP72. Int J Mol Sci 18:E69. doi:10.3390/ijms18010069.

43. Williams JM, Inoue T, Chen G, Tsai B. 2015. The nucleotide exchange factors Grp170 and Sil1 induce cholera toxin release from BiP to enable retrotranslocation. Mol Biol Cell 26:2181–2189. doi:10.1091/mbc.e15-01-0014.

Chapter 4: The γ-secretase binding-partner p120 catenin promotes HPV infection

Introduction

Human papillomaviruses (HPVs) are one of the most common sexually transmitted pathogens, and account for nearly all cases of cervical, anogenital, and oropharyngeal cancers (1). Despite a highly effective prophylactic vaccine against 7 high-risk and 2 low-risk HPVs, the virus still causes morbidity and mortality as a result of limited access to the vaccine itself, as well as an inability to combat disease in individuals already exposed to HPV (1, 2). Hence, clarifying HPV cell entry remains imperative as this might identify new therapeutic strategies.

Structurally, HPV is a nonenveloped DNA tumor virus composed of 72 pentamers of the major capsid protein L1 (3). Underlying L1 is the minor capsid protein L2 that varies in copy number (3). Protected inside the L1 pentamers is the 8-kilobase pair circular double-stranded DNA genome (4). HPV infection begins when L1 interacts with heparin sulfate proteoglycans on the plasma membrane or extracellular matrix (5-8). This stimulates viral conformational changes that allow the furin protease to cleave the N-terminus of L2 (7-11). The virus is then thought to be transferred to an unknown entry receptor, which initiates receptor-mediated endocytosis delivering HPV to the endosome (12). The low pH in this compartment, in conjunction with the peptidylprolyl isomerase cyclophilin, promotes partial uncoating of HPV, resulting in release of the majority of the L1 pentamers from the L2-viral genome complex (13, 14). Exposure of

L2 in turn enables this viral protein to insert into the endosomal membrane (15-18). Importantly, we demonstrated that the transmembrane protease γ-secretase promotes membrane insertion of L2 (18). L2 membrane insertion exposes the C-terminus of L2 (that harbors a retromer-binding motif) to the cytosol (19, 20). This then recruits the cytosolic retromer complex to HPV that routes the virus to the trans Golgi network (TGN) and then the Golgi (21-24). HPV remains in this compartment until mitosis, when it buds from the Golgi, trafficking to the nucleus to cause infection (25-29). As HPV in the endosome can also sort to the lysosome for degradation, the ability of the virus to target along the endosome-Golgi axis represents the committed infection step (30, 31). Within the endosome-Golgi axis, the decisive step is γ-secretase-dependent insertion of L2 into the endosome membrane (18, 32, 33, 34). In this context, a critical question is: how is HPV targeted to the γ-secretase complex?

Using an unbiased biochemical proteomics approach, our lab identified a cytosolic protein called p120 catenin (p120) as a potential novel binding partner of HPV L2 during virus entry (18). p120 belongs to the catenin family well-established for their interactions with cell surface-localized transmembrane adhesion receptors called cadherins (35-37). Importantly, p120 is also known to bind to γ-secretase (38). In fact, one crucial cellular function of p120 is to target cadherins to γ-secretase, enabling this transmembrane protease to cleave cadherins essential to elicit a cellular response (39). Here, using a loss-of-function strategy, we demonstrate that p120 promotes HPV infection by targeting the virus from the cell surface to γ-secretase in the endosome, thereby enabling γ-secretase to insert HPV L2 into the endosome membrane – a critical event during productive HPV entry. As HPV is not exposed to the cytosol at the cell

surface, the observed HPV-p120 interaction at the cell surface is likely mediated by an unknown receptor. We propose that the receptor-p120 complex engages HPV at the plasma membrane, delivering HPV to γ-secretase when the receptor-p120 complex itself is recruited to γ-secretase.

Materials and Methods

Antibodies and Inhibitors

M2 FLAG antibody was purchased from Sigma (St. Louis, MO). The p120 antibody was purchased from Santa Cruz Biotech (Santa Cruz, Ca). Antibody against the C-terminal fragment of PS1 was purchased from Cell Signaling Technologies (Danvers, MA). Anti-PD1 antibody was purchased from Abcam (Cambridge, MA). Anti-Bap31 antibody was purchased from Invitrogen (Carlsbad, CA) and anti- B actin antibody was purchased from Cell Signaling (Danvers, MA). The γ–secretase inhibitor XXI was purchased from Millipore and dissolved in DMSO and used at a concentration of 1μM.

DNA Constructs

The p16sheLL plasmid was a gift from Dr. John Shiller (National Cancer Institute, Rockville, MD; plasmid 37320, Addgene). The p16sheLL was used as in Zhang et al., 2014 (35) to produce the WT HPV16.L2F pseudovirus (PsV) with FLAG tagged L2, and WT HPV16 L1.

Cells

HeLa cells were purchased from American Type Culture Collection. The 293TT cells were a generous gift from Dr. Christopher Buck (National Cancer Institute, Rockville,

MD). Cells were cultured in DMEM (Thermo Fisher Scientific) and 10% fetal bovine serum (Corning) containing 10 mg/ml streptomycin and 10 U/ml penicillin (Thermo Fisher Scientific).

Pseudovirus Production

WT HPV16.L2F was produced according to Inoue et al., 2018 (33). Briefly, 293TT cells were co-transfected with p16sheLL.L2F along with indicated reporter construct (Gaussia luciferase or GFP-S) with polyethyleneimine (Polysciences Inc.). After 48 hrs, cells were harvested, lysed in 0.5% triton X-100, 10mM $MgCl_2$, 5mM $CaCl_2$, and 0.5 U/ml RNase A. Lysate was centrifuged on an optiprep gradient of 27, 33, and 39% at 300,000 g for 4 hours, at 16 ˚C, in a SW55 Ti rotor.

siRNA Transfection

siRNAs used in this study target the following sequences: PS1 siRNA: 5'-UCAAGUACCUCCCUGAAUG-3'; p120 siRNA: 5'-GCUAUGAUGACCUGGAUUA-3'. As a negative control, Allstar siRNA (Qiagen) was used. HeLa cells were seeded and simultaneously transfected (reverse transfected) with 75-100 nM siRNA using Lipofectamine RNAi MAX (Thermo Fisher Scientific) and incubated for at least 48 hours prior to infection or 24 hours prior to biochemical assays.

Infection studies

HeLa cells were seeded in 6 well plates and reverse transfected with indicated siRNAs for 72 hours, followed by infection with HPV16.L2F PsV (MOI~ 9-10) containing a

reporter plasmid encoding secreted Gaussia luciferase. Cells were treated with DMSO or compound XXI (1 μM) in DMSO at time of infection. At 48 hpi, 10 μl of supernatant was collected from each well and luciferase activity was measured using BioLux Gaussia Luciferase Assay Kit (NEB) according to manufacturer's instructions.

Immunoprecipitation of HPV16.L2F/ Mass Spectrometry

Immunoprecipitation of HPV16.L2F was performed as in Inoue et al., 2018 (18). Briefly, HeLa cells were infected or uninfected for 16 hrs before being lysed in 1% triton-X-100 in HN buffer (50mM Hepes, pH 7.5, 150 mM NaCl) and 1mM PMSF. After centrifugation, cell lysate was incubated with M2-FLAG antibody (0.3 μg/ml) for 2 hrs at 4˚C, followed by incubation with protein G-coated magnetic Dynabeads (Thermo Fisher Scientific). In the case of uninfected cells, lysates were mixed with purified PsV and functioned as a background control for post lysis binding. Proteins were eluted from beads using 0.1 mg/ml 3X FLAG peptide, followed by TCA precipitation. TCA-precipitated proteins were sent for mass spectrometry analysis (Taplin Mass Spectrometry Core Facility, Harvard Medical School).

Immunoprecipitation

HeLa cells were plated at 5 x 10^6 in 10 cm plates and incubated overnight. Cells were then infected with WT HPV16.L2F PsV (MOI ~100) for indicated times before lysis in 1% Decyl Maltose Neopenyl Glycol (DMNG) (Anatrace) in HN buffer and 1 mM PMSF. Lysed cells were centrifuged at 16,100 g for 10 min and resulting supernatant was incubated with M2 FLAG antibody overnight at 4˚C, rotating. Supernatant plus antibody

was then added to protein G-coated magnetic dynabeads for 1 hr at 4˚C, rotating. Beads were washed 3X in 0.1% DMNG in HN buffer. Beads were incubated at 95˚C for 10 minutes with 5X SDS sample buffer plus 2-mercaptoethanol (BME) and subjected to SDS-PAGE and immunoblotting with the indicated antibodies. Alternatively, cells were seeded and reverse transfected with indicated siRNAs for at least 24 hours prior to infection (Fig. 4-3A) before treatment as above. The bar graph in Fig. 4-3A shows relative values of L2-FLAG co-immunoprecipitated with PS1, where L2-FLAG co-immunoprecipitated with PS1 in scrambled siRNA treated cells is set to 100%. Values are normalized to PS1 band intensities. Bars represent the means ± standard deviations of at least three biological replicates. Significance determined using student's *t* test.

Alkali extraction assay

As in Inoue et al., (18), briefly, HeLa cells were seeded at 2.0 x 10^6 cells in 6 cm plates and infected with WT HPV16.L2F (MOI ~40-50) for 16 hrs. After 16 hrs, cells were collected and resuspended in HN buffer before being homogenized in 10 μM clearance ball bearing homogenizer (Isobiotech). Cell homogenate was then centrifuged at 16,100 x g, at 4˚C, for 10 min. Resulting supernatant was then centrifuged at 50,000 rpm, 4˚C, for 30 min in a TLA 100.3 rotor (Beckman). Pellet was treated with 25 μl of 10mM Tris-HCl (pH 7.5), 150 mM NaCl, 2mM $MgCl_2$, with 5mM DTT, and 50 units of Benzonase. This was incubated at 37˚C for 30 min. After 30 min, 225 μl of 0.1M Na_2CO_3 and 2 M Urea was added and incubated at 4˚C for 10 min. Next samples were centrifuged at 50,000 rpm, 4˚C for 30 min. Supernatant fraction was collected, and pellet was rinsed in HN buffer, and recentrifuged. Pellet and supernatant fraction were incubated at 95˚C for

10 min with 5X SDS running buffer plus BME, then subjected to SDS-PAGE and immunoblot with indicated antibodies. For quantification in Fig. 4-3B, bars represent relative values of L2-FLAG in pellet fraction, compared to L2-FLAG quantity in pellet fraction of scrambled siRNA treated cells, which is set to 100%. Values are normalized to Bap31 band intensities. Bars represent the means ± standard deviations of at least three biological replicates. Significance determined using student's *t* test.

Results

p120 binds to HPV16 L2 and promotes infection.

In order to study HPV entry and infection, we used a HPV16 pseudovirus (PsV) system composed of L1 and a C-terminally FLAG-tagged L2 encapsulating a luciferase reporter construct (WT HPV16.L2F) (3, 40). HPV16 PsV infection has been previously shown to mimic authentic HPV16 entry (3, 40). Using this PsV system in the context of an unbiased proteomics approach, we sought to identify host factors that bind to HPV16 L2 during entry. In this approach, an extract prepared from HeLa cells infected with WT HPV16.L2F was subjected to immunoprecipitation using an antibody against FLAG, and the bound material was eluted and analyzed by mass spectrometry (18). As a negative control, an extract prepared from uninfected HeLa cells was incubated with purified HPV16.L2F, and subjected to FLAG immunoprecipitation followed by mass spectrometry analysis; cellular proteins that bind to HPV16 L2 under this condition occurred during the extraction process, and are unlikely to represent factors that interact with the virus during entry.

Our results indicated that in addition to peptides corresponding to all 4 subunits of the γ-secretase complex (PS1, NICA, APH1A, and PEN2), 14 peptides corresponding to p120 catenin were present in the immunoprecipitated sample derived from the WT HPV16.L2F-infected extract (Fig. 4-1A); no peptides matching p120 were found in the sampled generated from the uninfected extract. Presence of p120 in the immunoprecipitated sample from the WT HPV16.L2F infected cells was verified by immunoblotting (Fig. 4-1B), demonstrating that HPV binds to p120. Importantly, when p120 was depleted via the siRNA approach in HeLa cells (Fig. 4-1C), WT HPV16.L2F infection was significantly attenuated (Fig. 4-1D), similar to the effect of knocking down PS1, as previously reported (18). These results indicate that p120 interacts with HPV-L2 and promotes HPV16 infection.

p120 binds to HPV16 L2 during early infection.

We next performed a time course experiment to assess when WT HPV16.L2F engages p120 during entry. HeLa cells incubated with WT HPV16.L2F for the indicated times were harvested, and the resulting cell extracts were subjected to immunoprecipitation using an antibody against FLAG. The bound material was analyzed by SDS-PAGE and immunoblotting. We found that p120 binds to the virus at the time of infection (0 hpi), with this interaction gradually disappearing after 7 hpi (Fig. 4-2A). Because previous studies showed that HPV reaches endosomal compartments 6-7 hpi, these findings suggest that p120 initiates binding to HPV at the cell surface, losing its affinity for the virus when HPV reaches the endosome (31, 41, 42). By contrast, γ-secretase (PS1) is reported to efficiently engage the virus only after 6 hpi (18). Thus,

HPV16 L2 interacts with p120 early during infection before the virus is recruited to the γ-secretase complex.

p120 promotes γ-secretase-dependent membrane insertion of HPV16 L2.

Our time course experiment revealed that as p120 binding to HPV16 L2 decreases, a corresponding increase in the γ-secretase-L2 interaction is observed, raising the possibility that p120 is required for L2 to target to γ-secretase. To test this, we asked if depleting p120 blocked the γ-secretase-L2 interaction, and found that it did (Fig. 4-3A, top panel; the extent of decrease is quantified in the right graph). This finding is consistent with the idea that p120 targets HPV L2 to γ-secretase.

Upon reaching γ-secretase, the L2 protein of HPV16 is inserted into the endosome membrane by the newly-ascribed chaperone activity of γ-secretase (18). We reasoned that if p120 is required to deliver L2 to γ-secretase, γ-secretase-dependent membrane insertion of L2 should similarly decrease when p120 is downregulated. To monitor membrane insertion of L2, we used the classic alkali extraction method, a rigorous biochemical approach that assesses whether a protein is a bona fide transmembrane protein. In this assay, WT HPV16.L2F-infected HeLa cells were disrupted mechanically, and the membrane fraction (containing the plasma, endosome, Golgi, and ER membranes) are collected by centrifugation. This membrane fraction was then resuspended in an alkaline carbonate solution containing the denaturant urea, and subjected to another round of centrifugation to produce a supernatant (S) and a pellet (P) fraction. Since treatment of alkali only perturbs the integrity of the membrane without affecting the ability of a transmembrane protein to remain as a membrane-inserted

protein, soluble luminal proteins (including protein disulfide isomerase [PDI]) can be found in the S fraction, while transmembrane proteins (including BAP31) reside in the P fraction (Fig. 4-3B). Thus, in this assay, L2 in the P fraction represents the membrane inserted form of L2. Importantly, the level of L2 in the P fraction markedly decreased when p120 was depleted (Fig. 4-3B, top panel; the extent of decrease is quantified in the graph to the right), indicating that in the absence of p120, HPV16 L2 fails to insert into the endosome membrane. This is consistent with the observation that p120 depletion blocks the interaction between L2 and γ-secretase (Fig. 4-3A). Together, our data suggest a scenario in which p120 targets HPV16 L2 to γ-secretase, thereby enabling γ-secretase to promote insertion of L2 into the endosome membrane – a critical infection step.

Discussion

High risk HPVs are the primary cause of cervical cancer worldwide and are associated with increasing rates of anogenital and oropharyngeal cancers. Despite HPV's significant impact on human health, much remains unknown regarding its infectious cellular entry. Upon receptor-mediated endocytosis, HPV reaches the endosome and is sorted to the Golgi *en route* for successful infection (12, 21-24). As endosome-localized HPV can also traffic to the lysosome where it is degraded, transport along the endosome-Golgi axis represents the productive entry route (30, 31). The decisive event in endosome-to-Golgi targeting of HPV is insertion of the HPV L2 protein into the endosome membrane (18). This is because upon membrane insertion, L2 is exposed to the cytosol, which in turn recruits the cytosolic retromer complex that

directs the virus to the Golgi (16, 18, 19-21). The mechanism by which L2 is inserted into the endosome membrane was recently revealed by our lab, demonstrating that the transmembrane protease γ-secretase in the endosome binds to and inserts L2 into the membrane (18). Despite this finding, how HPV is delivered to the γ-secretase complex remains enigmatic.

This study identified p120 catenin, an established binding-partner of γ-secretase, as a host cytosolic factor that promotes HPV16 infection (38). Mechanistically, it does so by targeting HPV16 L2 to γ-secretase, enabling γ-secretase to insert L2 into the endosome membrane. Our results demonstrate that the p120-HPV16 L2 interaction begins at the earliest time points during infection when the virus is localized to the cell surface. However, HPV16 L2 is not exposed to the cytosol until it is endocytosed and reaches the endosome. How then can p120 interact with HPV16 L2 at the plasma membrane? To reconcile this, we hypothesize that p120 must engage the virus via a transmembrane receptor.

We envision two models by which p120 targets HPV16 L2 to the endosome-localized γ-secretase. In the first model, p120 actively regulates initial endocytosis of HPV16 bound to the receptor-p120 complex at the plasma membrane, thereby promoting arrival of the viral particle to the endosome (Fig. 4-4A). In the second model, p120 exerts its role post endosome-arrival. Specifically, within the endosome, p120 targets HPV16 bound to the receptor-p120 complex to γ-secretase, delivering the virus to γ-secretase (Fig. 4-4B). We note that models 1 and 2 do not have to be exclusive: it is entirely possible that p120 exerts its action both at the step of initial endocytosis and in delivery of the virus to γ-secretase within the endosome. Clearly, additional experiments

are required to distinguish between these models. Regardless of the model, p120 clearly controls a critical infectious entry step. In this context, we recognize that while there are likely numerous host factors that also trigger endocytosis of HPV16, the subsequent intracellular transport pathways often result in a non-infectious fate.

In sum, our work here begins to reveal the mechanistic basis by which HPV16 is sorted from the endosome to the Golgi, the committed step in HPV entry. By identifying a new host component that supports HPV infection, these results should provide additional strategies to combat HPV-induced diseases.

Chapter 4 Figures

A.

	number of peptides corresponding to: p120 (CTND1)
uninfected	0
WT HPV16.L2F	14

B.

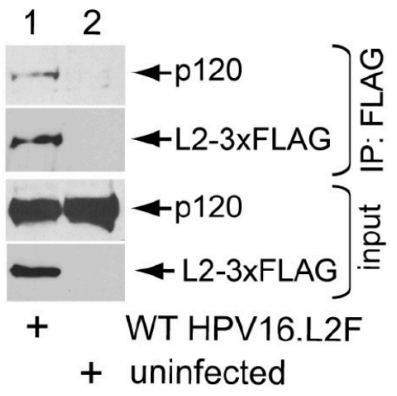

C.

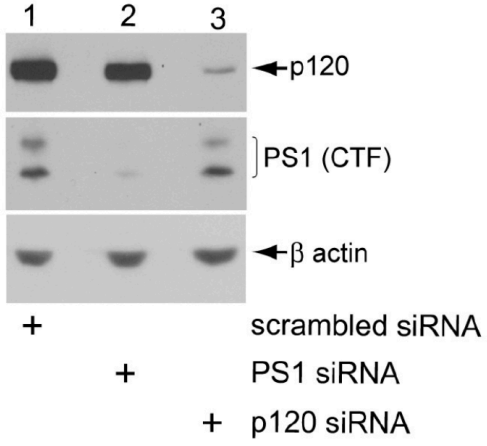

D.

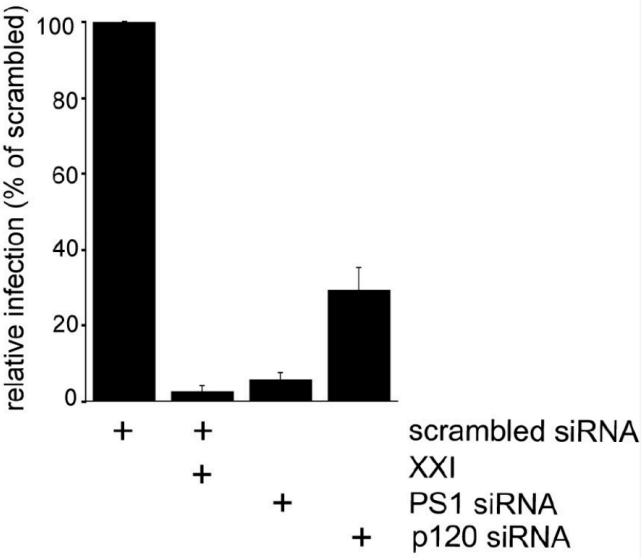

Figure 4-1 p120 binds HPV L2 and promotes infection.

A) Hela cells were infected, or mock infected with HPV16.L2F pseudovirus and L2-FLAG was immunoprecipitated. Immunoprecipitated samples were subjected to mass spectrometry. CTND1: gene encoding p120 catenin.
B) Hela cells were infected with HPV16.L2F pseudovirus or treated with DMSO for 6 hrs before a 1% DMNG lysis, and immunoprecipitation using M2 FLAG antibody and protein G dynabeads. Immunoprecipitated (IP) samples were subjected to SDS-PAGE and immunoblotting with indicated antibodies. Input represents 10% of whole cell lysate (WCL).
C) Hela cells were seeded and simultaneously transfected with indicated siRNAs. After 48 hrs, cells were lysed in 1% DMNG and WCL was subjected to SDS-PAGE and immunoblotting with indicated antibodies. PS1 (CTF): PS1 C terminal fragment.
D) Hela cells were seeded and transfected with indicated siRNA for 72 hrs, followed by 48 hr infection with HPV16.L2F pseudovirus. Alternatively, cells treated with compound XXI were simultaneously infected. HPV16.L2F infection was monitored by luciferase activity in culture supernatant. The graph represents relative value to cells transfected with control siRNA, which is set to 100%. Bars represent the means ± standard deviations from at least 3 biological replicates. Student's two-tailed *t* test was used to determine statistical significance.

A.

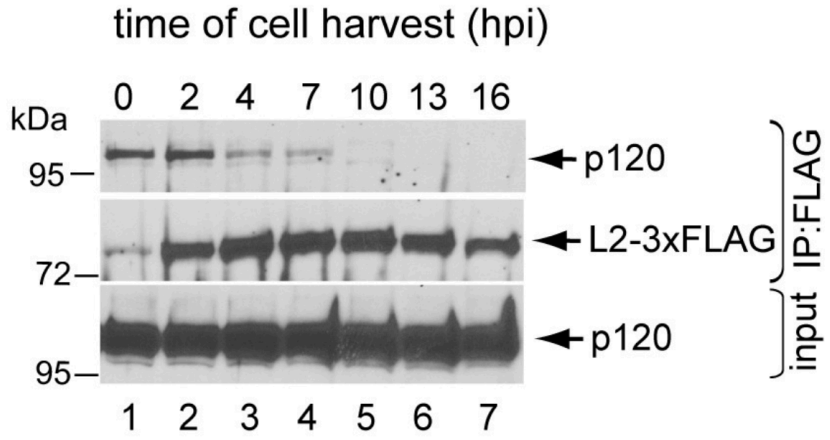
time of cell harvest (hpi)
0 2 4 7 10 13 16
kDa
95
72
95
p120
L2-3xFLAG
p120
IP:FLAG
input
1 2 3 4 5 6 7

Figure 4-2 The HPV L2 protein binds to p120 prior to engaging γ–secretase.

A) Hela cells were infected with HPV16.L2F (MOI~100) for the indicated times. Cells were harvested and lysed in 1% DMNG. L2-FLAG was immunoprecipitated from lysates and subjected to SDS-PAGE and immunoblotting with indicated antibodies. Input represents 10% of WCL.

A.

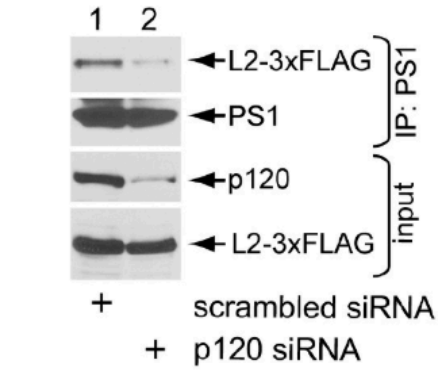
1
2
L2-3xFLAG
PS1
p120
L2-3xFLAG
IP: PS1
input
+
scrambled siRNA
+
p120 siRNA

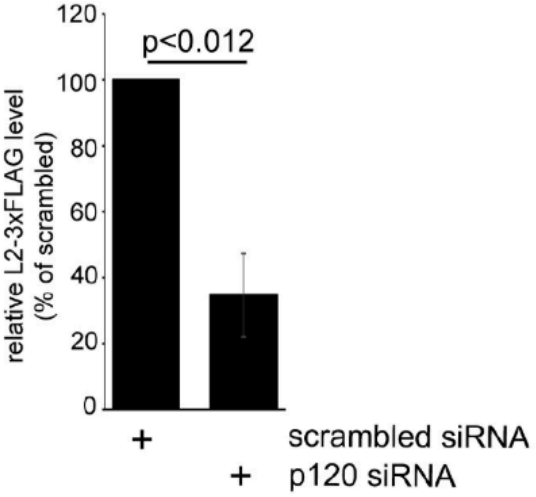
p<0.012
relative L2-3xFLAG level
(% of scrambled)
120
100
80
60
40
20
0
+
scrambled siRNA
+
p120 siRNA

B.

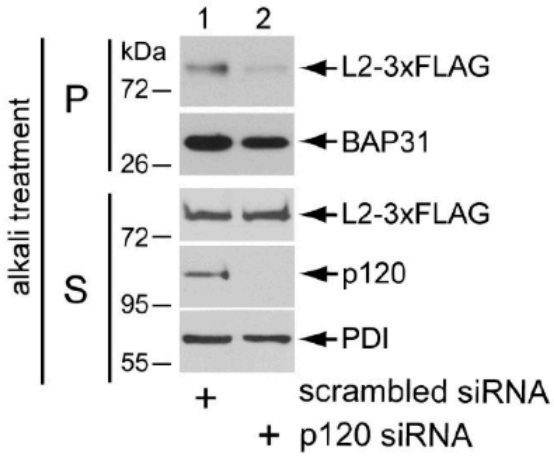
1
2
alkali treatment
P
S
kDa
72
26
72
95
55
L2-3xFLAG
BAP31
L2-3xFLAG
p120
PDI
+
scrambled siRNA
+
p120 siRNA

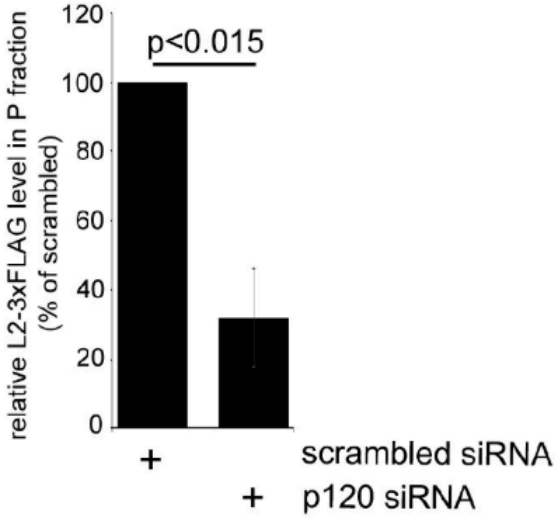
p<0.015
relative L2-3xFLAG level in P fraction
(% of scrambled)
120
100
80
60
40
20
0
+
scrambled siRNA
+
p120 siRNA

Figure 4-3 p120 promotes γ-secretase-dependent insertion pf HPV16 L2.

A) HeLa cells were seeded and simultaneously transfected with indicated siRNA for 24 hrs. After 24 hrs, cells were infected with HPV16.L2F (MOI~50) for 16 hrs before lysis in 1% DMNG. PS1 was immunoprecipitated from lysates and subjected to SDS-PAGE and immunoblotting with indicated antibodies. Input represents 10% of WCL. Graph: values are relative to PS1-L2 FLAG binding in cells treated with scrambled siRNA, which is set to 100%, after PS1 normalization. Bars represent the means ± standard deviations from at least 3 biological replicates. Student's two-tailed *t* test was used to determine statistical significance.
B) HeLa cells were seeded and simultaneously transfected with indicated siRNA for 24 hrs, followed by 16 hr infection with HPV16.L2F (MOI~50). After 16 hrs, cells were homogenized and membrane fraction was separated from cytosolic, mitochondria and nuclear fraction using centrifugation. Pellet fraction was treated with alkali reagents (pH ~11) with urea and DTT. Resulting fractions (P, pellet; S, supernatant) were subjected to SDS-PAGE and immunoblotting with the indicated antibodies. The amount loaded for the pellet fraction was 50% of the total pellet fraction. The amount loaded for the supernatant fraction was 7.5% of the total supernatant fraction. Bar graph represents means ± standard deviations from at least 3 biological replicates, and is relative to L2-FLAG level in pellet fraction of scrambled siRNA treated cells, which is set to 100%. Data are normalized to Bap31 levels. Student's two-tailed *t* test was used to determine statistical significance.

A.

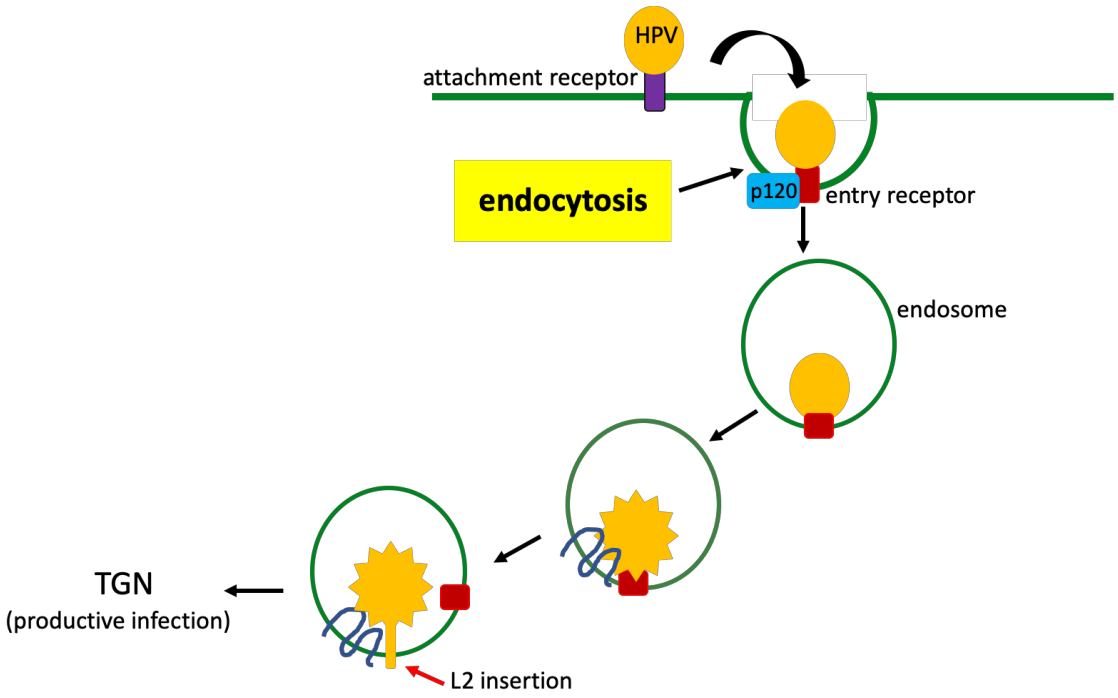
HPV
attachment receptor
endocytosis
p120
entry receptor
endosome
TGN
(productive infection)
L2 insertion

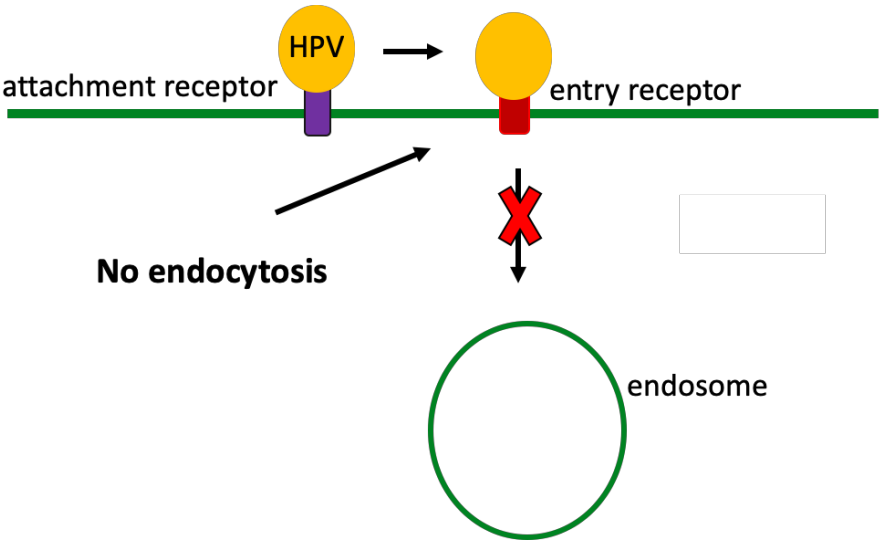
HPV
attachment receptor
entry receptor
No endocytosis
endosome

B.

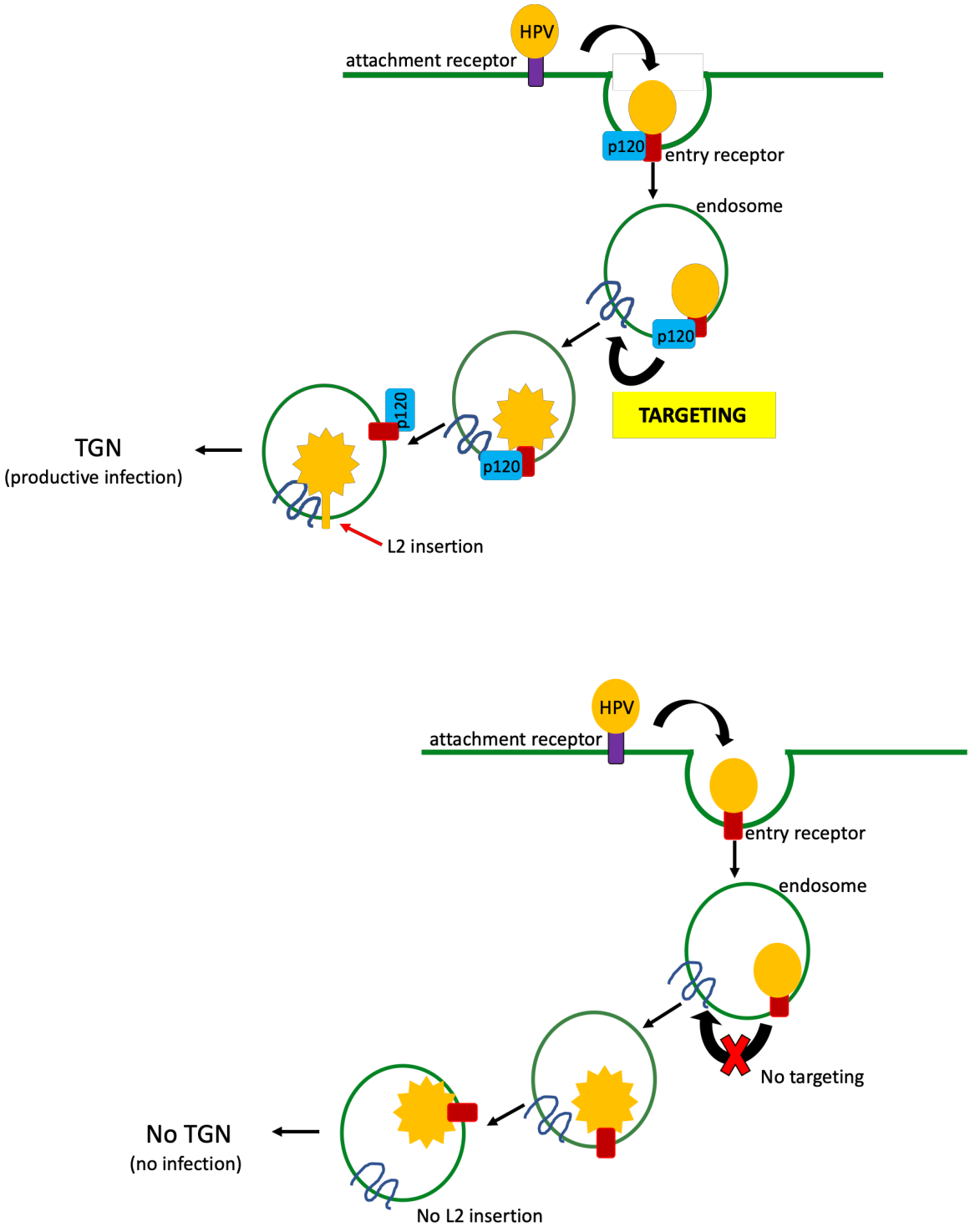
HPV
attachment receptor
p120
entry receptor
endosome
p120
TARGETING
TGN
(productive infection)
p120
p120
L2 insertion
HPV
attachment receptor
entry receptor
endosome
No targeting
No TGN
(no infection)
No L2 insertion

Fig. 4-4. Model of p120 promoting HPV infection.

A) In model A, p120 is necessary for HPV endocytosis. Upper graphic: HPV binds to HSPG (attachment receptor, purple) at the plasma membrane. After capsid conformational changes, HPV binds to the unknown entry receptor (red). P120 promotes endocytosis of the HPV-entry receptor complex. In the endosome, the HPV-receptor complex, along with p120, bind to γ-secretase (blue in endosomal membrane) for γ–secretase-mediated L2 insertion into the endosomal membrane, a decisive step in infection. HPV then traffics along the productive infection route to the trans golgi network (TGN) and the nucleus. Without p120 (lower graphic), HPV and the unknown entry receptor are not endocytosed, consequently, infection does not occur.
B) In model B, p120 targets HPV to γ-secretase. Upper graphic: HPV binds to HSPG (attachment receptor) at the plasma membrane. After capsid conformational changes, HPV binds to the unknown entry receptor. Although p120 associates with the unknown entry receptor, it is not necessary for HPV endocytosis. Once in the endosome, p120 targets HPV to γ-secretase for γ–secretase-mediated L2 insertion into the endosomal membrane, a decisive step in infection. HPV then traffics along the productive infection route to the trans golgi network (TGN) and the nucleus. Lower graphic: Without p120 (lower graphic), HPV and the unknown entry receptor are endocytosed, but HPV is not targeted to γ–secretase. Because HPV is not targeted to γ–secretase, L2 is not inserted through the endosomal membrane, and therefore unavailable for retromer binding and trans golgi network arrival. Consequently, infection does not occur.

References:

1) Lee LY, Garland SM. 2017. Human papillomavirus vaccination: the population impact. F1000Res 6:866.

2) Hildesheim A, Herrero R, Wacholder S, Rodriguez AC, Solomon D, Bratti MC, Schiller JT, Gonzalez P, Dubin G, Porras C, Jimenez SE, Lowy DR, Costa Rican HPVVTG. 2007. Effect of human papillomavirus 16/18 L1 viruslike particle vaccine among young women with preexisting infection: a randomized trial. JAMA 298:743-753.

3) Buck CB, Cheng N, Thompson CD, Lowy DR, Steven AC, Schiller JT, Trus BL. 2008. Arrangement of L2 within the papillomavirus capsid. J Virol 82:5190-5197.

4) Mallon RG, Wojciechowicz D, Defendi V. 1987. DNA-binding activity of papillomavirus proteins. J Virol 61:1655-1660.

5) Joyce JG, Tung JS, Przysiecki CT, Cook JC, Lehman ED, Sands JA, Jansen KU, Keller PM. 1999. The L1 major capsid protein of human papillomavirus type 11 recombinant virus-like particles interacts with heparin and cell-surface glycosaminoglycans on human keratinocytes. J Biol Chem 274:5810-5822.

6) Giroglou T, Florin L, Schafer F, Streeck RE, Sapp M. 2001. Human papillomavirus infection requires cell surface heparan sulfate. J Virol 75:1565-1570.

7) Johnson KM, Kines RC, Roberts JN, Lowy DR, Schiller JT, Day PM. 2009. Role of heparan sulfate in attachment to and infection of the murine female genital tract by human papillomavirus. J Virol 83:2067-2074.

8) Cerqueira C, Liu Y, Kuhling L, Chai W, Hafezi W, van Kuppevelt TH, Kuhn JE, Feizi T, Schelhaas M. 2013. Heparin increases the infectivity of Human Papillomavirus type 16 independent of cell surface proteoglycans and induces L1 epitope exposure. Cell Microbiol 15:1818-1836.

9) Richards, R.M., D.R. Lowy, J.T. Schiller, and P.M. Day. 2006. Cleavage of the papillomavirus minor capsid protein, L2, at a furin consensus site is necessary for infection. Proc. Natl. Acad. Sci. USA. 103:1522–1527.

10) Cerqueira C, Samperio Ventayol P, Vogeley C, Schelhaas M. 2015. Kallikrein-8 Proteolytically Processes Human Papillomaviruses in the Extracellular Space To Facilitate Entry into Host Cells. J Virol 89:7038-7052.

11) Calton, C.M., M.P. Bronnimann, A.R. Manson, S. Li, J.A. Chapman, M. Suarez-Berumen, T.R. Williamson, S.K. Molugu, R.A. Bernal, and S.K. Campos. 2017. Translocation of the papillomavirus L2/vDNA complex across the limiting membrane requires the onset of mitosis. PLoS Pathog. 13:e1006200.

12) Day PM, Lowy DR, Schiller JT. 2008. Heparan sulfate-independent cell binding and infection with furin-precleaved papillomavirus capsids. J Virol 82:12565-12568.

13) Smith JL, Campos SK, Wandinger-Ness A, Ozbun MA. 2008. Caveolin-1-dependent infectious entry of human papillomavirus type 31 in human keratinocytes proceeds to the endosomal pathway for pH-dependent uncoating. J Virol 82:9505-9512.

14) Bienkowska-Haba M, Williams C, Kim SM, Garcea RL, Sapp M. 2012. Cyclophilins facilitate dissociation of the human papillomavirus type 16 capsid protein L1 from the L2/DNA complex following virus entry. J Virol 86:9875-9887.

15) Bronnimann MP, Chapman JA, Park CK, Campos SK. 2013. A transmembrane domain and GxxxG motifs within L2 are essential for papillomavirus infection. J Virol 87:464-473.

16) DiGiuseppe, S., T.R. Keiffer, M. Bienkowska-Haba, W. Luszczek, L.G. Guion, M. Müller, and M. Sapp. 2015. Topography of the human papillomavirus minor capsid protein L2 during vesicular trafficking of infectious entry. J. Virol. 89:10442–10452.

17) Campos, S.K. 2017. Subcellular trafficking of the papillomavirus genome during initial infection: The remarkable abilities of minor capsid protein L2. Viruses. 9:370

18) Inoue T, Zhang P, Zhang W, Goodner-Bingham K, Dupzyk A, DiMaio D, Tsai B. 2018. gamma-Secretase promotes membrane insertion of the human papillomavirus L2 capsid protein during virus infection. J Cell Biol 217:3545-3559.

19) Pim, D., J. Broniarczyk, M. Bergant, M.P. Playford, and L. Banks. 2015. A novel PDZ domain interaction mediates the binding between human papillomavirus 16 L2 and sorting nexin 27 and modulates virion trafficking. J. Virol. 89:10145–10155

20) Popa, A., W. Zhang, M.S. Harrison, K. Goodner, T. Kazakov, E.C. Goodwin, A. Lipovsky, C.G. Burd, and D. DiMaio. 2015. Direct binding of retromer to human papillomavirus type 16 minor capsid protein L2 mediates endosome exit during viral infection. PLoS Pathog. 11:e1004699.

21) Bergant, M., and L. Banks. 2013. SNX17 facilitates infection with diverse papillomavirus types. J. Virol. 87:1270–1273.

22) Day PM, Thompson CD, Schowalter RM, Lowy DR, Schiller JT. 2013. Identification of a role for the trans-Golgi network in human papillomavirus 16 pseudovirus infection. J Virol 87:3862-3870.

23) Lipovsky A, Popa A, Pimienta G, Wyler M, Bhan A, Kuruvilla L, Guie MA, Poffenberger AC, Nelson CD, Atwood WJ, DiMaio D. 2013. Genome-wide siRNA screen identifies the retromer as a cellular entry factor for human papillomavirus. Proc Natl Acad Sci U S A 110:7452-7457.

24) Zhang W, Kazakov T, Popa A, DiMaio D. 2014. Vesicular trafficking of incoming human papillomavirus 16 to the Golgi apparatus and endoplasmic reticulum requires gamma-secretase activity. MBio 5:e01777-01714.

25) Pyeon D, Pearce SM, Lank SM, Ahlquist P, Lambert PF. 2009. Establishment of human papillomavirus infection requires cell cycle progression. PLoS Pathog 5:e1000318.

26) Aydin I, Weber S, Snijder B, Samperio Ventayol P, Kuhbacher A, Becker M, Day PM, Schiller JT, Kann M, Pelkmans L, Helenius A, Schelhaas M. 2014. Large scale RNAi reveals the requirement of nuclear envelope breakdown for nuclear import of human papillomaviruses. PLoS Pathog 10:e1004162.

27) Aydin I, Villalonga-Planells R, Greune L, Bronnimann MP, Calton CM, Becker M, Lai KY, Campos SK, Schmidt MA, Schelhaas M. 2017. A central region in the minor capsid protein of papillomaviruses facilitates viral genome tethering and membrane penetration for mitotic nuclear entry. PLoS Pathog 13:e1006308.

28) Calton CM, Bronnimann MP, Manson AR, Li S, Chapman JA, Suarez-Berumen M, Williamson TR, Molugu SK, Bernal RA, Campos SK. 2017. Translocation of the papillomavirus L2/vDNA complex across the limiting membrane requires the onset of mitosis. PLoS Pathog 13:e1006200.

29) DiGiuseppe S, Luszczek W, Keiffer TR, Bienkowska-Haba M, Guion LG, Sapp MJ. 2016. Incoming human papillomavirus type 16 genome resides in a vesicular compartment throughout mitosis. Proc Natl Acad Sci U S A 113:6289-6294.

30) Bergant Marušič, M., M.A. Ozbun, S.K. Campos, M.P. Myers, and L. Banks. 2012. Human papillomavirus L2 facilitates viral escape from late endosomes via sorting nexin 17. Traffic. 13:455–467.

31) Schelhaas M, Shah B, Holzer M, Blattmann P, Kuhling L, Day PM, Schiller JT, Helenius A. 2012. Entry of human papillomavirus type 16 by actin-dependent, clathrin- and lipid raft-independent endocytosis. PLoS Pathog 8:e1002657.

32) Huang HS, Buck CB, Lambert PF. 2010. Inhibition of gamma secretase blocks HPV infection. Virology 407:391-396.

33) Karanam B, Peng S, Li T, Buck C, Day PM, Roden RB. 2010. Papillomavirus infection requires gamma secretase. J Virol 84:10661-10670.

34) Zhang W, Kazakov T, Popa A, DiMaio D. 2014. Vesicular trafficking of incoming human papillomavirus 16 to the Golgi apparatus and endoplasmic reticulum requires gamma-secretase activity. MBio 5:e01777-01714.

35) Anastasiadis PZ, Reynolds AB. 2000. The p120 catenin family: complex roles in adhesion, signaling and cancer. J Cell Sci 113 (Pt 8):1319-1334.

36) Reynolds AB, Herbert L, Cleveland JL, Berg ST, Gaut JR. 1992. p120, a novel substrate of protein tyrosine kinase receptors and of p60v-src, is related to cadherin-binding factors beta-catenin, plakoglobin and armadillo. Oncogene 7:2439-2445.

37) Reynolds AB, Daniel J, McCrea PD, Wheelock MJ, Wu J, Zhang Z. 1994. Identification of a new catenin: the tyrosine kinase substrate p120cas associates with E-cadherin complexes. Mol Cell Biol 14:8333-8342.

38) Kiss A, Troyanovsky RB, Troyanovsky SM. 2008. p120-catenin is a key component of the cadherin-gamma-secretase supercomplex. Mol Biol Cell 19:4042-4050.

39) Kouchi Z, Barthet G, Serban G, Georgakopoulos A, Shioi J, Robakis NK. 2009. p120 catenin recruits cadherins to gamma-secretase and inhibits production of Abeta peptide. J Biol Chem 284:1954-1961.

40) Buck, C.B., D.V. Pastrana, D.R. Lowy, and J.T. Schiller. 2004. Efficient intracellular assembly of papillomaviral vectors. J. Virol. 78:751–757.

41) Day PM, Lowy DR, Schiller JT. 2003. Papillomaviruses infect cells via a clathrin-dependent pathway. Virology 307:1-11.

42) Becker M, Greune L, Schmidt MA, Schelhaas M. 2018. Extracellular conformational changes in the capsid of human papillomaviruses contribute to asynchronous uptake into host cells. J Virol doi:10.1128/JVI.02106-17.

Chapter 5. Conclusions and Future Directions

PyV

A host membrane acts as a critical barrier during entry of nonenveloped viruses (1). How these viruses penetrate a cellular membrane remains enigmatic, but insights into this process are slowly emerging. For the classic nonenveloped PyV SV40, penetration across the ER membrane to reach the cytosol represents the decisive infection step. During productive entry, SV40 is initially transported from the cell surface to the ER from where it crosses the ER membrane to access the cytosol and then the nucleus to cause infection (Fig. 1-1B) (2-9). Upon reaching the ER, host cues including the PDI family proteins in this compartment induce conformational changes to SV40, generating a hydrophobic viral particle that integrates into the ER membrane (10-14). To complete membrane penetration, a cytosolic ternary protein complex composed of Hsc70, Bag2, and SGTA, Hsp105 – forming the so-called extraction machinery – engages the ER membrane-integrated virus and ejects it into the cytosol (15-19). This thesis clarified the molecular basis of SV40's cytosol extraction process. Specifically, my results demonstrated that the Hsc70 chaperone first binds to the ER membrane-embedded virus. The ability of Hsc70 to engage the virus is due to the action of ER membrane J proteins (B12, B14, and C18), which converts low-affinity ATP-Hsc70 to high-affinity ADP-Hsc70 (15, 16, 20). Next, acting as a nucleotide exchange factor (NEF), Bag2 induces release of SV40 from Hsc70 by switching ADP-Hsc70 back to ATP-Hsc70 (19). Iterative rounds of binding and release of SV40 to and from Hsc70

"pulls" the virus out of the ER membrane. My analysis also revealed that SGTA regulates this Hsc70-dependent substrate binding-release cycle, either by inhibiting the activity of the J proteins or stimulating the NEF function (18). Hsp105 is likely involved in a reaction that disassembles the membrane-embedded SV40, presumably to enable efficient extraction of the virus (17).

Interestingly, although members of this extraction machinery are also components of the ERAD system that normally ejects cellular misfolded proteins from the ER into the cytosol, SV40 appears to hijack the extraction machinery in a novel way. The major difference is that ERAD substrates transport across the ER membrane by passing through a protein-conducting channel (formed by the Hrd1 transmembrane protein), while SV40 does not use a protein-based channel but instead penetrates the lipid bilayer of the ER to reach the cytosol (15-19, 21).

This situation raises a major conundrum: with a protein-conducting channel, the cytosol extraction machinery has a defined "docking site" where it can be recruited, and subsequently engage the translocating substrate (21, 22). However, in a situation where SV40 simply penetrates the lipid bilayer of the vast ER membrane network, where does the cytosol extraction machinery dock? Part of the explanation may lie in the observation that SV40 induces formation of cytosol entry sites in the ER membrane. For instance, SV40 triggers reorganization of the transmembrane J proteins B12, B14, and C18 to discrete sites in the ER called foci (15,16). Because these J proteins have their J-domain facing the cytosol, and because a J-domain binds to Hsc70, we anticipate that concentrating the J proteins to the foci should correspondingly recruit the cytosol

extraction machinery to the foci (16). Hence, in this scenario, a docking site on the ER membrane for the extraction machinery is in fact created by the incoming virus.

Although our analyses strongly support a model in which Hsc70, Bag2, SGTA, and Hsp105 form a ternary protein complex that ejects SV40 from the ER into the cytosol, many important questions remain. One obvious question is whether there are additional unidentified host factors present in the extraction complex? Addressing this question will require more rigorous biochemical approaches. For instance, a “sequential co-IP” approach coupled with mass spectrometry analysis should reveal if there are additional host factors present in the SV40-extraction machinery complex. In this context, establishing an *in vitro* reconstituted membrane transport system using purified cytosolic components will enable us to test whether there are minimum components required to drive ER-to-cytosol transport of SV40. Another outstanding question is how Hsp105-dependent disassembly of the virus is coupled to the extraction process. Does virus disassembly precede extraction, or vice versa?

One fascinating yet puzzling question surrounding this thesis work is that, while SV40 is thought to disguise as a misfolded substrate that hijacks elements of the ERAD machinery to gain access to the cytosol, the virus nonetheless escapes the degradative fate typically experienced by misfolded proteins in the cytosol. Indeed, how does SV40 evade the ubiquitin-dependent proteasome machinery once it reaches the cytosol? Thus far, none of the SV40 structural proteins have been reported to be polyubiquitinated, a post-translational modification appended to a substrate destined for proteasomal degradation. If in fact SV40 is not subjected to polyubiquitination, it is possible that recruitment of the extraction machinery (or other unidentified cytosolic

proteins) physically impedes the cascade of ubiquitination enzymes from gaining access to the viral proteins. Careful analysis of any potential post-translational modification imposed on cytosol-localized SV40 (by mass spectrometry) should reveal if the virus is polyubiquitinated. Similar to SV40, cholera toxin (CT) is yet another pathogenic agent that transports from the ER into the cytosol to induce cytotoxicity (23). Strikingly, CT avoids ubiquitination to evade the degradative fate in the cytosol. This occurs because CTA1, the catalytic subunit of CT which undergoes ER-to-cytosol transport, harbors few lysine residues that are conventional acceptor sites of ubiquitination (24). Thus evasion of polyubiquitination may be a conserved strategy to avoid proteasomal degradation during ER-to-cytosol membrane penetration of pathogens.

The last phase of productive SV40 infection requires trafficking of SV40 from the cytosol into the nucleus (8,9). Because SV40 does not experience significant disassembly in the ER, it must do so in the cytosol in order to cross the nuclear pore complex (NPC) and reach the nucleus. How cytosol-localized virus is disassembled is not entirely clear. It is possible that during entry into the cytosol from the ER, Hsp105 of the extraction machinery disassembles the virus, uncoating some of the VP1 pentamers. The resulting core viral particle, harboring a residual level of VP1 pentamers, VP2, VP3, and genome are then transported to the nucleus. Because our lab recently demonstrated that a dynein motor-dependent disassembly reaction is also required for SV40 infection, dynein might act in concert with Hsp105 to disassemble the cytosol-localized virus in preparation for nuclear entry (25). In such a scenario, ER membrane penetration of SV40 might be functionally coupled to its subsequent nuclear entry.

HPV

Paralleling the study of ER membrane penetration of SV40, another focus of my thesis is to elucidate endosome membrane penetration of HPV, a critical infection step. During productive entry, HPV is delivered from the cell surface to the endosome (26-29). In this compartment, the virus is targeted to the transmembrane protease γ-secretase that inserts the L2 viral protein into the membrane (30-33). This exposes a L2 retromer-binding domain to the cytosol that recruits the retromer complex, which in turn directs the virus to the Golgi (33-36). Golgi membrane fragmentation during mitosis generates Golgi-derived vesicles (GDVs) harboring HPV that enter the nucleus due to nuclear membrane disassembly at the onset of mitosis (37-41). In the nucleus, HPV is thought to penetrate the GDV membrane to complete its membrane penetration; when this occurs, HPV is deposited into the nucleoplasm where DNA synthesis can occur (40, 41). Thus, while HPV membrane insertion is initiated in the endosome, completion of virus membrane penetration is accomplished in the nucleus.

When HPV reaches the endosome, it can also sort to the lysosome where the virus is degraded (29, 42). Thus, for productive infection to take place, HPV must avoid this degradative fate and instead be targeted along the endosome-Golgi axis. The defining event in targeting HPV from the endosome to the Golgi is γ-secretase-dependent membrane insertion of L2. How then is HPV in the endosome targeted to the γ-secretase? My thesis work has provided some insight into this question.

Using an unbiased biochemical strategy, our lab previously found that HPV L2 potentially binds to a cytosolic protein called p120 catenin (31). Using standard co-IP

analysis, my results showed that the L2-p120 interaction begins at the cell surface and continues until the virus reaches the endosome. Moreover, HPV is known to bind to γ-secretase in the endosome (31). These observations raise the possibility that p120 targets HPV from the plasma membrane to γ-secretase in the endosome in order to support HPV infection. To test this hypothesis, I used a siRNA-mediated loss-of-function approach and found that p120 depletion blocked L2-HPV interaction, L2 insertion into the endosome membrane, and importantly, HPV infection. Because HPV L2 is not exposed to the cytosol at the plasma membrane, HPV's ability to bind to p120 at the cell surface must be mediated by an unknown transmembrane receptor. We therefore postulate that the receptor-p120 complex engages HPV at the plasma membrane, delivering the viral particle to γ-secretase in the endosome when the receptor-p120 complex itself is recruited to γ-secretase.

Clearly the key objective to address at this point is to identify the p120-associated receptor that binds to HPV at the cell surface. We are fully aware that this receptor may represent the long sought-after entry receptor of HPV. One approach to pinpoint this receptor is to determine host factors that bind to HPV prior to internalization. This could be accomplished by performing another IP-mass spectrometry study in which the experiment is designed so that HPV only engages cell surface molecules. (Our initial IP-mass spectrometry study examined host factors that bound to HPV post-internalization). Beyond this unbiased approach, another strategy is to test the function of transmembrane receptors known to bind to p120. In this context, p120 has been shown to associate with cadherins, which are transmembrane receptors well-established for their role in mediating cell-cell adhesion (43-46). In this case, p120

is believed to target cadherin to γ-secretase, enabling γ-secretase to proteolytically cleave cadherin and generate a cytosolic cleaved product that evokes a signaling response (46, 47). Interestingly, in a genome-wide RNAi screen, cadherin16 as well as many protocadherins were implicated as host factors that support HPV infection (35). Efforts are currently underway in using these two different strategies to identify the p120-interacting receptor that binds to HPV at the cell surface.

We recognize that there may not be only one single receptor that binds to p120 on the plasma membrane. In fact, different p120-binding receptors may engage HPV on the cell surface and promote endocytosis of the virus to the endosome. In the endosome, when p120 delivers the receptor to γ-secretase to potentially allow γ-secretase to cleave the receptor and elicit a cellular response, HPV is concomitantly targeted to the γ-secretase. It should be noted that while there is evidence in support of the presence of an entry receptor for HPV (48, 49), there is also a report suggesting that receptor-independent, macropinocytosis may be responsible for virus internalization (29). One possible explanation for these reported discrepancies is the use of different cell lines and pseudoviruses in the various studies.

In a model where a receptor-p120 complex targets HPV to γ-secretase in the endosome, an outstanding question is whether there is a conformation of HPV that is specifically recognized by γ-secretase. Previous analyses suggested that the majority of L1 pentamers are released from the L2-genome complex in the endosome (50, 51). This is believed to be caused by the low pH and the action of cyclophilin in the endosome (50, 52). Conceivably, L1 pentamer release enables sufficient L2 exposure that allows subsequent γ-secretase engagement. An experiment to test this possibility is

to disrupt the low pH and cyclophilin activity in the endosome, and assess if the HPV-γ-secretase interaction remains intact. Clearly, a high-resolution structure of the HPV-γ-secretase complex will provide unprecedented detail on the nature of the virus-protease interaction.

After HPV is properly delivered to γ-secretase by the receptor-p120 complex in the endosome, how does γ-secretase promote membrane insertion of L2? At present, we do not know the precise sequence of events leading to membrane insertion of L2. This is complicated by the fact that γ-secretase harbors 4 different subunits: PS1, NICA, APH1A, and PEN2 (53). Regardless of which γ-secretase subunits interact with L2, and in which specific order this takes place, we envision two models that may explain membrane insertion of L2. In the first model, membrane insertion of L2 is considered "dynamic". Here γ-secretase acts as a "plunger", actively inserting L2 into the lipid bilayer of the endosomal membrane. By contrast, in the second model, membrane insertion of L2 can be described as "passive". In this case, L2 passively diffuses in and out of the endosome membrane due to presence of a membrane-spanning domain in L2 (54). γ-secretase simply binds to and stabilizes L2 when it is within the plane of the bilayer. While we do not favor either model at this point, we presume that the dynamic model of L2 membrane insertion would require an energy source that enables γ-secretase to act as an insertase. This energy source might be derived from the low pH of the endosome, which has the capacity to induce structural rearrangements to γ-secretase essential for the insertion reaction.

From a structural standpoint, HPV and PyV appear very similar. Both viruses contain a circular, double stranded DNA genome that is encased by capsid proteins with

T=7 icosahedral symmetry (55-58). Both virus capsids have 72 pentamers of the major capsid protein (27, 55, 56, 58). Minor capsid proteins associate with the major capsid proteins: the VP2 or VP3 minor protein of PyV associates with a single VP1 pentamer, while the L2 capsid protein of HPV is associated with the L1 pentamer. In addition, the HPV and PyV virions are similar in size, at approximately 55 and 50 nm in diameter, respectively. Both viruses enter into the host cell, and arrive in the endosome (5,7,28,29). However, from the endosome, HPV and PyV take different routes throughout the cell (34, 59). If both viruses are structurally similar, why then do these viruses takes such different routes to traffic to the nucleus where viral genome replication occurs?

While there are many structural similarities between HPV and PyV, we propose three key differences between the virions that may account for such different routes of entry. First, at the amino acid sequence level, the major capsid proteins VP1 and L1 are quite different, with approximately 24% sequence homology. This is of significant importance when addressing a key protein-protein interaction: the initial binding to the entry receptor. GM1, the entry receptor used by SV40, targets the virus to the ER (2,3). During endocytosis and retrograde trafficking, transport to the Golgi is often observed; however, rarely are cargos trafficked to the ER (61). Interestingly, many bacterial toxins such as cholera toxin also bind to ganglioside receptors and are also trafficked to the ER (62). Perhaps the binding of cargos and pathogens to gangliosides provides a unique route in retrograde transport, enabling targeting from the cell surface to the ER. Hence attachment to a specific entry receptor may dictate the cellular destination of the receptor-bound ligand.

Second, a key difference between HPV and PyV is the presence of recruiting domains on the minor capsid proteins. Specifically, HPV's L2 protein contains a binding motif near the cytosolically exposed C-terminus that recruits the retromer, a cytosolic complex that directs a cargo (e.g. HPV) from the endosome to the Golgi (35,36). Importantly, neither the VP2 or VP3 minor proteins of PyV contain such a domain. Thus, during entry, PyV does not reach the Golgi. Precisely why HPV evolved to contain a retromer binding domain is unknown.

For nonenveloped DNA viruses, trafficking of the viral DNA to the nucleus from the cell surface poses specific challenges. Specifically, while a virus must sufficiently disassemble so that its genome can access the cellular replication machinery, the genome must also remain hidden or shielded from the host cytosolic immune factors that could potentially recognize the viral DNA. Therefore, a third key difference between HPV and PyV is their timeline for uncoating and genome exposure, which may be a result of capsid stability. While both virus capsids contain both intra- and inter-pentameric disulfide bonds, the extent and strength of these disulfide bonds may vary (55,56,63). As capsid disassembly is an obligate step in infection, viruses likely target to specific organelles to promote their uncoating. In the case of SV40, ER chaperones and protein disulfide isomerase (PDI) located in the ER are needed to disrupt capsid disulfide bonds and expose hydrophobic VP2 and VP3 (10-14). In the ER, the viral genome is not exposed and is likely not fully exposed until later steps in cytosolic trafficking as the virus nears the nucleus. Under this circumstance, the viral capsid has been disassembled, and the viral genome likely remains safeguarded by the minor capsid proteins.

Unlike PyV, HPV disassembly occurs in the endosome where low pH and cyclophilins clearly play a role in segregation of L1 from the L2-viral genome complex (50, 51, 52). Why cyclophilins disassemble HPV but not PyV is not known, but this may be due to the strength and rigidity of the different capsids. Importantly, HPV attachment to the primary attachment receptor at the cell surface facilitates capsid conformational changes proposed to partially expose the minor capsid protein L2 (64-66). Perhaps this conformational change starts capsid disassembly and makes further disassembly possible in the endosome. Because only L2 is cytosolically exposed upon interaction with γ-secretase, the viral genome remains shielded from host cytosolic immune factors (31,36,41,54). In fact, throughout HPV trafficking, the viral genome remains shielded from the cytosol (41, 67). It is possible that, unlike PyV, after endosomal disassembly, the HPV viral genome is not safeguarded by L2 alone, and therefore maintains protection from host cytosolic immune factors by remaining safeguarded in the lumen of the endosome and TGN. In this circumstance, the virus is disassembled yet protected from the host immune response. Thus, while HPV and PyV have significant structural similarities from a low-resolution viewpoint, distinct variation in viral entry and trafficking occurs due to key differences.

Despite variation in mechanisms of nonenveloped virus entry, important aspects are shared. Specifically, nonenveloped viruses must traffic to specific sites in the cell where at least partial viral disassembly occurs. In addition, membrane penetration must occur at these sites in order for productive trafficking to continue and ultimately lead to DNA replication. For example, similar to HPV, the non-enveloped adenovirus traffics to the endosome where membrane penetration occurs. However, endosomal membrane

penetration by the lytic protein VI of adenovirus results in complete disruption and penetration of the endosomal membrane, akin to the complete penetration of the ER membrane by SV40 (1,68). In the cytosol, the adenovirus genome remains partially coated and is transported to the nuclear pore complex where complete disassembly occurs before entry into the nucleus (69).

Another nonenveloped DNA virus, parvovirus, undergoes endocytosis and similar to HPV, must penetrate the endosomal membrane. As in HPV entry, the pH of the endosome plays an important role in parvovirus membrane penetration, where the phospholipase domain in its capsid protein VP1 disrupts membrane integrity (70, 71). Again, similar to SV40, complete penetration of the endosomal membrane occurs. While pH is important for exposure of the phospholipase, the virion remains intact upon delivery to the cytosol and during transport to the nucleus (70,71). This would prevent recognition of the viral genome by host cytosolic factors. Clearly, while nonenveloped viruses have evolved different mechanisms of membrane penetration, two key aspects are generally observed for nonenveloped virus entry. First, the virus must traffic to specific sites in the cell where partial disassembly or conformation changes to the virus capsid structure occur. And second, at these specific locations, membrane penetration must occur. Membrane penetration is a decisive infection step and is necessary for delivery of the virus to the nucleus where DNA replication ensues.

Overall summary

In sum, my thesis study elegantly depicts how two distinct nonenveloped viruses exploit host machineries to support their membrane penetration process. As host membranes represent crucial barriers to infection, clarifying the molecular mechanism

of virus membrane penetration will likely have therapeutic implications. For PyV, my results revealed how protein quality control machineries - residing in both the ER and cytosol – are co-opted to promote ER membrane penetration. For HPV, my findings unveiled how a cytosolic adaptor of a transmembrane protease is exploited to support endosomal membrane penetration of HPV. I believe insights from my thesis should lay the foundation for novel therapeutic approaches against PyV- and HPV-induced diseases. As an example, because host Hsp70 chaperone machineries regulate Zika virus infection, new Hsp70 inhibitors have recently been developed and shown to curtail Zika virus-induced disease (72). Given that these Hsp70 machineries also impact PyV infection, the new Hsp70 inhibitors might also be effective in combating PyV diseases. Finally, beyond the field of virology, I anticipate that illuminating membrane penetration of viruses will also inform fundamental cellular membrane transport processes.

References:

1) Tsai, B. Penetration of nonenveloped viruses into the cytoplasm. Annu Rev Cell Dev Biol. 2007, 23: 23-43.

2) Tsai, B.; Gilbert, J.M.; Stehle, T.; Lencer, W.; Benjamin, T.L.; Rapoport, T.A. Gangliosides are receptors for murine polyoma virus and SV40. EMBO J. 2003, 22, 4346–4355.

3) Campanero-Rhodes, M.A.; Smith, A.; Chai, W.; Sonnino, S.; Mauri, L.; Childs, R.A.; Zhang, Y.; Ewers, H.;Helenius, A.; Imberty, A.; et al. N-glycolyl GM1 ganglioside as a receptor for simian virus 40. J. Virol. 2007, 81, 12846–12858.

4) Ewers, H.; Romer, W.; Smith, A.E.; Bacia, K.; Dmitrieff, S.; Chai, W.; Mancini, R.; Kartenbeck, J.; Chambon, V.;Berland, L.; et al. GM1 structure determines SV40-induced membrane invagination and infection.Nat. Cell Biol. 2010,12, 11-18.

5) Engel, S.; Heger, T.; Mancini, R.; Herzog, F.; Kartenbeck, J.; Hayer, A.; Helenius, A. Role of endosomes in simian virus 40 entry and infection. J. Virol. 2011, 85, 4198-4211.

6) Kartenbeck, J.; Stukenbrok, H.; Helenius, A. Endocytosis of simian virus 40 into the endoplasmic reticulum. J. Cell Biol. 1989, 109, 2721–2729.

7) Qian, M.; Cai, D.; Verhey, K.J.; Tsai, B. A lipid receptor sorts polyomavirus from the endolysosome to the endoplasmic reticulum to cause infection. PLoS Pathog. 2009, 5, e1000465.

8) Nakanishi, A.; Clever, J.; Yamada, M.; Li, P.P.; Kasamatsu, H. Association with capsid proteins promotes nuclear targeting of simian virus 40 DNA. Proc. Natl. Acad. Sci. USA 1996, 93, 96–100.

9) Clever, J.; Yamada, M.; Kasamatsu, H. Import of simian virus 40 virions through nuclear pore complexes. Proc. Natl. Acad. Sci. USA 1991, 88, 7333–7337.

10) Walczak, C.P.; Tsai, B. A PDI family network acts distinctly and coordinately with ERp29 to facilitate polyomavirus infection. J. Virol. 2011, 85, 2386–2396.

11) Inoue, T.; Dosey, A.; Herbstman, J.F.; Ravindran, M.S.; Skiniotis, G.; Tsai, B. ERdj5 Reductase Cooperates with Protein Disulfide Isomerase To Promote Simian Virus 40 Endoplasmic Reticulum Membrane Translocation. J. Virol. 2015, 89, 8897–8908.

12) Magnuson, B.; Rainey, E.K.; Benjamin, T.; Baryshev, M.; Mkrtchian, S.; Tsai, B. ERp29 triggers a conformational change in polyomavirus to stimulate membrane binding. Mol. Cell 2005, 20, 289–300.

13) Rainey-Barger, E.K.; Mkrtchian, S.; Tsai, B. The C-terminal domain of ERp29 mediates polyomavirus binding, unfolding, and infection. J. Virol. 2009, 83, 1483–1491.

14) Gilbert, J.; Ou, W.; Silver, J.; Benjamin, T. Downregulation of protein disulfide isomerase inhibits infection by the mouse polyomavirus. J. Virol. 2006, 80, 10868–10870.

15) Walczak, C.P.; Ravindran, M.S.; Inoue, T.; Tsai, B. A cytosolic chaperone complexes with dynamic membrane J-proteins and mobilizes a nonenveloped virus out of the endoplasmic reticulum. PLoS Pathog. 2014, 10, e1004007.

16) Bagchi, P.; Walczak, C.P.; Tsai, B. The endoplasmic reticulum membrane J protein C18 executes a distinct role in promoting simian virus 40 membrane penetration. J. Virol. 2015, 89, 4058–4068.

17) Ravindran, M.S.; Bagchi, P.; Inoue, T.; Tsai, B. A Non-enveloped Virus Hijacks Host Disaggregation Machinery to Translocate across the Endoplasmic Reticulum Membrane. PLoS Pathog. 2015, 11, e1005086.

18) Dupzyk, A.; Williams, JM.; Bagchi, P.; Inoue, T.; Tsai, B. 2017. SGTA-Dependent Regulation of Hsc70 Promotes Cytosol Entry of Simian Virus 40 from the Endoplasmic Reticulum. J Virol 91.

19) Dupzyk, A.; Tsai, B. 2018. Bag2 Is a Component of a Cytosolic Extraction Machinery That Promotes Membrane Penetration of a Nonenveloped Virus. J Virol 92.

20) Goodwin, E.C.; Lipovsky, A.; Inoue, T.; Magaldi, T.G.; Edwards, A.P.; Van Goor, K.E.; Paton, A.W.; Paton, J.C.; Atwood, W.J.; Tsai, B.; et al. BiP and multiple DNAJ molecular chaperones in the endoplasmic reticulum are required for efficient simian virus 40 infection. MBio 2011, 2, e00101–e00111.

21) Brodsky, J.L. Cleaning up: ER-associated degradation to the rescue. Cell 2012, 151, 1163–1167.

22) Ye, Y.; Meyer, H.H.; Rapoport, T.A. The AAA ATPase Cdc48/p97 and its partners transport proteins from the ER into the cytosol. Nature 2001, 414, 652–656.

23) Tsai B, Rodighiero C, Lencer WI, Rapoport TA. 2001. Protein disulfide isomerase acts as a redox-dependent chaperone to unfold cholera toxin. Cell 104**:**937-948.

24) Rodighiero C, Tsai B, Rapoport TA, Lencer WI. 2002. Role of ubiquitination in retro-translocation of cholera toxin and escape of cytosolic degradation. EMBO Rep 3:1222-1227.

25) Ravindran MS, Spriggs CC, Verhey KJ, Tsai B. 2018. Dynein engages and disassembles cytosol-localized SV40 to promote infection. J Virol doi:10.1128/JVI.00353-18.

26) Volpers C, Unckell F, Schirmacher P, Streeck RE, Sapp M. 1995. Binding and internalization of human papillomavirus type 33 virus-like particles by eukaryotic cells. J Virol 69:3258-3264.

27) Joyce JG, Tung JS, Przysiecki CT, Cook JC, Lehman ED, Sands JA, Jansen KU, Keller PM. 1999. The L1 major capsid protein of human papillomavirus type 11 recombinant virus-like particles interacts with heparin and cell-surface glycosaminoglycans on human keratinocytes. J Biol Chem 274:5810-5822.

28) Day PM, Lowy DR, Schiller JT. 2003. Papillomaviruses infect cells via a clathrin-dependent pathway. Virology 307:1-11.

29) Schelhaas M, Shah B, Holzer M, Blattmann P, Kuhling L, Day PM, Schiller JT, Helenius A. 2012. Entry of human papillomavirus type 16 by actin-dependent, clathrin- and lipid raft-independent endocytosis. PLoS Pathog 8:e1002657.

30) Huang HS, Buck CB, Lambert PF. 2010. Inhibition of gamma secretase blocks HPV infection. Virology 407:391-396.

31) Inoue T, Zhang P, Zhang W, Goodner-Bingham K, Dupzyk A, DiMaio D, Tsai B. 2018. gamma-Secretase promotes membrane insertion of the human papillomavirus L2 capsid protein during virus infection. J Cell Biol 217:3545-3559.

32) Karanam B, Peng S, Li T, Buck C, Day PM, Roden RB. 2010. Papillomavirus infection requires gamma secretase. J Virol 84:10661-10670.

33) Zhang W, Kazakov T, Popa A, DiMaio D. 2014. Vesicular trafficking of incoming human papillomavirus 16 to the Golgi apparatus and endoplasmic reticulum requires gamma-secretase activity. MBio 5:e01777-01714.

34) Day PM, Thompson CD, Schowalter RM, Lowy DR, Schiller JT. 2013. Identification of a role for the trans-Golgi network in human papillomavirus 16 pseudovirus infection. J Virol 87:3862-3870.

35) Lipovsky A, Popa A, Pimienta G, Wyler M, Bhan A, Kuruvilla L, Guie MA, Poffenberger AC, Nelson CD, Atwood WJ, DiMaio D. 2013. Genome-wide siRNA screen identifies the retromer as a cellular entry factor for human papillomavirus. Proc Natl Acad Sci U S A 110:7452-7457.

36) Popa A, Zhang W, Harrison MS, Goodner K, Kazakov T, Goodwin EC, Lipovsky A, Burd CG, DiMaio D. 2015. Direct binding of retromer to human papillomavirus type

16 minor capsid protein L2 mediates endosome exit during viral infection. PLoS Pathog 11:e1004699

37) Pyeon D, Pearce SM, Lank SM, Ahlquist P, Lambert PF. 2009. Establishment of human papillomavirus infection requires cell cycle progression. PLoS Pathog 5:e1000318.

38) Aydin I, Weber S, Snijder B, Samperio Ventayol P, Kuhbacher A, Becker M, Day PM, Schiller JT, Kann M, Pelkmans L, Helenius A, Schelhaas M. 2014. Large scale RNAi reveals the requirement of nuclear envelope breakdown for nuclear import of human papillomaviruses. PLoS Pathog 10:e1004162.

39) Aydin I, Villalonga-Planells R, Greune L, Bronnimann MP, Calton CM, Becker M, Lai KY, Campos SK, Schmidt MA, Schelhaas M. 2017. A central region in the minor capsid protein of papillomaviruses facilitates viral genome tethering and membrane penetration for mitotic nuclear entry. PLoS Pathog 13:e1006308.

40) Calton CM, Bronnimann MP, Manson AR, Li S, Chapman JA, Suarez-Berumen M, Williamson TR, Molugu SK, Bernal RA, Campos SK. 2017. Translocation of the papillomavirus L2/vDNA complex across the limiting membrane requires the onset of mitosis. PLoS Pathog 13:e1006200.

41) DiGiuseppe S, Luszczek W, Keiffer TR, Bienkowska-Haba M, Guion LG, Sapp MJ. 2016. Incoming human papillomavirus type 16 genome resides in a vesicular compartment throughout mitosis. Proc Natl Acad Sci U S A 113:6289-6294.

42) Bergant Marušič, M., M.A. Ozbun, S.K. Campos, M.P. Myers, and L. Banks. 2012. Human papillomavirus L2 facilitates viral escape from late endosomes via sorting nexin 17. Traffic. 13:455–467.

43) Reynolds AB, Daniel J, McCrea PD, Wheelock MJ, Wu J, Zhang Z. 1994. Identification of a new catenin: the tyrosine kinase substrate p120cas associates with E-cadherin complexes. Mol Cell Biol 14:8333-8342.

44) Anastasiadis PZ, Reynolds AB. 2000. The p120 catenin family: complex roles in adhesion, signaling and cancer. J Cell Sci 113 (Pt 8):1319-1334.

45) Reynolds AB, Herbert L, Cleveland JL, Berg ST, Gaut JR. 1992. p120, a novel substrate of protein tyrosine kinase receptors and of p60v-src, is related to cadherin-binding factors beta-catenin, plakoglobin and armadillo. Oncogene 7:2439-2445.

46) Kiss A, Troyanovsky RB, Troyanovsky SM. 2008. p120-catenin is a key component of the cadherin-gamma-secretase supercomplex. Mol Biol Cell 19:4042-4050.

47)Kouchi Z, Barthet G, Serban G, Georgakopoulos A, Shioi J, Robakis NK. 2009. p120 catenin recruits cadherins to gamma-secretase and inhibits production of Abeta peptide. J Biol Chem 284:1954-1961.

48)Selinka HC, Florin L, Patel HD, Freitag K, Schmidtke M, Makarov VA, Sapp M. 2007. Inhibition of transfer to secondary receptors by heparan sulfate-binding drug or antibody induces noninfectious uptake of human papillomavirus. J Virol 81:10970-10980.

49)Becker M, Greune L, Schmidt MA, Schelhaas M. 2018. Extracellular conformational changes in the capsid of human papillomaviruses contribute to asynchronous uptake into host cells. J Virol doi:10.1128/JVI.02106-17.

50)Bienkowska-Haba M, Williams C, Kim SM, Garcea RL, Sapp M. 2012. Cyclophilins facilitate dissociation of the human papillomavirus type 16 capsid protein L1 from the L2/DNA complex following virus entry. J Virol 86:9875-9887.

51)DiGiuseppe S, Bienkowska-Haba M, Guion LGM, Keiffer TR, Sapp M. 2017. Human papillomavirus major capsid protein L1 remains associated with the incoming viral genome throughout the entry process. J Virol doi:10.1128/JVI.00537-17.

52)Smith JL, Campos SK, Wandinger-Ness A, Ozbun MA. 2008. Caveolin-1-dependent infectious entry of human papillomavirus type 31 in human keratinocytes proceeds to the endosomal pathway for pH-dependent uncoating. J Virol 82:9505-9512.

53)Lu, P., X.C. Bai, D. Ma, T. Xie, C. Yan, L. Sun, G. Yang, Y. Zhao, R. Zhou, S.H.W. Scheres, and Y. Shi. 2014. Three-dimensional structure of human γ-secretase. Nature. 512:166–170.

54)Bronnimann, M.P., J.A. Chapman, C.K. Park, and S.K. Campos. 2013. A transmembrane domain and GxxxG motifs within L2 are essential for papillomavirus infection. J. Virol. 87:464–473.

55)Liddington, R.C.; Yan, Y.; Moulai, J.; Sahli, R.; Benjamin, T.L.; Harrison, S.C. Structure of simian virus 40 at 3.8-A resolution. Nature 1991, 354, 278–284.

56)Stehle, T.; Gamblin, S.J.; Yan, Y.; Harrison, S.C. The structure of simian virus 40 refined at 3.1 A resolution. Structure 1996, 4, 165–182.

57)DeCaprio, J.A.; Garcea, R.L. A cornucopia of human polyomaviruses. Nat. Rev. Microbiol. 2013, 11, 264–276.

58)Buck CB, Cheng N, Thompson CD, Lowy DR, Steven AC, Schiller JT, Trus BL. 2008. Arrangement of L2 within the papillomavirus capsid. J Virol 82:5190-5197.

59)Kartenbeck, J.; Stukenbrok, H.; Helenius, A. Endocytosis of simian virus 40 into the endoplasmic reticulum. J. Cell Biol. 1989, 109, 2721–2729.

60)Bienkowska-Haba M, Williams C, Kim SM, Garcea RL, Sapp M. 2012. Cyclophilins facilitate dissociation of the human papillomavirus type 16 capsid protein L1 from the L2/DNA complex following virus entry. J Virol 86:9875-9887.

61)Geiger R, Luisoni S, Johnsson K, Greber UF, Helenius A. 2013. Investigating endocytic pathways to the endoplasmic reticulum and to the cytosol using SNAP-trap. Traffic 14:36-46.

62)Williams JM, Tsai B. 2016. Intracellular trafficking of bacterial toxins. Curr Opin Cell Biol 41**:**51-56.

63)Sapp M, Fligge C, Petzak I, Harris JR, Streeck RE. 1998. Papillomavirus assembly requires trimerization of the major capsid protein by disulfides between two highly conserved cysteines. J Virol 72:6186-6189.

64)Selinka HC, Giroglou T, Nowak T, Christensen ND, Sapp M. 2003. Further evidence that papillomavirus capsids exist in two distinct conformations. J Virol 77:12961-12967.

65)Richards RM, Lowy DR, Schiller JT, Day PM. 2006. Cleavage of the papillomavirus minor capsid protein, L2, at a furin consensus site is necessary for infection. Proc Natl Acad Sci U S A 103:1522-1527.

66)Day PM, Lowy DR, Schiller JT. 2008. Heparan sulfate-independent cell binding and infection with furin-precleaved papillomavirus capsids. J Virol 82:12565-12568.

67)DiGiuseppe S, Bienkowska-Haba M, Sapp M. 2016. Human Papillomavirus Entry: Hiding in a Bubble. J Virol 90**:**8032-8035.

68)Wiethoff CM, Nemerow GR. 2015. Adenovirus membrane penetration: Tickling the tail of a sleeping dragon. Virology 479-480**:**591-599.

69)Kilcher S, Mercer J. 2015. DNA virus uncoating. Virology 479-480**:**578-590.

70)Cotmore SF, Tattersall P. 2007. Parvoviral host range and cell entry mechanisms. Adv Virus Res 70**:**183-232.

71)Farr GA, Zhang LG, Tattersall P**.** 2005. Parvoviral virions deploy a capsid-tethered lipolytic enzyme to breach the endosomal membrane during cell entry. Proc Natl Acad Sci U S A 102**:**17148-17153.

72) Taguwa S, Yeh MT, Rainbolt TK, Nayak A, Shao H, Gestwicki JE, Andino R, Frydman J. 2019. Zika Virus Dependence on Host Hsp70 Provides a Protective Strategy against Infection and Disease. Cell Rep 26:906-920 e903.